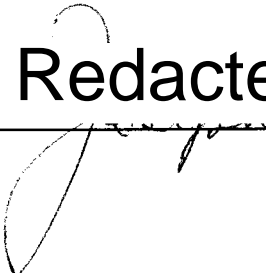


AN ABSTRACT OF THE THESIS OF

Philip R. Minarik for the degree of Doctor of Philosophy in Physical Chemistry presented on July 29, 1996. Title: Coherent Anti-Stokes Raman Spectroscopy of Acetylene Nanoclusters.

Redacted for Privacy

Abstract approved:



---

Joseph W. Nibler

Coherent Anti-Stokes Raman spectroscopy was used to study the formation and phase development of small clusters formed by condensation in a supersonic jet. The clusters were generated from several acetylene / helium mixtures with different initial temperature and pressure conditions. The clusters exhibited two phase transitions, liquid - cubic solid and cubic solid - orthorhombic solid, which were studied to determine various physical properties of acetylene, especially the interfacial free energy of the phases.

Homogeneous nucleation theory was used to relate the interfacial free energy to measured rates of nucleation of cubic solid in a liquid host and of orthorhombic solid in a cubic solid host. The analysis required an estimate of mean cluster size, and the measured rate of cooling, the diameters of the clusters were determined to be from 10 nm in the most dilute gases to 20 nm in the neat samples. For neat acetylene samples, the nucleation rate was  $1.4 \times 10^{29}$  to  $2.8 \times 10^{28} \text{ m}^{-3}\text{s}^{-1}$  and for acetylene mixed with helium, the rate was  $1.8 \times 10^{29}$  -  $3.8 \times 10^{31} \text{ m}^{-3}\text{s}^{-1}$ . These data lead to estimates of 10.1 to 11.6 mJ / m<sup>2</sup> for the

interfacial free energy of the liquid - solid transition and  $2 \text{ mJ} / \text{m}^2$  for the solid - solid phase transition. These results can be compared with the values of  $11.7 \text{ mJ} / \text{m}^2$  for the liquid - solid transition and  $8.7 \text{ mJ} / \text{m}^2$  for the solid - solid transition from Turnbull.

For very dilute expansions, new spectral features were seen which are attributed to molecules on the surface of very small clusters. This conclusion is consistent with similar cluster studies on  $\text{CO}_2$  where new features were also seen and attributed to molecules on the surface layer.

Coherent Anti-Stokes Raman Studies of Acetylene Nanoclusters

by

Philip R. Minarik

A THESIS

submitted to

Oregon State University

in partial fulfillment of  
the requirements for the  
degree of

Doctor of Philosophy

Presented July 29, 1996  
Commencement June 1997

Doctor of Philosophy thesis of Philip R. Minarik presented on July 29, 1996

APPROVED:

Redacted for Privacy

---

Major Professor, representing Chemistry

Redacted for Privacy

---

Chair of Department of Chemistry

Redacted for Privacy

---

Dean of Graduate School

I understand that my thesis will become part of the permanent collection of Oregon State University libraries. My signature below authorizes release of my thesis to any reader upon request.

Redacted for Privacy

---

Philip R. Minarik, Author

## TABLE OF CONTENTS

	<u>Page</u>
1. Introduction.....	1
1.1 Clusters.....	1
1.1.1 Aggregation.....	1
1.1.2 Small Clusters.....	2
1.1.3 Large Clusters.....	3
1.1.4 Very Large Clusters.....	4
1.2 Methods of Studying Clusters.....	5
1.2.1 Preparation of Samples.....	5
1.2.2 Spectroscopies.....	5
1.3 This Cluster Study.....	7
2. Background.....	9
2.1 Raman Scattering.....	9
2.1.1 CARS Amplitude Expression.....	9
2.1.2 Interference Effects.....	15
2.2 Free Jet Expansions.....	16
2.3 Nucleation Theory.....	17
2.3.1 Thermodynamic Aspects.....	18
2.3.2 Kinetic Aspects.....	22
2.3.2.1 Cluster Formation.....	22
2.3.2.2 Cluster - Cluster Collisions and Growth.....	23

## TABLE OF CONTENTS (Continued)

	<u>Page</u>
2.3.3 Expansion Conditions for Acetylene.....	24
3. Instrumentation and Techniques.....	28
3.1 CARS System.....	28
3.1.1 Overall Layout.....	28
3.1.2 Nd: Yag Laser.....	28
3.1.3 Dye Laser.....	30
3.1.4 Alignment Procedure for Generating CARS Signal.....	31
3.1.5 Detection System.....	32
3.1.6 Bad Shot Detector.....	33
3.2 Spectroscopic Techniques.....	35
3.2.1 Jet Samples.....	35
3.2.2 Cryostat.....	37
3.2.3 CARS in the Cryostat.....	38
3.2.4 I <sub>2</sub> Calibration.....	41
3.2.5 Spectral Calibration.....	41
4. Equilibrium Phases of Acetylene.....	44
4.1 Introduction.....	44
4.1.1 Background.....	44
4.1.2 This Study.....	44
4.1.3 Bulk Phase Samples.....	46

## TABLE OF CONTENTS (Continued)

	<u>Page</u>
4.2 Data Analysis.....	47
4.2.1 Gas Phase Data.....	47
4.2.2 Data for Bulk Acetylene.....	48
5. Neat Acetylene Clusters.....	54
5.1 Cluster Spectra and Temperatures.....	54
5.1.1 Experimental Conditions.....	54
5.1.2 Monomer Results.....	54
5.1.3 Cluster Results.....	58
5.2 Mean Cluster Size.....	64
5.3 Liquid - Solid Phase Transition.....	67
5.3.1 Isothermal Transition.....	67
5.3.2 Adiabatic Transition.....	69
5.3.3 Crystal Growth Rate Calculation.....	70
5.3.4 Nucleation Rate.....	71
5.3.5 Interfacial Free Energy.....	72
5.3.6 Solid - Solid Interfacial Free Energy.....	76
6. Acetylene Mixes.....	81
6.1 Mix Data.....	81
6.1.1 Experimental Conditions.....	81

## TABLE OF CONTENTS (Continued)

	<u>Page</u>
6.1.2 First Phase Formed for All Conditions.....	82
6.2 Cooling Curves and Phase Transitions.....	93
6.2.1 Adiabatic Nature of Cooling.....	93
6.2.2. Liquid - Solid Interfacial Free Energy.....	93
6.2.3 Solid - Solid Interfacial Free Energy.....	95
6.3 New Features in the Acetylene Spectrum.....	97
6.3.1 1960 cm <sup>-1</sup> Feature.....	87
6.3.2 Assignment of the New Feature as the B <sub>3g</sub> Peak.....	101
6.3.3 Assignment as Surface Layer of Acetylene Clusters.....	101
6.3.4 Cluster Diameter Calculation.....	102
6.3.5 Diffuse Feature near 1963 cm <sup>-1</sup> .....	103
6.4 Discussion.....	106
6.5 Conclusions.....	109
Bibliography.....	111
Appendix.....	115
AI CARS Fitting Program.....	116
AI.1 To Fit a Spectrum.....	116
AI.1.1 CARS Spectra of Neighboring Peaks.....	116
AI.1.2 CARS Spectra Models.....	116
AI.2 The Program.....	117

AI.2.1 Nonlinear Spectra Calculations.....	118
--	-----

## LIST OF FIGURES

<u>Figure</u>	<u>Page</u>
2.1	Energy required to add a monomer to a cluster as a function of cluster radius is calculated for acetylene.....20
2.2	Free energy for addition of acetylene monomers to clusters at varying supersaturation ratios.....21
2.3	The number of collisions per $X/D$ is calculated for clusters of 23 nm diameters and 6 nm diameters.....26
2.4	Isentropic expansions of four of the initial conditions used in these studies are plotted with the coexistence curve for acetylene.....27
3.1	Schematic diagram of the apparatus used for the CARS experiments.....29
3.2	Two S-branch lines of $\text{CO}_2$ are compared at the frequency extremes where shots were considered good.....34
3.3	Evacuated cell into which cold gas is pulsed to produce the supersonic jet expansion.....36
3.4	Cryostat sample holder cell with quartz windows and indium gaskets mounted on a copper body.....39
3.5	Cryogenic cooling stack which was used to prepare the bulk phase samples....40
3.6	Comparison of jet and bulk monomer scans for calibration.....43
4.1	Cubic solid unit cell (shaded molecules are in a separate plane) $a = 6.091 \text{ \AA}$ ....45
4.2	Orthorhombic unit cell (dark molecules are in the plane of the page others are below).....45
4.3	Correlation diagram for acetylene.....45
4.4	CARS spectra of all three condensed phases of acetylene.....51
4.5	Frequency of the $\nu_2$ peak as a function of temperature.....52
4.6	Frequency of the $\nu_2$ peak of liquid acetylene as a function of temperature.....52

## LIST OF FIGURES (Continued)

<u>Figure</u>	<u>Page</u>
4.8	Frequency of the $\nu_2$ peak of cubic solid acetylene as a function of temperature.....53
4.9	Frequency of the $\nu_2$ peak of orthorhombic acetylene as a function of temperature.....53
5.1	Neat acetylene at 233 K and 14 atm produces nearly 80% clustering with liquid acetylene as the dominant phase.....55
5.2	Monomer Q-branch spectra for the first 85 X/D.....56
5.3	Rotational temperature of the monomer is estimated in the jet spectra.....57
5.4	The liquid to cubic solid transition can be seen in clusters very close to the nozzle.....59
5.5	The cubic solid to orthorhombic solid phase transition is seen late in the jet...60
5.6	Temperature of all phases of the clusters are graphed vs. X/D.....63
5.7	Cubic solid temperatures are fit with cooling curves by adjusting final temperature and cluster diameter.....66
5.8	Qualitative plots of the adiabatic and isothermal phase transition models are plotted with the data.....68
5.9	The fraction of clusters frozen $\ln(1-F(t))$ is fit with equation 5.6 using a cluster diameter of 20 nm to give a nucleation rate $J$ of $1.4 \times 10^{29} \text{ m}^{-3}\text{s}^{-1}$ .....73
5.10	The fraction of orthorhombic solid vs. time is plotted and fit with eq. 5.6 to give a rate of $2.8 \times 10^{28} \text{ m}^{-3}\text{s}^{-1}$ .....77
5.11	Interfacial free energy is plotted as a function of supercooling with $\nu = 22 \text{ cm}^{-1}$ , $E = 394 \text{ J/mol}$ and $J = 2.8 \times 10^{28} \text{ m}^{-3}\text{s}^{-1}$ .....80
6.1	50% acetylene in He, 220 K, 7 atm. showing the complete liquid to solid transition in $\sim 18 \text{ nm}$ clusters.....85

## LIST OF FIGURES (Continued)

<u>Figure</u>	<u>Page</u>
6.2	12% acetylene in He, 200 K, 29 atm. showing a large new feature.....86
6.3	12% acetylene in He, 200 K, 27 atm. showing the complete transition from cubic solid to orthorhombic solid, and a new feature at 1960 cm <sup>-1</sup> .....87
6.4	10% acetylene in He, 213 K, 27 atm. showing the complete cubic solid to orthorhombic solid transition.....88
6.5	4% acetylene in He, 185 K, 31 atm. showing a new feature at 1960 cm <sup>-1</sup> .....89
6.6	The first condensed phase of acetylene which is seen depends on the mix and the initial conditions.....92
6.7	Temperature vs. X/D curves for the 50% mix (dashed lines) and the neat (Solid lines) jets, both have the liquid to cubic solid phase transition.....94
6.8	Fraction of clusters frozen in the 50% mix fit with equation 5.6 giving a nucleation rate of $1.8 \times 10^{29} \text{ m}^{-3}\text{s}^{-1}$ .....96
6.9	Cooling curve fit to the cubic temperature data of the 50% mix jet gives an 18 nm diameter for the clusters.....96
6.10	The fraction of orthorhombic solid present vs. Time in a 12% 27 atm. jet is fit with eq. 5.6 to give a nucleation rate of $3.8 \times 10^{31} \text{ m}^{-3}\text{s}^{-1}$ .....99
6.11	The fraction of orthorhombic acetylene present in the 10% 213 K jet are plotted and fit with eq. 5.6 to give a nucleation rate of $1.4 \times 10^{31} \text{ m}^{-3}\text{s}^{-1}$ .....99
6.12	A spectrum from a 12% mix at 29 atm (top) is compared to a similar neat acetylene spectrum.....100
6.13	Cluster sizes are calculated from the surface to volume ratio yielding cluster diameters of around 10 nm.....104
6.14	A graph of a 12% spectrum and two 4% spectra, the latter of which show a broad feature while the former has a narrower surface feature.....105

## LIST OF TABLES

<u>Table</u>	<u>Page</u>
4.1 Bulk acetylene data with $\nu_2$ frequencies and widths for spectra at the recorded temperatures.....	50
5.1 Neat acetylene jet data; frequencies, temperatures, and percentages.....	61
5.2 Physical constants for acetylene.....	65
6.1 Amix: 50% acetylene in He, 220 K, 7 atm.....	83
6.2 Emix: 12% acetylene in He, 200 K, 29 atm.....	83
6.3 Imix: 4% acetylene in He, 185 K, 31 atm.....	83
6.4 Gmix: 12% acetylene in He, 200 K, 27 atm.....	84
6.5 Hmix: 10% acetylene in He, 213 K, 27 atm.....	84
6.6 Percent clustering for acetylene mixes.....	90
6.7 Temperature of acetylene condensed phases.....	91
6.8 Results for all data.....	98
6.9 Interfacial Free Energies.....	108

# Coherent Anti-Stokes Raman Spectroscopy of Acetylene Nanoclusters

## 1 Introduction

### 1.1 Clusters

Over the past decade, coherent anti-Stokes Raman spectroscopy (CARS) has been used in this lab to study simple clusters ranging from two to billions of molecular units. As part of this effort, Kyung Lee carried out a study of acetylene clusters which demonstrated the ability of CARS to distinguish between several different phases in acetylene clusters. Subsequent technical improvements made by Alan Richardson to the cluster spectroscopy system made it possible to do studies similar to Lee's at much higher spectral resolution. It was the aim of this study to use this improved resolution to take the work initiated by Lee further by studying the mechanism and rates of the acetylene phase transitions with a primary goal of determining interfacial energies between phases. This quantity is of interest because it plays a key role in all models of the nucleation process, yet it is very difficult to determine by experimental methods.

#### 1.1.1 Aggregation

In the gas phase, molecules interact only very weakly with other molecules since the separations are very large. In the liquid and solid phases, molecules are held close to

each other by intermolecular forces; and are much more ordered. There is a clear difference between the physical environment of the molecules in the gaseous, liquid and two solid phases, which can be distinguished spectroscopically. A condensing supersonic jet provides a means of creating a sample of many aggregations of small numbers of molecules, called clusters, which can be in gas, liquid, or solid form. Combining this preparation method with CARS allows one to monitor the evolution of these phases and to measure transition rates between them. The jet method of cluster production also permits production of clusters of widely varying sizes.

#### 1.1.2 Small Clusters

The goal of many investigations has been to learn how the molecules interact with each other and arrange themselves when two or three units aggregate. Among others, the E.R. Bernstein group examined the clustering of a number of molecules using mass spectroscopy along with photoionization / fluorescence spectra to characterize cluster vibrations.<sup>1</sup> This group studied the association of aromatic hydrocarbons with rare gases,<sup>2</sup> other small gases<sup>3</sup> and each other to form dimers.<sup>4</sup> Other authors have also examined the association of multiple noble gases atoms with a single aromatic hydrocarbon molecule.<sup>5,6</sup>

The main interest in making small clusters has been to determine how the molecules are oriented. The geometry of HF..N<sub>2</sub>, for example, has been studied by the Nesbitt group.<sup>7</sup> They noticed an extreme red shift in the fundamental stretch when HF was clustered with a single nitrogen.<sup>8</sup> From rotational structure in this band, the geometry was found to be close to a linear arrangement. HF multimers of (2 - 8) units have been

seen as well and, in combination with ab initio computations the structures of these clusters were also determined.<sup>9</sup> As another example, rotational constants of multimers of H<sub>2</sub>O<sup>10</sup> and carbon<sup>11</sup> have been determined through high resolution spectroscopy and used to establish the configurations of the molecules in the clusters. As the number of H<sub>2</sub>O or C units increased, to  $n > 5$ , the spectra become congested. For  $n \geq 6$ , carbon clusters have been shown to be linear<sup>12</sup>, and water clusters have complex orientations involving low energy pseudo-rotations between configurations. The ongoing field of research on such systems provides considerable insight into the intermolecular forces which are present as molecules interact.

### 1.1.3 Large Clusters

Clusters with an even larger number of molecules in them ( $>100$ ) are of interest even though the rotational structure can no longer be resolved. These clusters are more representative of the macroscopic condensed phases of molecules, and one is limited to vibrational spectroscopic measurements. For example, the internal vibrations of carbon dioxide have been studied for clusters in this size range by our group at OSU using CARS. For CO<sub>2</sub>, it has been possible to observe the low frequency external librational modes in crystalline clusters<sup>13</sup>. With clusters of moderate size, a significant fraction of the molecules are on the surface of the cluster and one might hope to spectroscopically distinguish these molecules from the bulk. Indeed, for CO<sub>2</sub> clusters, such surface molecules are seen to have a unique peak in the CARS spectrum<sup>14</sup>. Surface features have

also been seen on clusters coated by molecules of a different type, for example Scoles has done work with SF<sub>6</sub> deposited on the surface of noble gas clusters<sup>15</sup>.

#### 1.1.4 Very Large Clusters (n > 10,000)

Very large clusters can be used to study the bulk phase properties and phase transitions of the liquids and solids. This is an effective way of studying homogeneous phase transitions because clusters can have very few impurities per sample and they do not have containing walls to initiate heterogeneous phase transitions. Previous OSU work has shown that large nitrogen<sup>16,17</sup> and acetylene<sup>18</sup> clusters exhibit phase transitions upon cooling in supersonic jets. Bartell has also done extensive work in this area using electron diffraction methods. Both types of studies have proven to be particularly useful in measuring phase changes of clusters cooled in molecular beams.<sup>19</sup> These techniques are sensitive to the phases present in the sample, and both can be used to measure factors which govern the nucleation process in clusters.<sup>20</sup> Energies involved in the nucleation and growth processes have been determined by the diffraction method<sup>21</sup> and it has also been used to show that the phase transition between liquid and solid phase is an adiabatic event<sup>22</sup>. The latter observation was in part motivational for this work.

## 1.2 Methods of Studying Clusters

### 1.2.1 Preparation of Samples

Small clusters has been formed in a vapor cell by rapidly cooling a sample of gas in a long path length chamber<sup>23</sup>. Another technique, called the enclosive flow cooling method, employs a vertical cell in which warm gas is flowed into a cold background gas where it nucleates and forms droplets.<sup>24</sup> However, in most cluster studies, and in our work, clusters are formed during the cooling that occurs on expanding a high pressure gas out of a nozzle into a vacuum. Studies of nozzle types have been done to determine the shape of the nozzle which produces the most efficient clustering conditions.<sup>25</sup> To form the smallest clusters, expansions are done at high nozzle temperatures and low driving pressures. For studies using infrared absorption spectroscopy, the nozzle openings are typically slits<sup>10</sup> of 2 cm - 10 cm in length, which are needed to give a long sample path length. It is also possible to deposit molecules on the surface of clusters, for example Scoles devised a pickup method in which an effusive jet of SF<sub>6</sub> molecules was used to coat cold Ar core clusters formed in a supersonic jet.<sup>26</sup>

### 1.2.2 Spectroscopies

Mass spectroscopy has been one of the major techniques used for cluster studies in the last 15 years. It is usually combined with some selective method of ionization. Two-color resonant ionization has been used with time-of-flight mass spectroscopy for many studies<sup>2</sup>. Often, optical forms of spectroscopy are combined with mass spectroscopy.

Infrared laser spectroscopy combined with quadrupole mass spectroscopy was used to study ethylene clusters<sup>27</sup>. Electron diffraction has proven to be a useful technique in determining the phase of larger clusters<sup>28,29</sup>. Most optical studies have focused on smaller clusters. Laser induced fluorescence spectroscopy has provided a simple and sensitive technique for probing clusters which emit light after they absorb a photon<sup>30</sup>. Fluorescence spectroscopy can be done at high resolution which is well suited for the study of rotations in small clusters. Hole burning spectroscopy has also been used as a means of examining small clusters<sup>31,32</sup>. This technique was shown to be useful in distinguishing between isomers of clusters, which was not previously possible in electronic mass selection spectroscopy. Direct absorption microwave spectroscopy has been used to view some clusters, including Ar - HCN and (HCN)<sub>2</sub><sup>33</sup>, and also C<sub>n</sub>O clusters<sup>34</sup>.

Infrared absorption is by far the most widely used technique of absorption spectroscopy. Far IR lasers are used to probe the low frequency spectra of clusters with high resolution and the results have been used as a basis for interpreting astronomical far IR spectra of cold molecules in space<sup>35</sup>. The spectral range of these IR lasers is quite limited however, and Fourier transform IR spectroscopy provides a method of viewing clusters with high resolution over larger spectral ranges<sup>36</sup>. Advances in the technique of IR absorption have been applied to a number of systems by Scoles. The bolometric detection of laser-dissociated molecules has allowed very sensitive detection of low density samples, particularly of SF<sub>6</sub> molecules which have been coated onto the surface of noble gas clusters<sup>37</sup>. Often, frequency-differencing techniques are used with a narrow line width ion laser, and a tunable ring dye laser to produce IR laser light which is tunable and

of high resolution<sup>38</sup>. These laser systems or IR diode laser systems are typically employed with a pulsed slit nozzle in a multipass spectrometer to increase the distance of interaction.<sup>39</sup>

Nonlinear laser techniques are used in a few labs, including ours at OSU. Techniques such as Coherent Anti-Stokes Raman Spectroscopy (CARS) and Coherent Stimulated Raman Scattering (CSRS) have been shown to be useful in studying Raman active vibrations in larger clusters<sup>40,41</sup>. These methods permit studies of clusters at a resolution of  $\sim 0.007 \text{ cm}^{-1}$  or better<sup>42</sup>. Following the evolution of clusters in a jet is a unique capability of these point-probing techniques. The small overlap region of crossed, focused laser beams allows one to pinpoint a region for study in an expanding jet<sup>17</sup> whereas most multipass absorption methods sample large volumes.

### 1.3 This Cluster Study

Some previous work on acetylene was done in this lab by Lee<sup>43</sup>, who studied the production and low resolution spectroscopy of the three condensed phases present in acetylene expansions. The present work uses a higher resolution system to do an in-depth study of the phase transitions of such acetylene expansions. The objective was to determine the interfacial free energies of the liquid and solid phases, a physical quantity that is very hard to measure. The interfacial free energy of the cubic solid and orthorhombic solid was also of interest. A model of nucleation and propagation rates in the phase transition provides a means of calculating the interfacial energies. As part of this

work, sizes of clusters are determined by methods previously used and also with new Rayleigh scattering techniques. Finally, we have noted new spectral features of acetylene in extremely small clusters, features not seen in any known bulk phase. These new features are thought to be due to surface layers and or metastable structures that exist only for small clusters. These various aspects of this thesis work will be discussed in the following chapters.

## 2. Background

### 2.1 Raman Scattering

#### 2.1.1 CARS Amplitude Expression

As part of the analysis of CARS spectra done with this work, the peak intensities and areas are used to determine the number of molecules which contribute to a signal.

The following is a development after that of Tolles and Harvey<sup>44</sup> of the intensity expression for CARS as a function of the polarizability and the number of molecules.

The polarization  $P$  of a molecule can be expressed as a power series in the electric field  $E$

$$P = \chi^{(1)} \cdot E + \chi^{(2)} \cdot E_1 E_2 + \chi^{(3)} \cdot E_1 E_2 E_3 + \dots \quad (2.1)$$

The first order coefficient  $\chi^{(1)}$  is responsible for linear phenomena such as infrared absorption and Raman scattering. The second order susceptibility is important in summing and differencing of the frequencies of two incident light photons by non isotropically ordered media as shown by Shen et al.<sup>45</sup> This second order interaction is used to probe surfaces where molecules arrange in such a fashion that there is no local bulk inversion symmetry. A second order effect will become identically zero if the medium has inversion symmetry, because every sum or difference produced will have a complimentary beam produced  $180^\circ$  out of phase, thereby producing complete cancellation. Thus it can be

ignored for isotropic media like gases and liquids. The  $\chi^3$  term is the lowest order non-linear term in the expansion which can generate a signal from bulk, randomly arranged samples and it is the term of interest in the development of CARS.

At time  $t$ , the net electric field on a sample can be represented as a sum of components of frequencies  $\omega_m$  propagating in the  $z$  direction with wave vectors  $k_m = \omega_m n_m / c$ .

$$E(z, t) = \sum [ 1/2 E_m(\omega_m, z) (\cos\theta_m i + e^{i\phi} \sin\theta_m j) e^{i(\omega_m t + k_m z)} ] \quad (2.2)$$

Here  $\theta_m$  is the angle the plane of polarization makes with the  $x$  axis or the  $i$  vector  $\phi$  measures the ellipticity of the polarization and  $E_m$  is the amplitude of frequency component  $m$ . We examine the polarization vector which is produced by three vertically polarized incident waves as used in CARS, where  $\omega_3 = 2\omega_1 - \omega_2$  is

$$P(\omega_3) = 1/8 [ (\chi^{(3)}_{1111})^2 E_1^2 E_2 e^{i(2k_1 - k_2)z - (2\omega_1 - \omega_2)t} + \text{c.c.} ] \quad (2.3)$$

Here c.c. indicates the complex conjugate of the first term. This coherent anti-Stokes Raman polarization results from Raman pumping a level at the beat frequency  $\omega_1 - \omega_2$  so as to generate an anti-Stokes signal at  $\omega_1 - \omega_2 + \omega_1 = \omega_3$ . The connection to the molecule is the complex 4<sup>th</sup> rank tensor  $\chi^3$ , which can be broken into frequency dependent (resonant) and independent (non-resonant) parts

$$\chi^{(3)} = \chi^{nr} + \chi^{rs}. \quad (2.4)$$

The non-resonant contribution is usually minimal compared to the resonant signal and can be considered a constant background.

An expression for  $\chi$  can be derived classically, or quantum mechanically. Placzek's development, as described by Tolles<sup>46</sup>, will be used here. This model starts by assuming the linear polarizability  $\alpha$  can be expressed in a power series in the molecular coordinate  $q$ .

$$\alpha = \alpha_0 + (d\alpha/dq)_0 q + \dots \quad (2.5)$$

A resulting force on the oscillator is produced by an oscillating electric field  $E$  interacting with the dipole ( $\alpha E$ ) which the field induces in the molecule.

$$F = 1/2 (d\alpha/dq)_0 E^2 \quad (2.6)$$

The motion of the electron cloud with respect to vibrational coordinate  $q$  can be described as a damped harmonic oscillator of effective mass  $m$ . When the driving force due to the field is added to 2.6, one obtains the equation of motion

$$(d^2q/dt^2) + \Gamma(dq/dt) + \omega^2 q - 1/2m (d\alpha/dq)_0 E^2 = 0 \quad (2.7)$$

For simplicity's sake, we consider the condition for the  $\chi_{1111}$  susceptibility tensor element in which one constrains the polarizations of all the fields to one direction. This gives the largest signal experimentally, and it simplifies the electric field expression in eq. 2.2 since  $\cos\theta = 1$  and  $\sin\theta = 0$ . Also, if we assume that the fields are all linearly polarized, the  $\sin\phi$  term is 0. This leads to the simplified expression for the electric field

$$E_i(\omega_i) = 1/2[A_i e^{i(kz - \omega t)} + \text{c.c.}] \quad (2.8)$$

Substituting this into eq 2.6, there arise three components, two at  $2\omega_1$  and  $\omega_1 + \omega_2$  which are representative of non-resonant scattering, and one

$$E^2(\omega, t) = 1/4 [E_1 E_2 e^{i(\omega_1 - \omega_2)t} + \text{c.c.}] \quad (2.9)$$

which is responsible for driving the transition at  $\omega_1 - \omega_2$ . Substituting eq 2.6 into eq. 2.7, we can solve for  $q$ , yielding

$$q = 1/8m (d\alpha/dq)_0 \{E_1 E_2 e^{i(\omega_1 - \omega_2)t} / [\omega_v^2 - (\omega_1 - \omega_2)^2 + i\Gamma(\omega_1 - \omega_2)]\} + \text{c.c.} \quad (2.10)$$

Noting that the oscillator is driven at  $\omega_1 - \omega_2$ ,  $P$  from equation 2.3 is given by

$$P = \chi E = N(d\alpha/dq)_0 q (\omega_1 - \omega_2) E \quad (2.11)$$

where  $N$  is molecular density or population of a pumped state. The susceptibility can be described by substituting the value for  $q(\omega_1 - \omega_2)$  from equation 2.10 onto 2.11 giving

$$3\chi(\omega_3) = N/m(d\alpha/dq)_0^2 [1/(\omega_v^2 - (\omega_1 - \omega_2)^2 - i\Gamma(\omega_1 - \omega_2))] \quad (2.12)$$

Using the definition for the Raman scattering cross section of a molecule in a radiation field,

$$(d\sigma/d\omega) = (\hbar/2m\omega_v) (d\alpha/dq)_0^2 (\omega^4/c) \quad (2.13)$$

the susceptibility can be described in terms of the cross section  $(d\sigma/d\Omega)$ , vibrational transition frequency  $\omega_v$ , laser frequencies  $\omega_1$  and  $\omega_2$ , and molecular populations  $N$  as

$$\chi^{(3)} = (2Nc^4/\hbar\omega_v^4)(d\sigma/d\Omega) [\omega_v/(\omega_v^2 - (\omega_1 - \omega_2)^2 - i\Gamma(\omega_1 - \omega_2))] \quad (2.14)$$

From this the resonance condition occurs when  $|\omega_1 - \omega_2| = \omega_v$ , i.e. the denominator goes to  $-i\Gamma(\omega_1 - \omega_2)$ , which maximizes  $\chi^{(3)}$ . Intensities of the resultant beam at  $\omega_3$  are a function of  $|\chi^{(3)}|^2$  and therefore a function of the square of the population, since  $\chi^{(3)} \propto N$ . For relatively small changes in the field strength and population the intensity can be described by

$$I = (4\pi^2\omega_3/c^2)^2 I_1^2 I_2 |\chi^{(3)}|^2 z^2 \quad (2.15)$$

where  $z$  is the distance of interaction and  $I_i$  is the intensity of the beam of frequency  $\omega_i$ .

Each peak has a width and intensity associated with it, as indicated in the expression

$$\chi = B\omega_v / [\omega_v^2 - (\omega_1 - \omega_2)^2 - \Gamma(\omega_1 - \omega_2)] \quad (2.16)$$

where  $B$  is a set of constants including real and imaginary parts which include populations, scattering cross sections, and other fundamental constants mentioned earlier,  $\omega_v$  is the vibrational frequency of the Raman transitions, and  $\omega_1$ ,  $\omega_2$ , and  $\Gamma$  are pump frequency, probe frequency and HWHM line width, respectively. This is only the resonant portion of the susceptibility; there is also the addition of a purely real non-resonant part which effects the line shapes.

In the case of a single resonant transition, the real  $\chi'$ , non-resonant  $\chi^{nr}$ , and imaginary  $\chi''$  parts of the susceptibility equations combine to give

$$\chi = \chi' + \chi^{nr} + i\chi'' \quad (2.17)$$

and the CARS signal is proportional to

$$|\chi|^2 = (\chi' + \chi^{nr})^2 + (\chi'')^2 \quad (2.18)$$

This yields a total line shape for the CARS signal which is a simple addition of the squares of the susceptibilities as has been shown by Tolles et al.<sup>46</sup>

### 2.1.2 Interference Effects

The CARS spectrum of a system involving two close peaks requires consideration of interference between the peaks. This is applicable in regions where there are two coexisting phases of acetylene, as previously viewed by Lee<sup>43</sup> and as found with the present work. Two close peaks will contribute to a total susceptibility, in a non-linear way due to the squared dependence of the signal intensity on the total susceptibility leading to the expression

$$|\chi|^2 = (\chi_1' + \chi_2' + \chi^{nr})^2 + (\chi_1'' + \chi_2'')^2 \quad (2.19)$$

Multiplying through gives

$$|\chi|^2 = (\chi_1'^2 + \chi_2'^2) + (\chi_1''^2 + \chi_2''^2) + (2\chi_1'\chi_2' + 2\chi_1''\chi_2'') + (2\chi_1'\chi^{nr} + 2\chi_2'\chi^{nr} + \chi^{nr2}) \quad (2.20)$$

which produces the last two cross term groupings which wouldn't appear from simple addition of the independent  $\chi^2$  terms. The effect is to produce peak shifts and line asymmetries which will turn out to be an important consideration in deducing accurate resonant frequencies. This matter is addressed in a program presented in appendix 1 which yields true resonance frequencies for spectra with closely positioned peaks.

## 2.2 Free Jet Expansions

Samples examined in this work were in both bulk and clustered states. Bulk samples were generated in a cryostat in which a gas was condensed to the appropriate phase between quartz windows to allow optical probing by CARS. Cluster samples were generated in a free jet expansion where cooling, nucleation, and condensation occur during rapid expansion of gas into a vacuum. Free jets are made by expanding a gas from a high pressure reservoir through a small nozzle into a vacuum chamber. Initial temperature and pressure of the sample are critical in determining the initial products of the abrupt expansion.

One of the main features of the free jet is the cooling that occurs as molecules travel through the jet. This is achieved through flow work being done on the gas because, as the gas expands, its velocity increases. The change in enthalpy per unit mass can be directly related to the change in velocity through the relation

$$v^2 = 2(H_0 - H) = 2C_p(T_0 - T) \quad (2.21)$$

which is for an ideal gas with constant  $C_p$  over the temperature range of interest. The velocity can be related to the mach number  $M$  by  $M = v/(\gamma RT/W)^{1/2}$  using  $W$  for molecular mass and  $\gamma=C_p/C_v$  for the heat capacity ratio. The mach number is a useful parameter to characterize the expansion as a function of position, defined in units of  $X/D$ . Here,  $X$  is distance from the nozzle and  $D$  is the diameter of the nozzle. The mach number increases

as  $X/D$  increases. Empirical expressions for  $M$  as a function of  $\gamma$  are given by Miller et. al.<sup>47</sup> and are derived from measurements of very large continuously-flowing jets.

Quantities of interest are temperature, pressure and density, all of which can be shown to be simple

$$\frac{T}{T_0} = \left(1 + \frac{\gamma - 1}{2} M^2\right)^{-1} \quad V = \left(\frac{\gamma R T_0}{W}\right)^{\frac{1}{2}} \cdot \left(1 + \frac{\gamma - 1}{2} M^2\right)^{-\frac{1}{2}} \cdot M \quad (2.22)$$

$$\frac{P}{P_0} = \left(\frac{T}{T_0}\right)^{\frac{\gamma}{\gamma - 1}} \quad \frac{\rho}{\rho_0} = \left(\frac{T}{T_0}\right)^{\frac{1}{\gamma - 1}}$$

functions of  $M$  and  $\gamma$  (eq. 2.22). From these, it is found that temperature, pressure and density all drop quickly as one probes along the center line of the expansion, while velocity and mach number values increase. The rapid temperature drop is the phenomenon of greatest interest, since as the thermal energy of individual molecules lowers, dipole and Van der Waals interactions cause molecules to stick together. The onset of this nucleation phenomenon is a function of the free energy of the system.

### 2.3 Nucleation Theory

The nucleation of molecules can be assessed using either a thermodynamic or kinetic model. J. E. McDonald<sup>48,49</sup> considered both methods and his treatment be outlined

here. The nucleation process is assumed to be homogeneous in nature, and to apply at near equilibrium conditions. For a non equilibrium jet expansion, effective local temperatures and pressures are defined by position in the jet as described in the last section. It should be noted, however, that condensing jet properties are slightly different from those of a free jet, which assumes only monomers, so that no account of the heat of condensation due to clustering is taken into account. For the discussion here, we consider a homogeneous neat sample with a negligible amount of condensation but in later modeling of cooling curves, condensation is treated explicitly after the manner described by Richardson.

### 2.3.1 Thermodynamic Aspects

The quantity of interest when calculating nucleation properties of a system from a thermodynamic point of view is the system free energy. As with all chemical reactions, a favorable (negative)  $\Delta G$  must exist for the condensation reaction to proceed. In the nucleation case,  $\Delta G$  is a function of cluster radius  $r$ , surface tension  $\sigma$ , density of the condensed phase  $\rho$ , and the supersaturation ratio  $S$ .

$$S = p/p' \quad (2.23)$$

where  $p$  is the gas pressure and  $p'$  is defined as the cluster vapor pressure at a particular temperature. For a supersaturation ratio  $S > 1$ , condensation will occur.  $\Delta G$  is the difference between the surface energy and the bulk free energy. When the bulk energy

overcomes the surface energy, molecules will tend to aggregate, increasing the cluster radius  $r$ . Since an increase in  $r$  comes from an increase in number of molecules, the bulk energy will be increased faster than surface energy with addition of molecules. This makes it favorable to add molecules. The expression for  $\Delta G$  is simply a surface ( $r^2$ ) term minus a volume term,

$$\Delta G = 4\pi r^2 \sigma - (4/3)\pi r^3 \rho RT \ln S. \quad (2.24)$$

Here  $\sigma$  is the surface tension,  $\rho$  is the density of the solid, and  $r$  is the radius of the cluster. A plot of  $\Delta G$  as a function of  $r$  for  $S = 2$  is shown in fig 2.1. This clearly shows that for small  $r$  it is unfavorable to add molecules (increase  $r$ ). The case where  $S = 1$ , shown in fig. 2.2 in a graph of  $\Delta G$  as a function of number of molecules for varying  $S$ , displays a continual rise in the free energy as radius increases, which is expected for a non-supersaturated gas. For  $S > 1$ , there is a maximum of the energy of the system for a particular radius  $r^*$  which is dependent on  $S$ . This maximum corresponds to the point at which the free energy starts to decrease with addition of monomers to the cluster. This point defines the critical radius

$$r^* = 2\sigma/\rho RT \ln S \quad (2.25)$$

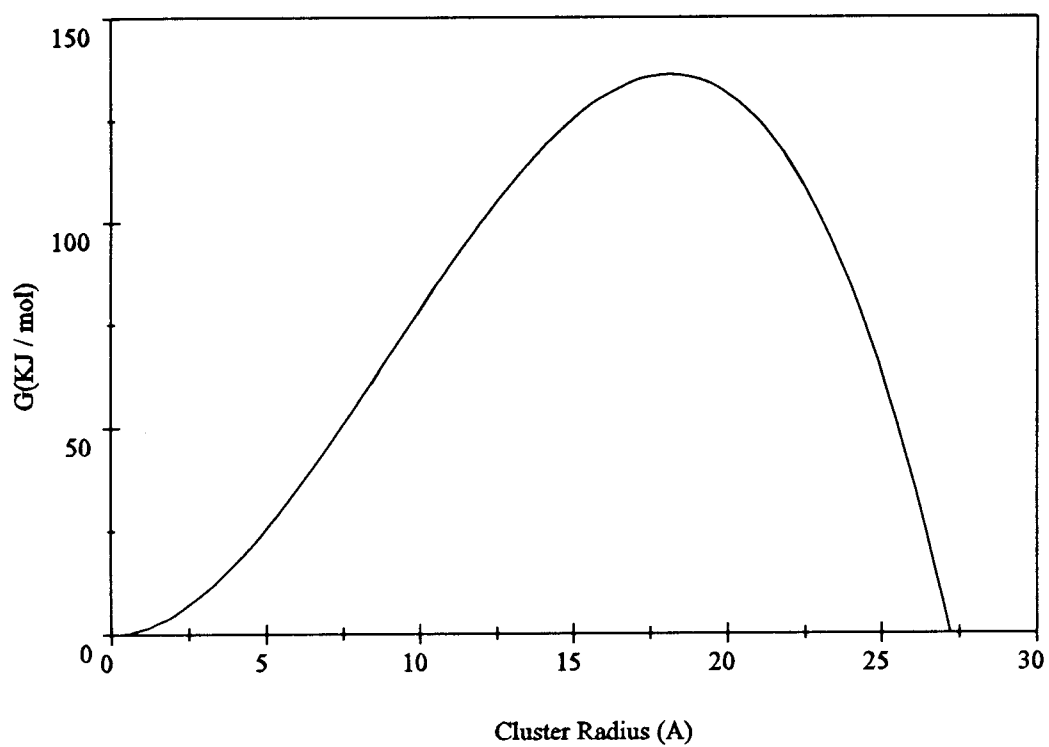


Fig. 2.1 Energy required to add a monomer to a cluster as a function of cluster radius is calculated for acetylene. A value of  $S = 2$  is assumed.

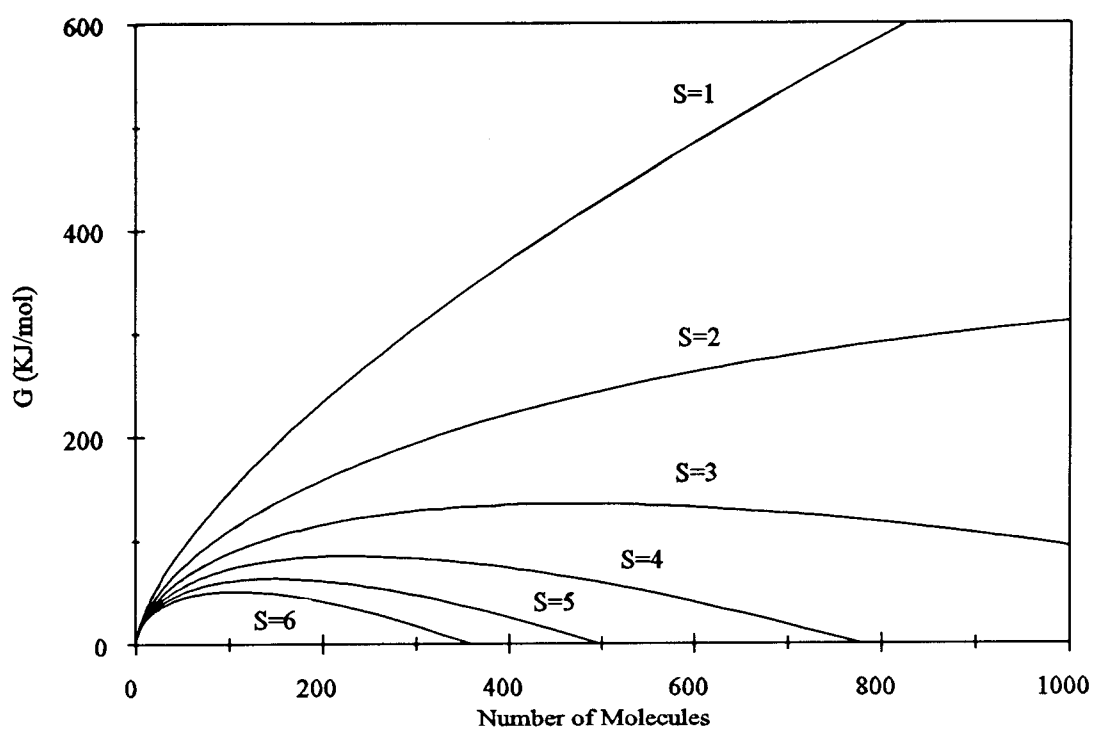


Fig. 2.2 Free energy for addition of acetylene monomers to clusters at varying supersaturation conditions.

When the system achieves a population of clusters with radii greater than  $r^*$ , fast growth occurs for the clusters because it is favorable to add more monomers.

Substituting  $r^*$  into the free energy equation gives

$$\Delta G^* = 16\pi\sigma^3/3(\rho RT \ln S) = 4\pi r^{*2}\sigma/3 \quad (2.26)$$

This shows that raising  $S$  will lower  $\Delta G^*$ , which makes sense, because increasing the supersaturation ratio should make it energetically easier to form clusters. Large values of  $S$  can be obtained experimentally by raising source pressure and or lowering the temperature of the jet expansion gas to achieve condensing conditions.

### 2.3.2 Kinetic Aspects

#### 2.3.2.1 *Cluster Formation*

If we consider clusters as spherical objects of radius  $r$  in a sample of gas which has a density  $\rho$  and a mean molecular velocity  $v = (2\pi mkT)^{1/2}$ , the collision rate of gas molecules onto clusters is

$$R = 4\pi r^2 \rho v \quad (2.27)$$

If a fraction  $q$  of the impacting monomers stick, the condensation rate would be

$$C = 4\pi r^2 q p / (2\pi m k_B T)^{1/2} \quad (2.28)$$

for a system of molecules with mass  $m$  and vapor pressure  $p$  at a temperature  $T$ . The condensation rate for clusters with the critical radius is found to be

$$C^* = 4\pi 4\sigma^2 q p / (2\pi m k_B T)^{1/2} (\rho R T \ln S)^2 \quad (2.29)$$

if the critical radius  $r^*$  (eq. 2.25) is inserted. The rate of escape  $E$  is equal to the critical condensation rate if the radius is exactly  $r^*$ , i.e. there is neither energy gain nor loss for adding or subtracting units at this point. The evaporation to condensation rate ratio for any value of  $S > 1$  is

$$E/C = S^{(r^*-r)/r} \quad (2.30)$$

The radius  $r$  is related to the number of molecules  $g$  in the cluster by  $4/3\pi r^3 \rho = g$ .

### 2.3.2.2 Cluster - Cluster Collisions and Growth

Just as monomer collisions from the last section contribute to cluster growth, cluster - cluster collisions could have an impact on the growth of clusters. A calculation of the number of collisions in the jet was done using gas kinetic theory. Monomer - monomer, monomer - cluster, and cluster - cluster collision rates were calculated from

$$z_{12} = (\rho_1 \rho_2) / (\rho_1 + \rho_2) \pi (1/2(d_1 + d_2)^2) (8RT/\mu\pi)^{1/2}. \quad (2.31)$$

Cluster diameters of both 23 and 6 nm were used, because those are typical values deduced in some of our expansions of acetylene. A graph of  $z_{12}$  (fig. 2.3) shows that cluster - cluster collisions occur, on the average, at a rate of less than one per X/D unit. Since only a fraction results in coalescence, we make the assumption that cluster growth is due solely to the addition of monomers, and not to cluster - cluster collisions.

### 2.3.3 Expansion Conditions for Acetylene

It is useful to examine the relation of temperature and pressure of an expansion mixture, plotted on a graph of log P vs. log T along with the vapor - liquid - solid coexistence curve to generate a picture of the saturation condition of the expanding jet<sup>43</sup>. The conditions for four expansions are included in fig. 2.4. The straight lines are the isentropic expansions of the gas which are derived from  $P/P_0 = (T/T_0)^{C_p/R}$ , assuming a constant heat capacity of the gas. It is interesting to note that the neat expansion trace starts in the region of supersaturated gas on this graph, indicating that condensation could have occurred prior to expanding the gas out of the nozzle. However the conditions of the expansion revealed by the CARS spectra show that there is a significant amount of monomer present and we believe fig. 2.4 cannot be taken too literally. In particular, the temperature of the gas at the nozzle will be somewhat higher than the thermocouple indicates due to resistive heating in the nozzle solenoid and heat being transferred through the body of the vacuum cell. An increase in temperature of 30 K, or a decrease of 100 psi

in initial pressure, would put the line on the vapor side of the coexistence curve.

Moreover one can imagine that even if the initial expansion contains small liquid droplets, the jet properties would not be significantly altered in the later jet. In both the case of liquid being sprayed out and the case of highly nucleating jets significant condensation occurs in the expansion, and in both cases one has clusters going through later liquid - solid and solid- solid phase transitions.

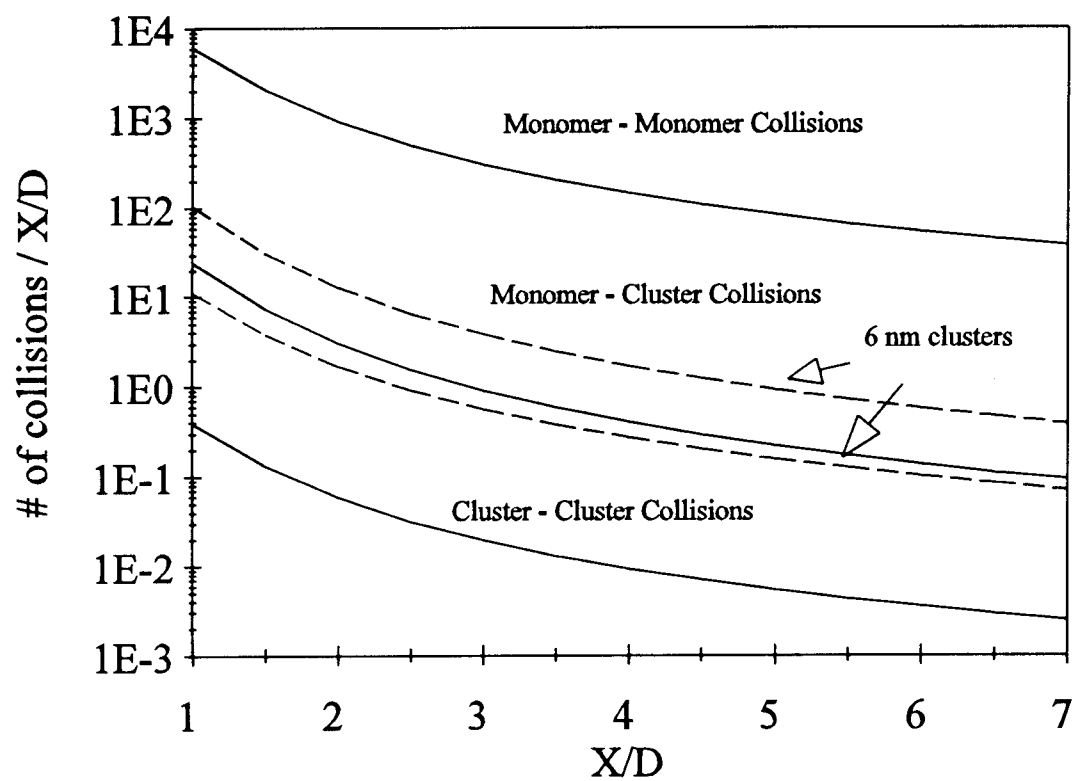


Fig. 2.3 The number of collisions per  $X/D$  is calculated for clusters of 23 nm diameters and 6 nm (dashed lines) diameters. The sample is assumed to be 80% condensed phase.

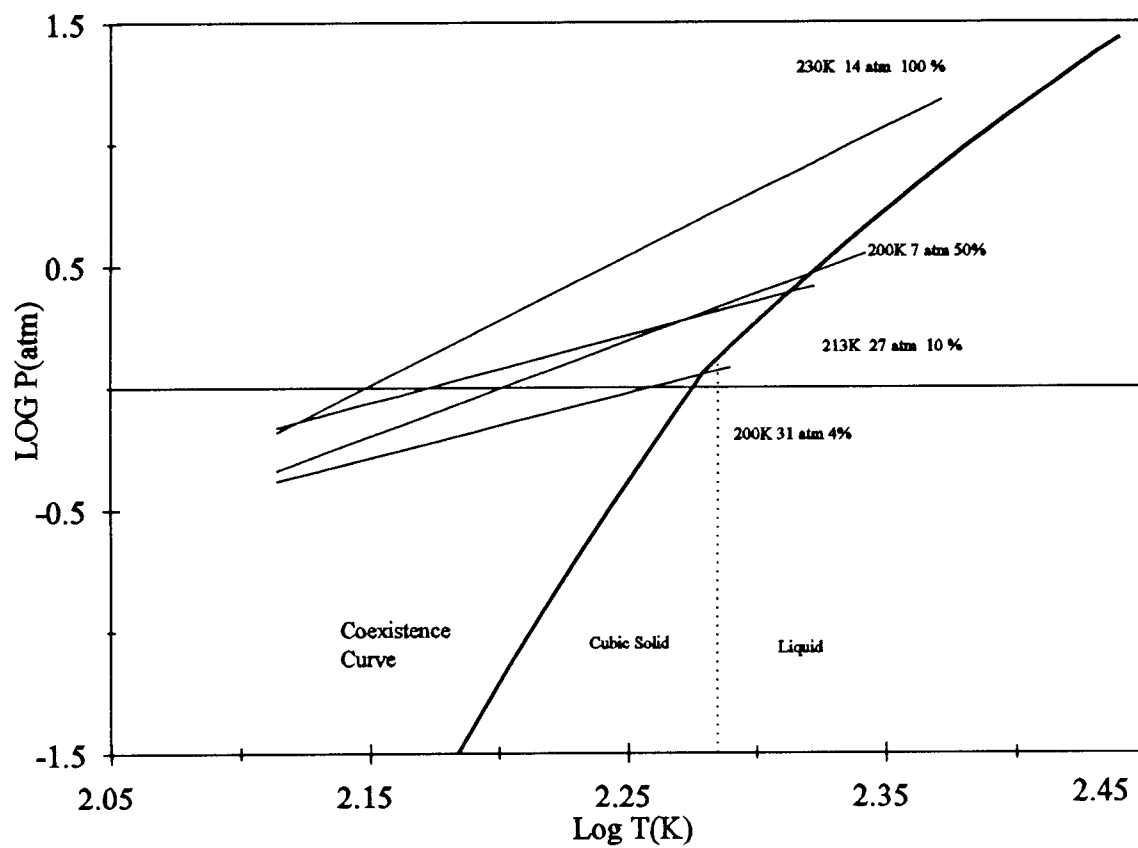


Fig. 2.4 Isentropic expansions of four of the initial conditions used in these studies are plotted with the coexistence curve for acetylene.

## 3. Instrumentation and Techniques

### 3.1 CARS System

#### 3.1.1 Overall Layout

The experimental results described in this thesis were obtained on the CARS system shown in figure 3.1. The elements in this diagram will be described in some detail below.

#### 3.1.2 Nd:YAG Laser

The primary laser is a "seeded" Quanta Ray DCR-1A Nd:YAG laser which produces a pulsed 1064 nm infrared beam at 10 Hz. A Lightwave Electronics S-100 infrared diode laser pumps a monolithic Nd:YAG crystal to give cw single frequency "seed" light of about 2 mW. This output is injected into the oscillator cavity of the pulsed YAG laser to produce single mode operation. Pulses are generated with a spectral width of about  $0.003 \text{ cm}^{-1}$ . Pulses are about 8 ns in duration as measured using photodiodes with response times of 1 ns. The laser has trigger outputs which can be accessed for timing of the detection system.

The 1064 nm output from the laser is doubled using a 97% deuterated KDP crystal. The resulting 532 nm beam is separated from the infrared pulse using a Pellin-Broca prism. The separated IR beam is then dumped immediately for safety. The green beam (which is on the order of 100 mJ/pulse) is divided by a beam splitter, with 2/3 used

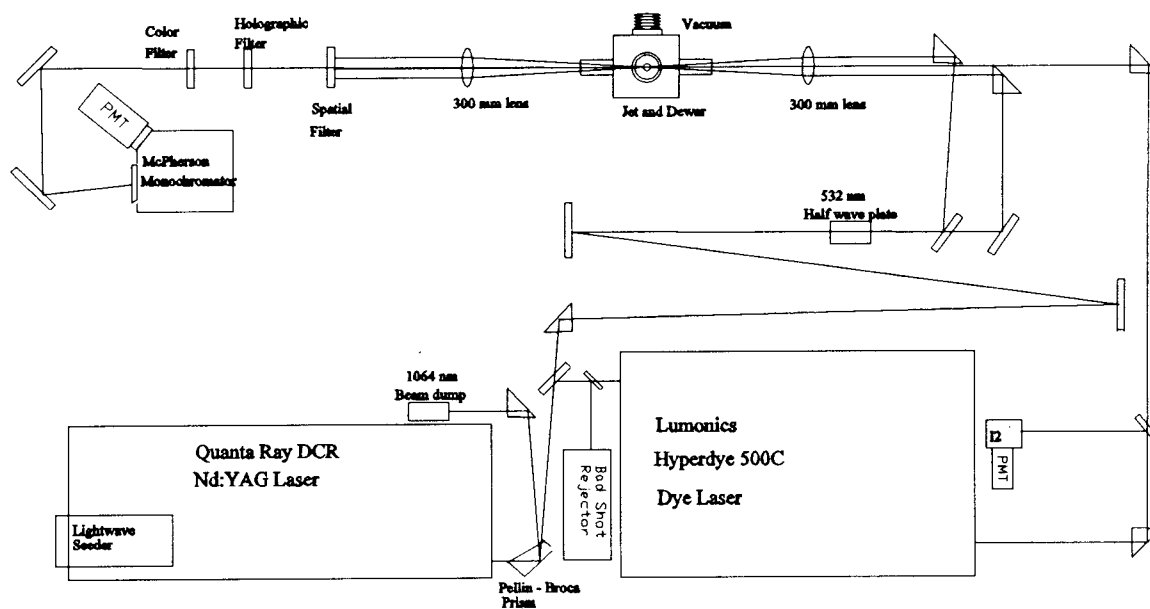


Fig. 3.1 Schematic diagram of the apparatus used for the CARS experiments.

to pump a Lumonics Hyperdye-500 tunable dye laser. The remaining light is steered through a time-delay path which is adjusted to provide temporal overlap of the green Nd:YAG beams with the lower frequency dye beam. A rotatable 532 nm half wave plate is used to assure vertical polarization of the Nd:YAG beams. This half wave plate can be adjusted with a sample in place to achieve a maximum signal, thus assuring optimum polarization conditions. After the half wave plate, the beam is split by a 50% reflecting dichroic mirror to achieve the so-called folded BOXCARS geometry. The beams are turned by prisms on a micrometer stage, allowing fine tuning in spatial overlap. Typically this is done while a sample is in place to optimize the signal.

### 3.1.3 Dye Laser

The Lumonics Hyperdye-500 is a tunable dye laser which uses a grating in the oscillator cavity to scan frequencies. The grating is a 2400 grooves / mm holographic grating which is run in 5th order to achieve line widths on the order of  $0.04 \text{ cm}^{-1}$ . This is greater than the  $0.002 \text{ cm}^{-1}$  resolution which the stepper motor is capable of producing. The 532 nm pump beam is introduced through a half wave plate which is adjustable to give vertical polarization, which is necessary for optimum dye efficiency. This is done by measuring the power output of the dye laser while tuning the half wave plate for maximum power.

The initial dye laser beam is produced by pumping of an oscillator cavity by the Nd:YAG pump beam. The resultant oscillator output is passed through a telescope which expands and steers the beam to fill the amplifier. Amplification is achieved by pumping a

Bethune cell amplifier. This is an amplification stage which is used for the efficient use of the pump beam and good beam quality which results from uniform illumination of the dye by the pump beam. Typically, a 10 mJ/pulse dye output can be produced. This value is dependent on the dye used and the frequency of the laser with relation to the power curve of the dye.

#### 3.1.4 Alignment Procedure for Generating CARS Signal

Beams from the YAG and dye lasers are passed through the region where the sample will be located. The temporal profiles of the beams are then measured with a photodiode. Typically, the dye laser output is generated with a time delay with respect to the input pulse. This delay can be seen as the difference in arrival times of the two YAG beams and the dye beam. This difference is typically 7-8 ns. Accordingly, an optical delay of the 532 nm beam about 2 m is used to achieve maximum overlap. Once the beams are coincident in time, the system must be set to have all beams focusing on the point of the sample. The 532 nm beams are focused through a 300 mm lens onto the sample. The dye beams will focus at a different position from that of the 532 nm beam because of the difference in frequency and the achromatic nature of the lens. To compensate for this, a telescope is used in the dye beam so that the divergence can be adjusted to focus it at the same point as the 532 nm beams. Once a common focal point has been established, the beams can be spatially overlapped. The overlap is done through drilling a pinhole in a brass sheet with the dye laser. This pinhole is used as a guide for the 532 beam (initially reduced in intensity to prevent drilling a new hole) which is steered to go through the hole.

Once all temporal, focal, and spatial overlapping has been achieved, a sample is introduced. Initially, a known static sample gas is used to generate a CARS signal to allow further alignment of the beams spatially. Typically, a sample is chosen for alignment whose transition is known to be close to the transition in the sample being studied. This keeps the experimenter from having to change dyes after the alignment is completed.

### 3.1.5 Detection System

Anti-Stokes beams generated in the folded BOXCARS geometry are spatially separated from the pump and probe beams. This spatial separation allows one to direct the blue light through an aperture to discriminate it from green pump and orange probe beams. A holographic filter for the 532 nm light is employed after this spatial filter to further reduce any remaining green light. Colored filters (usually Corning glass 5-57 and/or 5-60) may also be used if the amount of background from the dye laser is limiting the instrumental sensitivity. The signal is sent into a McPherson single grating monochromator after the filtering stage. Photons are detected by an RCA 31034 photomultiplier operated at a voltage ranging from 1000 to 1750 V. Output is sent to SRS SR250 gated integrators, and the integrated signal is digitized with a Scientific Solutions Lab Master A/D conversion board. Data acquisition and dye laser control are achieved through the interface with a Tangent 80386 computer using software that was written primarily by A. Richardson<sup>50</sup>.

### 3.1.6 Bad Shot Detector

To ensure the pump frequency stability and to improve the CARS signal to noise ratio, use was made of a bad shot rejector which was built at OSU for the purpose of detecting laser shots that are not seeded and are multi- mode. The basic construction of the bad shot detector is a pair of photodiodes that monitor two small reflections of the 532 nm laser beam. One beam is sent through an iodine cell, and the other is not. The frequency of the seeder is set so that it produces light that, when frequency doubled, lies on a strong iodine absorption line. The detectors differentiate between the light levels of the two beams. If the laser is not seeding at the desired absorption frequency (due to multimode lasing), the two detector outputs will be comparable, and a TTL pulse is generated by the detector to note that a bad shot has occurred. During single mode operation, the detector puts out no TTL pulse, indicating that the laser is running single mode. During signal averaging, the data acquisition software uses the output pulse of the bad shot rejector to exclude any bad shots thus significantly improving the signal to noise ratio.

The pump frequency range over which the bad shot rejector functions can be determined as follows. One first scans over a narrow CARS transition while the seeder is set to the lowest frequency at which a good shot is indicated. This produces a CARS peak at a given stokes frequency. If the seeder is then set to the highest frequency that still produces good shots, and the CARS transition scanned, the same peak will now be shifted to the blue. The difference in peak centers gives a measure of frequency error that is possible due to seeder drifting. This is illustrated in figure 3.2 which shows the S-

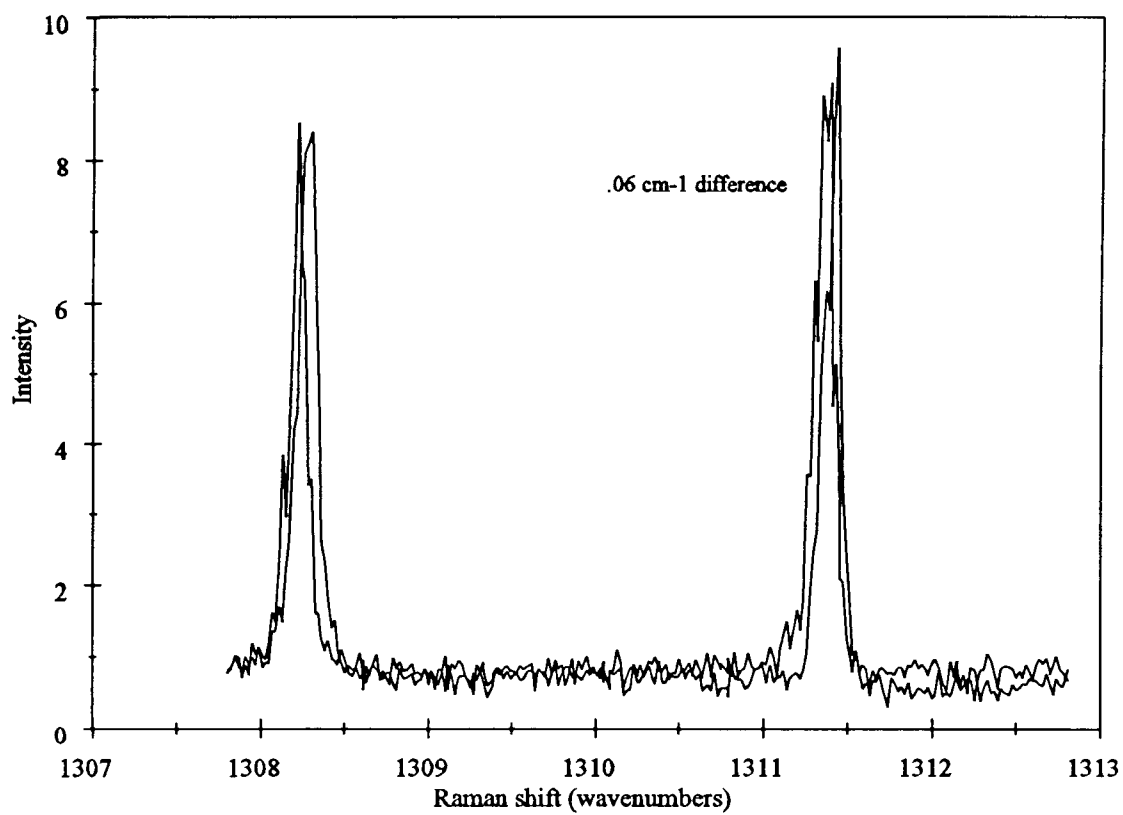


Fig. 3.2 Two S-branch lines of CO<sub>2</sub> are compared at the frequency extremes where shots were considered good. This shows a 0.06 cm<sup>-1</sup> drift is possible.

branch lines of  $\text{CO}_2$  scanned after setting the seeder at extreme positions where the bad shot rejector was recording good shots. The difference in the two peak centers is  $0.06 \text{ cm}^{-1}$ . The maximum error that can be ascribed to the seeder drift is thus  $0.06 \text{ cm}^{-1}$ , which is of the order of the resolution of the dye laser.

## 3.2 Spectroscopic Techniques

### 3.2.1 Jet Samples

All of the jet spectra were recorded for expansions produced in a vacuum cell shown schematically in figure 3.3. In the sample cell the pumping speed is sufficient to maintain pressures of less than 1 torr even when a high pressure pulse is used to form the supersonic jet expansion. Cold free jet expansion conditions are maintained until the gas reaches the mach disc, where gas reheats due to background collisions with the background gas. The mach disc position is a function of the background pressure  $P_b$  and the nozzle pressure  $P_0$ . The position is approximately at  $X/D = 2/3(P_0/P_b)^{1/2}$ , which, for nozzle pressures 10,000 times that of the background gas, is at  $X/D = 67$ . The  $X/D$  ranges for the phase transition studies are always in the free jet at positions before the mach disc.

The cell has windows on either side for laser entry for spectroscopy. These windows are held at Brewster's angle so that there is a minimum of reflected light, maximizing the power transmitted through the windows. Inside the cell is mounted a Bosch fuel injector which has been adapted for use as a gas expansion nozzle. The

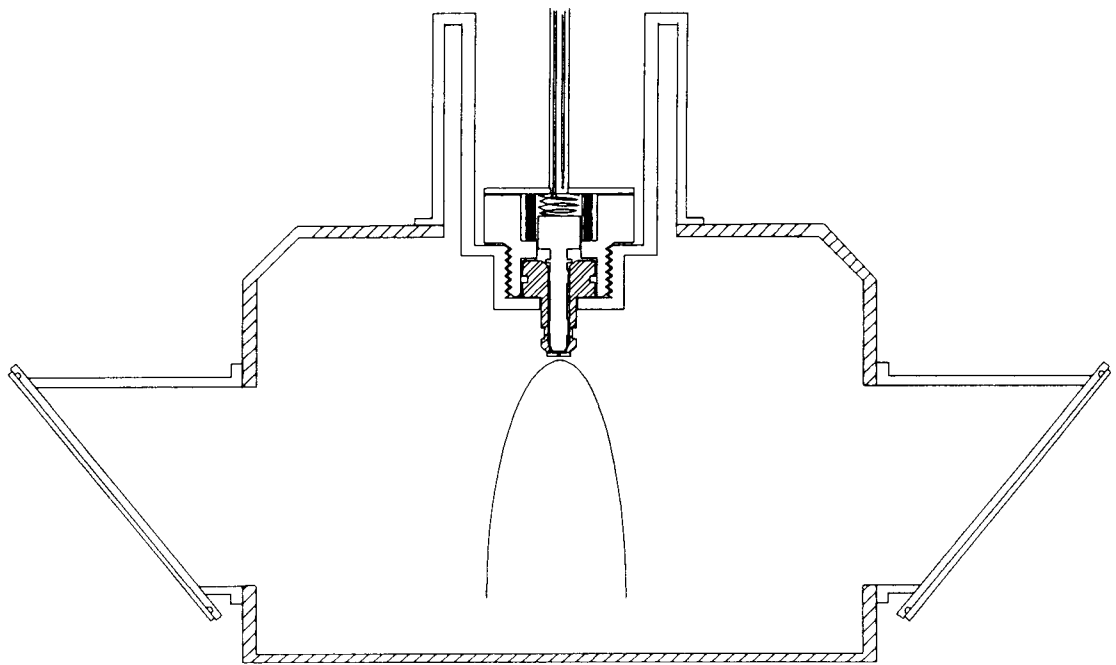


Fig. 3.3 Evacuated cell into which cold gas is pulsed to produce the supersonic jet expansion.

modifications include threading the body for mounting purposes and applying a shim type nozzle to the end. In the case of the neat acetylene expansions, the nozzle diameter was 0.24 mm, allowing a large X/D scanning range.

The solenoid is driven by a pulse driver which was constructed at OSU. The driver essentially uses an SCR switch to dump the charge of a capacitor through the solenoid windings of the magnetic pulsed valve, at typically 150-350 V. The valve opening is synchronized with the laser pulses by a Hewlett Packard 222A pulse generator, which has variable delay and width capability to provide a clean TTL pulse to the pulse driver. This allowed overlap of the jet pulse and the laser pulse (10 ns). Given these widths, the jet can be considered to be a static source on the time scale of the probing lasers.

### 3.2.2 Cryostat

Bulk phase samples were taken in a sample cell shown in fig. 3.4 which consisted of a copper body screwed into the bottom of the cold finger on the APD Cryogenics HC-4MK1 cryostat pictured in fig. 3.5. Indium gaskets were placed on the surface of a spacer inside the cell and quartz windows were pressed down on the indium gasket to achieve a seal. Samples were introduced into the cell through a stainless steel tube soldered into an upper corner of the cell. Gas was introduced into the cell interior after evacuating the system. Temperatures were lowered to a point where liquid started to condense and to fill the cell. Solids were made by slowly approaching the melting point of the sample and slowly stepping down through the melting point until the entire sample was frozen.

Slower rates of freezing tend to produce better crystals. An optically clear sample could easily be made over night using a temperature stepping procedure. This procedure was also used for preparation of colder solid phases in acetylene. Once a good crystal was made, scans were done from low temperatures to higher temperatures to allow continuous scanning from phase to phase. Temperatures could be controlled either through the use of the Lakeshore 330 Autotuning Temperature controller, or the interfacing computer could control the 330 through the IEEE interface on the controller.

The vacuum system on the cryostat included a roughing pump and a diffusion pump which was measured to have vacuums on the order of  $10^{-6}$  torr. A minimum vacuum of  $10^{-3}$  torr is required for operation of the cryostat. Laser beams probed the samples through side mounted windows held at Brewster's angle.

### 3.2.3 CARS in the Cryostat

Taking spectra of samples which are located between two sapphire windows of the cryostat cell requires overlapping three beams between the windows. A difficulty occurs if the focused laser power densities are too high for the windows to withstand. Also overlapping and focusing of high power beams in the sample can cause thermal decomposition, especially in the case of the solid samples. Accordingly the CARS input lasers were overlapped at a position approximately 1 cm beyond the focus (from a 30 cm lens) to avoid the possibility of burning the sample. This reduced the CARS intensity slightly, but, due to the high sample density, the signal was adequate to allow a thorough scan of all three phases of acetylene.

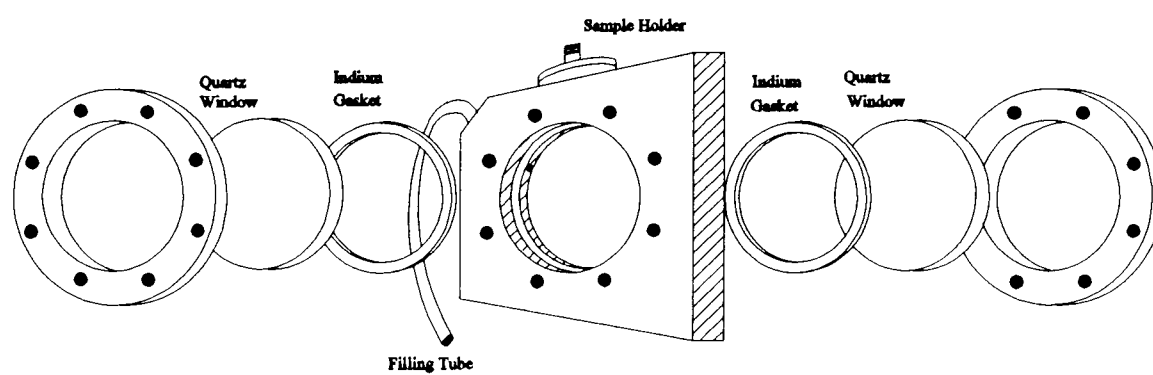


Fig. 3.4 Cryostat sample holder cell with quartz windows and indium gaskets mounted on a copper body.

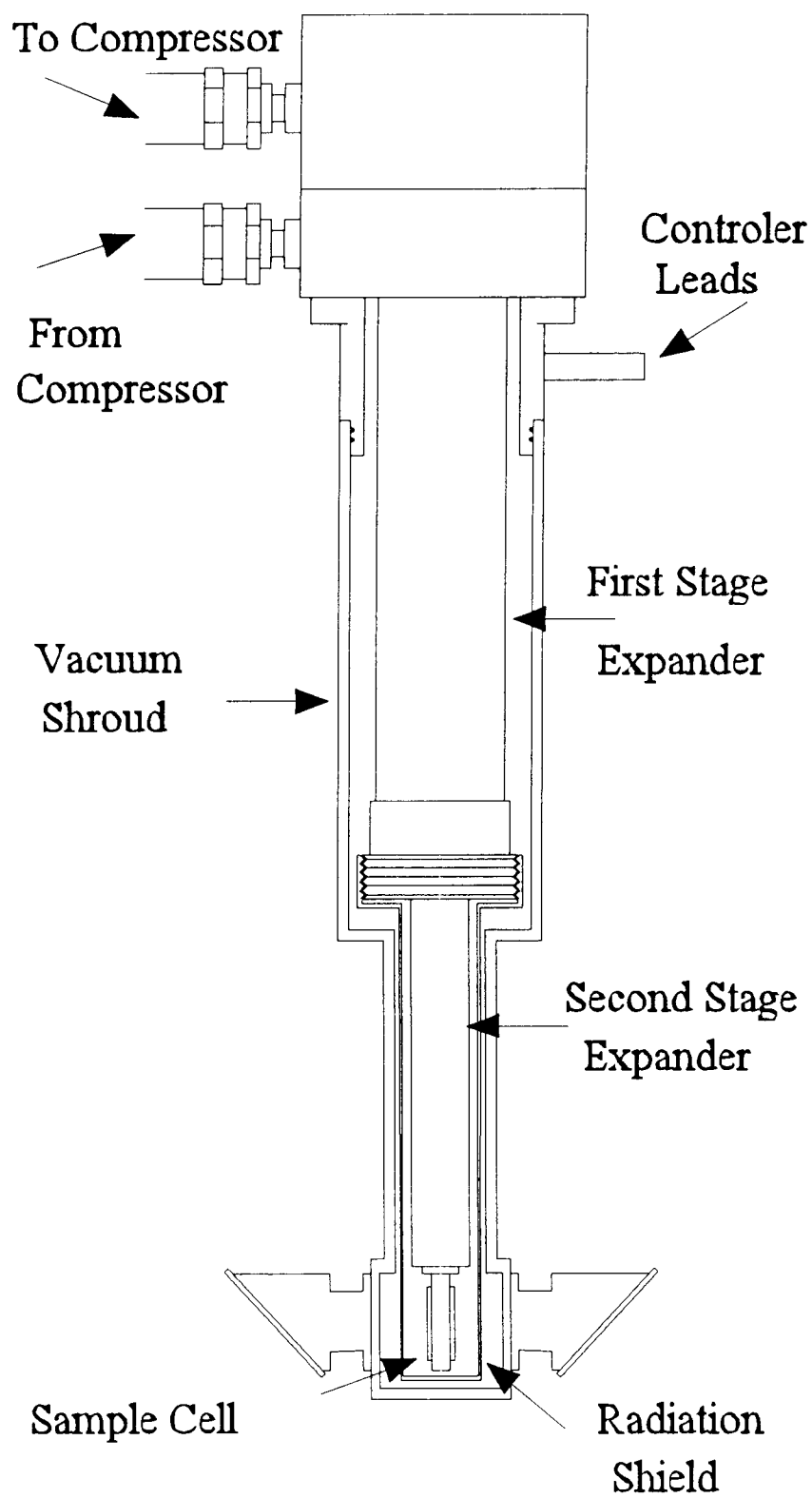


Fig 3.5 Cryogenic cooling stack which was used to prepare the bulk phase samples.

### 3.2.4 I<sub>2</sub> Calibration

The dye laser frequency was calibrated by sending a portion of the dye laser beam into an iodine cell where fluorescence is measured perpendicular to the dye beam. Signals were detected with an RCA IP28A photomultiplier held at voltages ranging from 500 to 1000 V. The detection, integration, and digitization scheme used for the iodine as was the same as that used for the CARS signal. This allowed continuous monitoring of the position of the dye frequency during scanning. The iodine lines could be compared to the wavenumber values located in the iodine atlas<sup>51</sup>. This number and the wavenumber value of the Nd:YAG laser were used to calculate the frequency of CARS transitions.

### 3.2.5 Spectral Calibration

To better calibrate independent data sets, an "internal standard" was used. The internal standard for acetylene is the monomer Q-branch rotational spectrum. This spectrum is unchanging in frequency, and all other CARS transition frequencies can be related to it.

Before each data set was taken, a monomer scan was done at high resolution. Each of the rotational lines in the monomer spectrum was fit and compared to the literature value. An average deviation between the fit values and the literature values was obtained for each data set. The deviation could be applied to the spectra to adjust the peak frequencies to the true frequencies. Figure 3.6 shows two of the monomer scans with the resolved rotational structure.

To calibrate the spectra to accurate absolute frequencies, higher resolution spectra

of acetylene gas Q-branch were taken with each data set. Fitting the best peaks in the monomer spectra taken with the bulk orthorhombic, bulk cubic and liquid, and the jet spectra, Q-branch line centers were compared to theoretical centers to find how far away from the correct frequency the lasers were. The advantage of this is that all peak frequency numbers are absolute once the offset is calculated. Calculating the centers of each of the Q-branch lines with  $\nu_0 = 1974.317$  and  $B' - B'' = -0.006187^{56}$ , an offset could be found for each data set by comparing the calculated centers with the fitted centers. Bulk orthorhombic data was  $1.24 \text{ cm}^{-1}$  low, the bulk cubic and liquid data set was  $1.41 \text{ cm}^{-1}$  low, and the jet data was  $0.981 \text{ cm}^{-1}$  low. After adjusting each to the real frequency, temperature fits could be made.

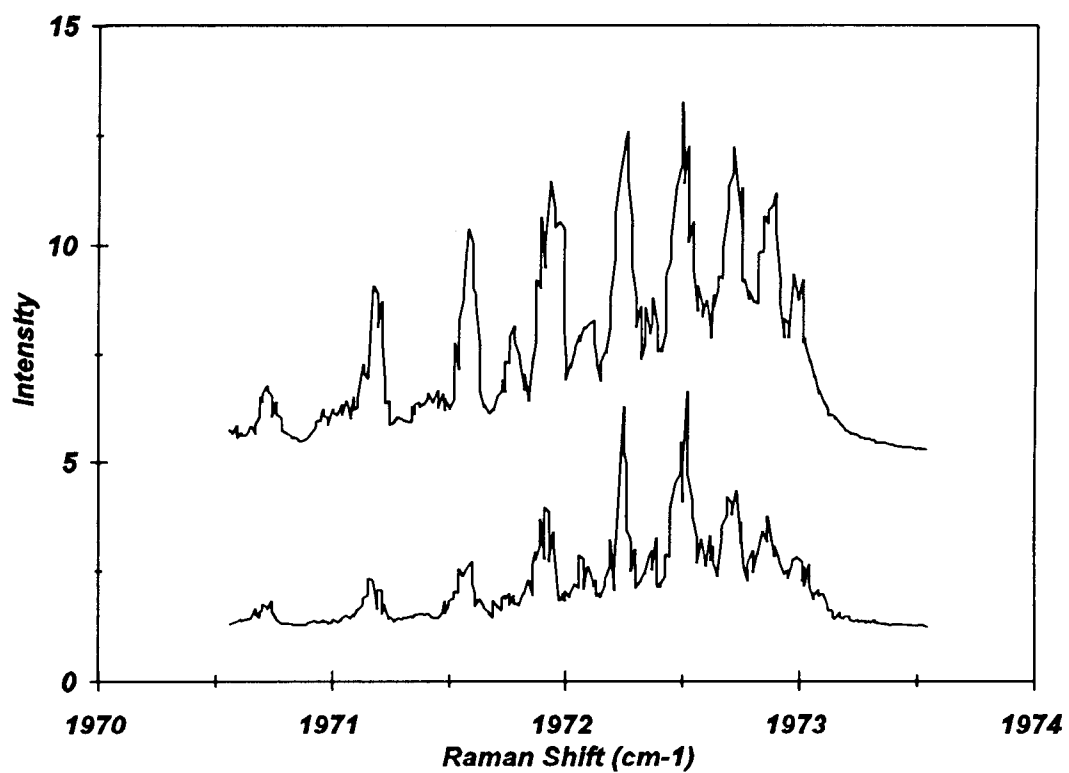


Fig. 3.6 Comparison of jet and bulk monomer scans for calibration

## 4. Equilibrium Phases of Acetylene

### 4.1 Introduction

#### 4.1.1 Background

At low pressures ( $\sim 1 - 5$  atm.), acetylene exists in three condensed phases: liquid, cubic solid, and orthorhombic solid.<sup>57</sup> Unit cell structures of the solid phases and unit cell lengths are known from X-ray data<sup>58</sup> and are shown in figs. 4.1 and 4.2. We have prepared all three phases in a cryostatic cell and examined the vibrational spectra described below. These measurements of equilibrium samples were necessary since the existing data were not of sufficient accuracy to allow use of the temperature dependent frequencies of the peaks to determine the phases and temperatures of clusters formed in jets.

#### 4.1.2 This Study

The frequency of the  $C\equiv C$  stretch ( $\nu_2$ ) vibrational transition is known to change significantly for different phases and temperatures of acetylene. The fundamental frequency for the  $\nu_2$  vibration in the gas is  $1974.317\text{ cm}^{-1}$ . Depending on the temperature in liquid acetylene it is found between  $1960\text{ cm}^{-1}$  and  $1957\text{ cm}^{-1}$ , for cubic solid it is found from  $1956\text{ cm}^{-1}$  to  $1954\text{ cm}^{-1}$ , and for orthorhombic solid it is found between  $1952\text{ cm}^{-1}$  and  $1949\text{ cm}^{-1}$ , depending on the temperature. The general shift to lower frequency can be attributed to an increase in intermolecular interactions which arise from shrinking intermolecular distances. In the case of the solid, the structure can be viewed as being made up of pairs of molecules in which the hydrogens of one unit point toward the

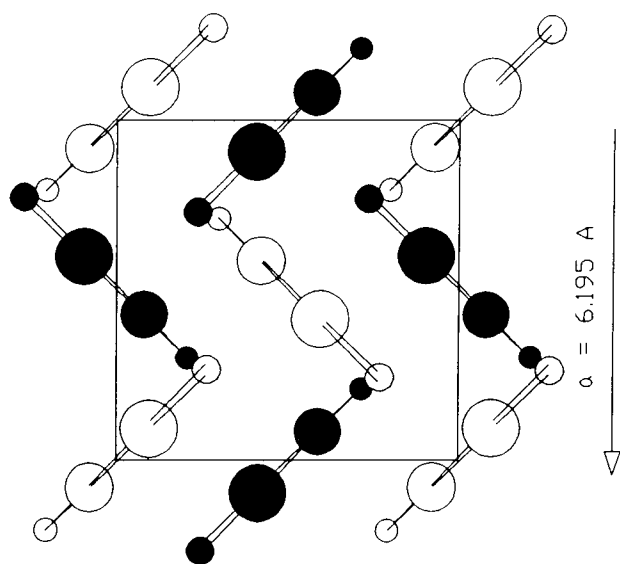


Fig. 4.1 Cubic solid unit cell (shaded molecules are in a separate plane)  $a = 6.091 \text{ \AA}$ .

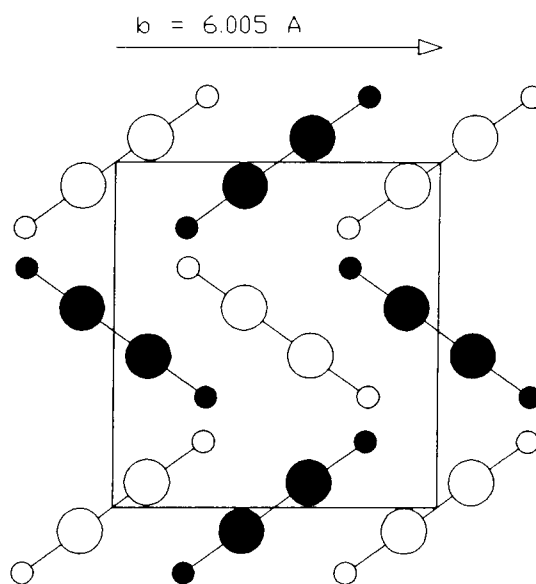


Fig. 4.2 Orthorhombic unit cell (dark molecules are in the plane of the page others are below).  $a = 6.195 \text{ \AA}$ ,  $b = 6.005 \text{ \AA}$ ,  $c = 5.546 \text{ \AA}$ .

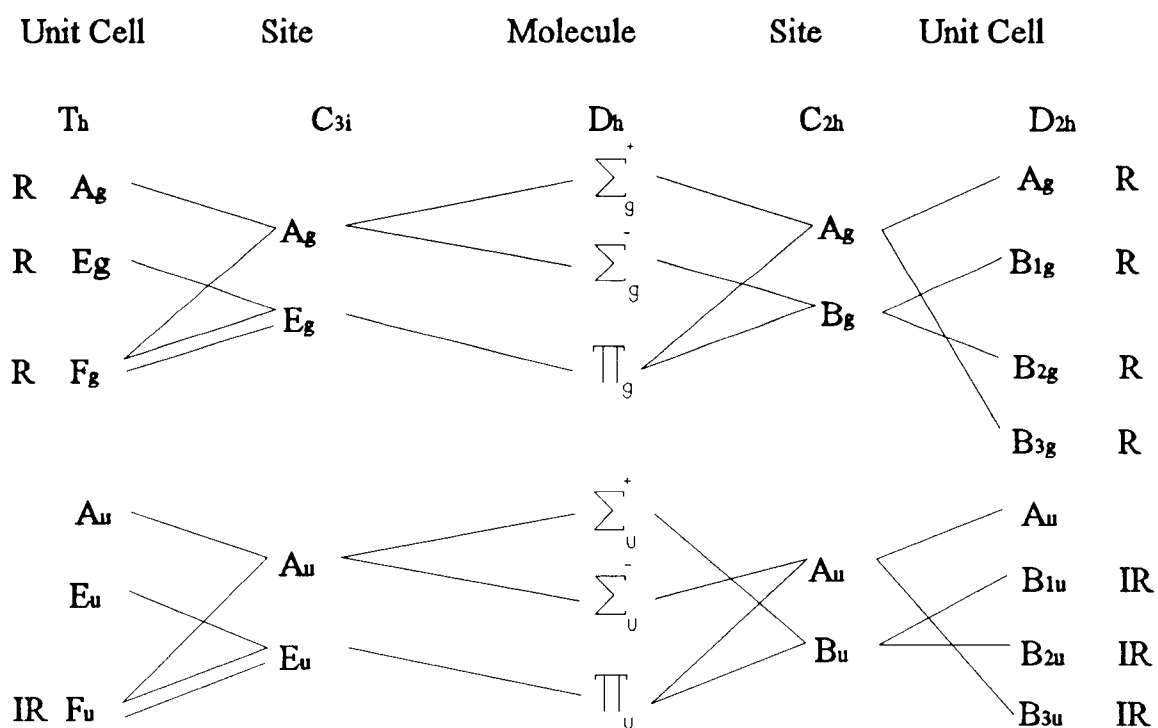


Fig. 4.3 Correlation diagram for acetylene.

electron rich triple bond of the other. With cooling this separation decreases and the C≡C bond is effectively weakened, resulting in a lower frequency for the  $\nu_2$  vibration. This vibrational frequency shift also can be correlated with the observed changes in the lattice dimensions, as shown by van Nes and Bolhuis,<sup>58</sup> who show a plot of the temperature dependence of the cubic phase lattice parameter.

In fact one expects two Raman active peaks for both the cubic and orthorhombic solids, according to the correlation diagrams<sup>59</sup> in fig. 4.3. However, the bulk spectra are dominated by the intense  $A_g$  peak for both phases and all of the information for acetylene will be based on the  $A_g$  position of the  $\nu_2$  vibration in the solid phases. We also note that the width of the peak decreases as the temperature decreases in the bulk samples but this information proved not very useful in determining jet properties.

#### 4.1.3 Bulk Phase Samples

Bulk phase data is obtained from samples which are made in a cryostatic cell, described in the previous chapter. Samples are prepared through introduction of a gas into the evacuated cryostatic cell at 5 atm and 220 K, thus giving the liquid form. It was easy to fill the cell with acetylene because the liquid level could be viewed as it rose in the cell. Once the cell was full, the sample was cooled very slowly (0.5 K steps every 5 min) through the phase transition temperature to yield an optically clear solid. The cubic solid sample was then cooled to a point just above the cubic - orthorhombic phase transition temperature and the spectra were taken as the sample was warmed. The reason for taking spectra as the sample is warmed is that a full set of data which included both the liquid and

cubic solid could be taken quickly. This is because there was no need to spend time annealing an optically clear solid, thus minimizing the possibility of instrumental frequency and laser power drift.

Orthorhombic data was obtained in a similar manner with some slight modifications. A cubic sample was obtained in the same way as was previously stated and the temperature was lowered to 140 K. This cubic sample was then cooled in 0.2 K steps every 5 min to 130 K. The slower temperature drop is needed because the sample tends to fracture as it goes through the phase transition. A reasonably clear sample was obtained, and scanned using CARS, as with the cubic and liquid phases. As noted by Richardson, the phase transition temperature was indicated by a pronounced change in the scattering levels at 137.5 K, about midway between values of 133<sup>61</sup> and 142<sup>64</sup> reported by others. We have used our value of 137.5 in our latter calculations because we believe it to be most accurate.

## 4.2 Data Analysis

### 4.2.1 Gas Phase Data

Spectra of the  $\nu_2$  Q-branch of gas phase acetylene have been shown previously in fig. 3.6. We note that well resolved Q-branches are seen only for samples at relatively low pressure (5 - 100 torr). Accurate values for these frequencies have been reported in the literature<sup>60</sup> and can be calculated from the relation

$$Q_J = 1974.317 - 0.006189 J(J+1) \quad (4.1)$$

These frequencies were used as primary calibration points for some of the Raman shifts observed for the condensed phases.

#### 4.2.2 Data for Bulk Acetylene

The liquid-solid data in table 4.1 shows that the  $\nu_2$  vibrational frequency is shifted from the gas phase value by 10 to 20  $\text{cm}^{-1}$ , depending on the phase and temperature being studied (fig. 4.4). The  $\nu_2$  frequency in each phase is shifted slightly to the red as temperature drops, and large discontinuous red shifts occur at phase transitions. The peak center frequencies taken at several temperatures yield a frequency vs. temperature curve which can be fit to a polynomial for each phase. Peak widths also vary slightly as the temperature drops, and a correlation between temperature and width can be made. In principle, line widths could give a measure of temperature. This has the advantage that accurate knowledge of the absolute frequency of the peak center is not required, but rather only the relative width. Widths are more sensitive to sample crystallinity, however, and we have found that features in cluster samples are always 2-3 times as broad as those in bulk samples. Thus we make measurements based on the position of the  $A_g$  peak which we can measure absolutely relative to the gaseous monomer as described in ch. 3.

Plotted in figs 4.5 - 4.8 are the  $\nu_2$  frequencies as functions of temperature. The liquid data was fit to a linear relation, but cubic and orthorhombic data were best

reproduced with a quadratic function. Only orthorhombic data above 70 K was used because no clusters were seen below this temperature. The resultant relations are:

$$\text{Liquid} \quad v = 1950.791 + 0.04352 T \quad (4.2)$$

$$\text{Cubic} \quad v = 1954.881 - 0.01652 T + 9.660 \times 10^{-5} T^2 \quad (4.3)$$

$$\text{Ortho} \quad v = 1950.165 + 0.00762 T + 6.2833 \times 10^{-5} T^2 \quad (4.4)$$

Given the frequencies of the  $\nu_2$  transition for a large cluster formed in the jet, these relations can be used to deduce the cluster temperatures. Since our later interest is in calculating T from  $\nu$ , the data were also fit to the expressions

$$\text{Liquid} \quad T = -17.4201 + 22.898 (1950 - \nu) \quad (4.5)$$

$$\text{Cubic} \quad T = -720.65 + 302.944 (1950 - \nu) - 24.63508 (1950 - \nu)^2 \quad (4.6)$$

$$\text{Ortho} \quad T = 3.34 + 74.238 (1950 - \nu) - 7.76913 (1950 - \nu)^2 \quad (4.7)$$

Table 4.1 Bulk acetylene data with  $\nu_2$  frequencies and widths for spectra at the recorded temperatures.

T(K)	Liquid	FWHM	T(K)	Cubic	FWHM	T(K)	Ortho	FWHM
234.1	1960.969	1.180	192.4	1955.270	0.280	131.0	1951.231	0.230
231.1	1960.844	1.260	192.0	1955.266	0.260	128.0	1952.146	0.210
228.1	1960.744	1.260	190.0	1955.230	0.280	124.8	1952.115	0.250
225.1	1960.636	1.400	188.0	1955.192	0.280	120.0	1952.027	0.250
222.1	1960.459	1.380	185.8	1955.152	0.320	119.0	1951.959	0.250
219.0	1960.300	1.280	183.9	1955.097	0.280	116.1	1951.881	0.250
216.1	1960.145	1.280	181.9	1955.087	0.340	113.3	1951.840	0.210
213.1	1960.124	1.200	179.9	199.026	0.320	110.0	1951.779	0.330
210.1	1959.867	1.380	178.0	1955.016	0.340	107.2	1951.692	0.250
207.2	1959.802	1.360	176.0	1954.969	0.300	104.3	1951.645	0.310
204.1	1959.701	1.440	174.0	1954.912	0.340	101.2	1951.564	0.290
201.2	1959.535	1.140	172.0	1954.898	0.360	98.30	1951.508	0.350
189.2	1959.403	1.180	170.0	1954.857	0.360	95.5	1951.451	
195.1	1959.298	1.100	168.0	1954.854	0.280			
193.3	1959.219	1.040	164.0	1954.796	0.360			
			163.9	1954.782	0.380			
			161.9	1954.712	0.320			
			160.0	1954.714	0.380			
			158.0	1954.692	0.480			
			156.0	1954.642	0.500			
			154.0	1954.640	0.380			
			152.0	1954.579	0.480			
			149.9	1954.579	0.520			
			148.0	1954.565	0.560			
			146.0	1954.529	0.540			
			143.9	1954.478	0.520			
			141.9	1954.493	0.460			
			140.0	1954.458	0.800			
			137.9	1954.448	0.56			

\*Data is contained in ace\*\*\*\*.prn and arc\*\*\*\*.prn files where \*\*\*\* is the temperature

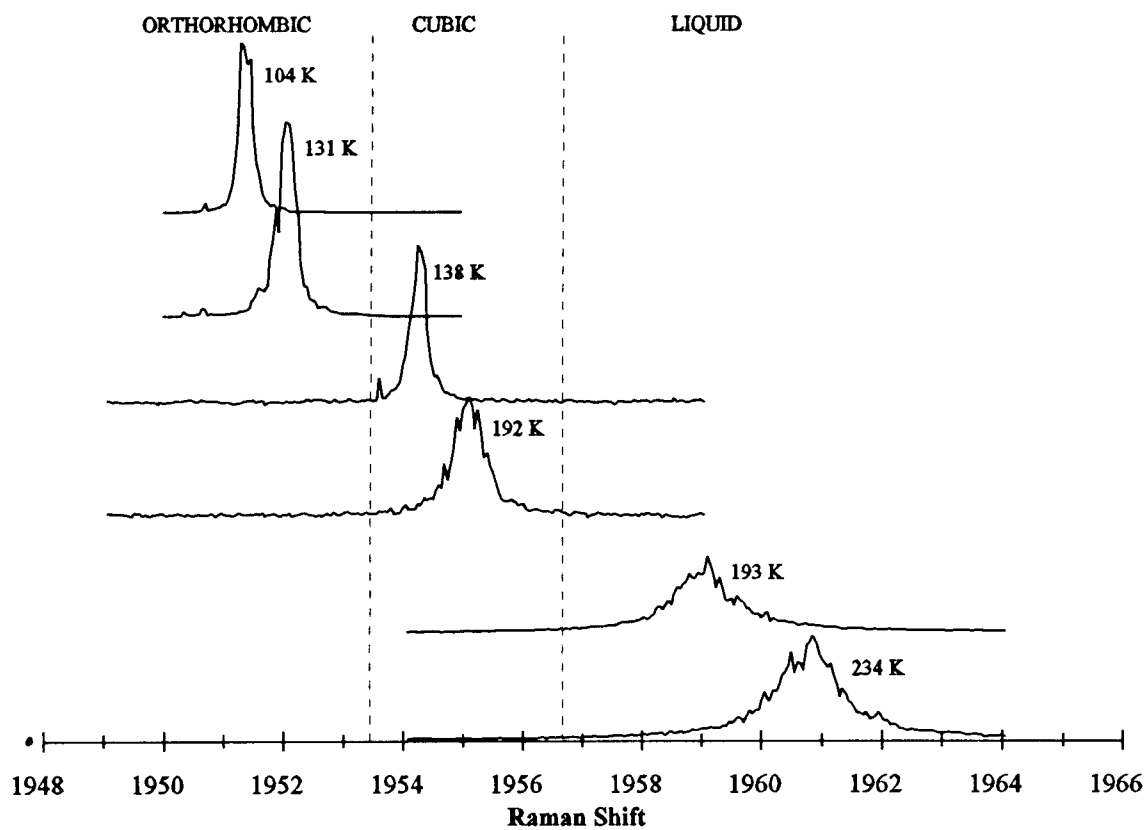


Fig. 4.4 CARS spectra of all three condensed phases of acetylene.

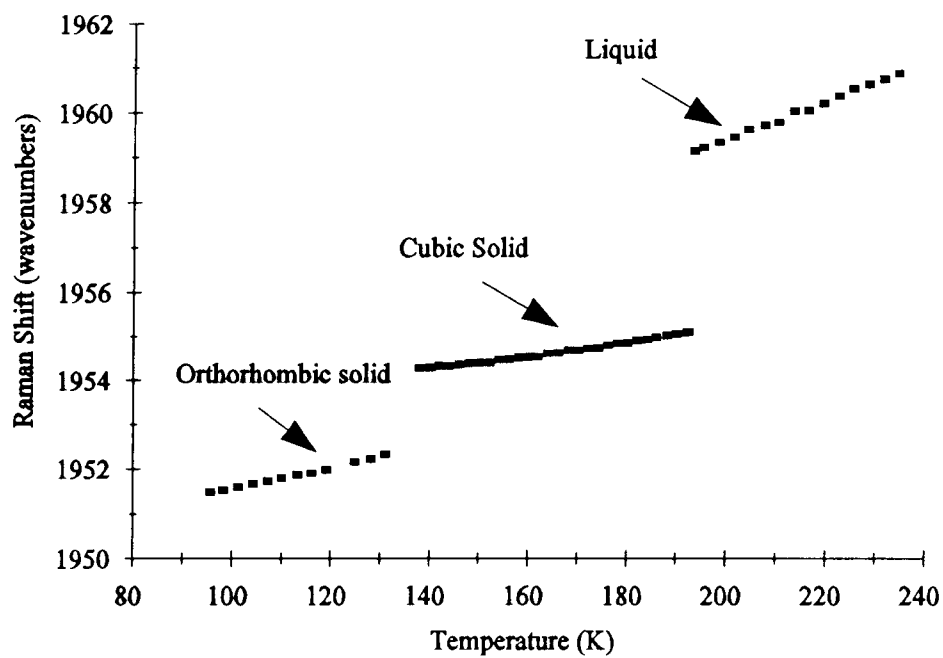


Fig. 4.5 Frequency of the  $\nu_2$  peak as a function of temperature.

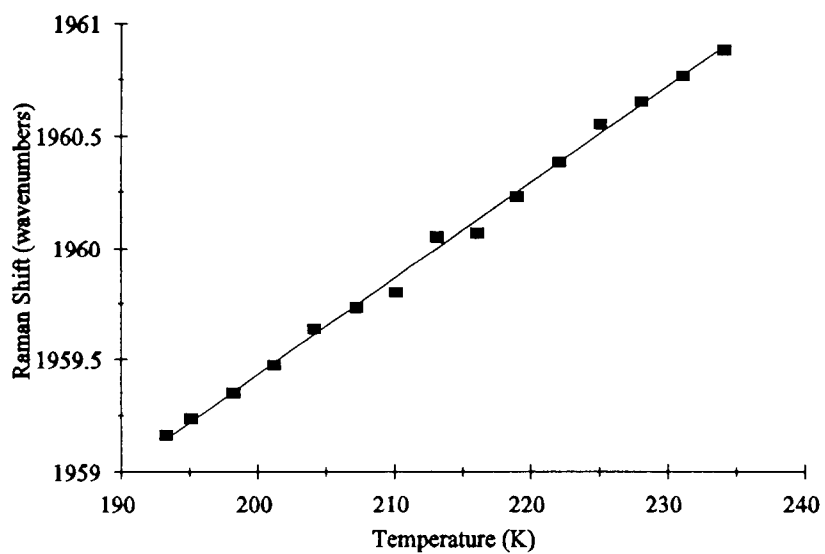


Fig. 4.6 Frequency of the  $\nu_2$  peak of liquid acetylene as a function of temperature.

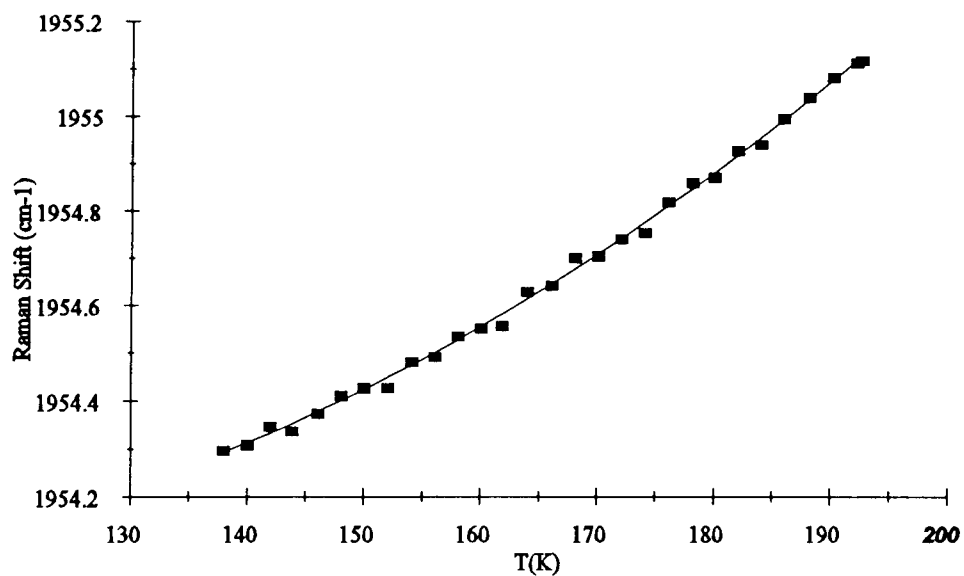


Fig. 4.7 Frequency of the  $\nu_2$  peak of cubic solid acetylene as a function of temperature.

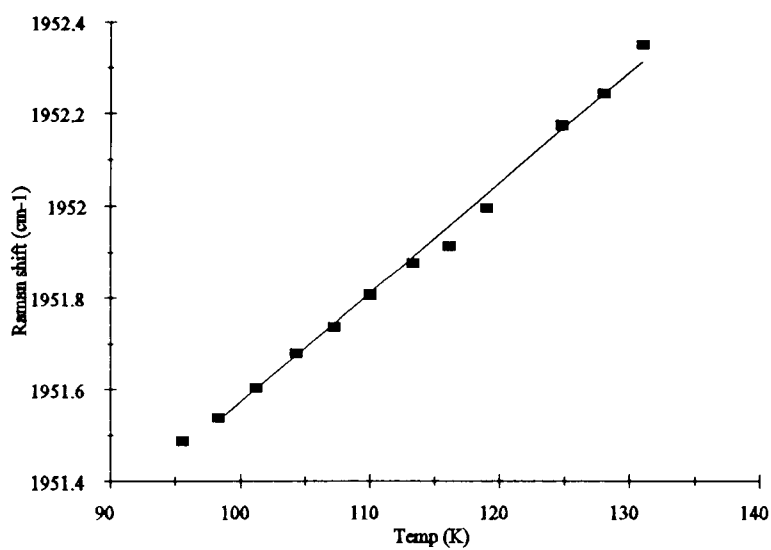


Fig. 4.8 Frequency of the  $\nu_2$  peak of orthorhombic solid acetylene as a function of temperature.

## 5. Neat Acetylene Clusters

### 5.1 Cluster Spectra and Temperatures

#### 5.1.1 Experimental Conditions

Acetylene was pulsed out of a nozzle into a vacuum chamber to produce a supersonic gas jet which cooled rapidly and began to condense into small liquid droplets. A number of experiments were performed to find optimal conditions for the production of large clusters and the data presented here are from one extensive series of measurements. For this study the nozzle temperature and pressure were kept stable at 233 K and 14 atm, conditions which are very near the condensation point of the gas, to make it more favorable for the gas to nucleate. The extensive clustering which occurred is seen in fig. 5.1, where approximately 80% of the molecules are in the condensed phase. The large peak at  $1958\text{ cm}^{-1}$  is due to liquid clusters, while the smaller peak at  $1974\text{ cm}^{-1}$  is due to the uncondensed monomer.

#### 5.1.2 Monomer Results

Fig. 5.2 shows the change in the monomer Q-branch as a function of X/D and, by comparison with the room temperature scan of fig. 3.6, the narrowing due to rotational cooling early in the expansion is clear. Although the low J rotational structure was not resolved in the jet spectra, modeling of the overall contours was done to obtain rough rotational temperatures. These are displayed in Fig. 5.3, along with the translational

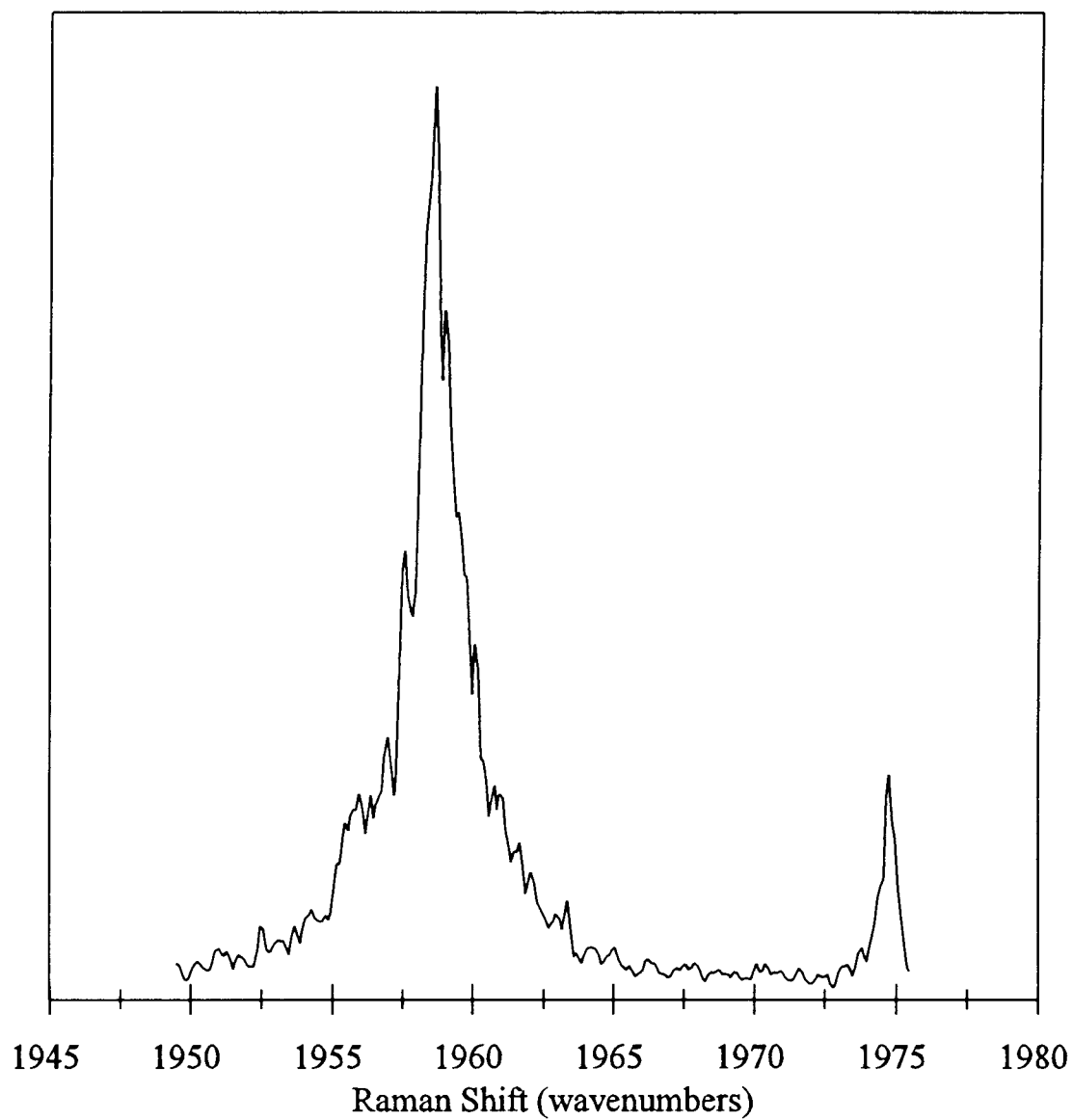


Fig. 5.1 Neat acetylene at 233 K and 14 atm produces nearly 80% clustering with liquid acetylene as the dominant phase.

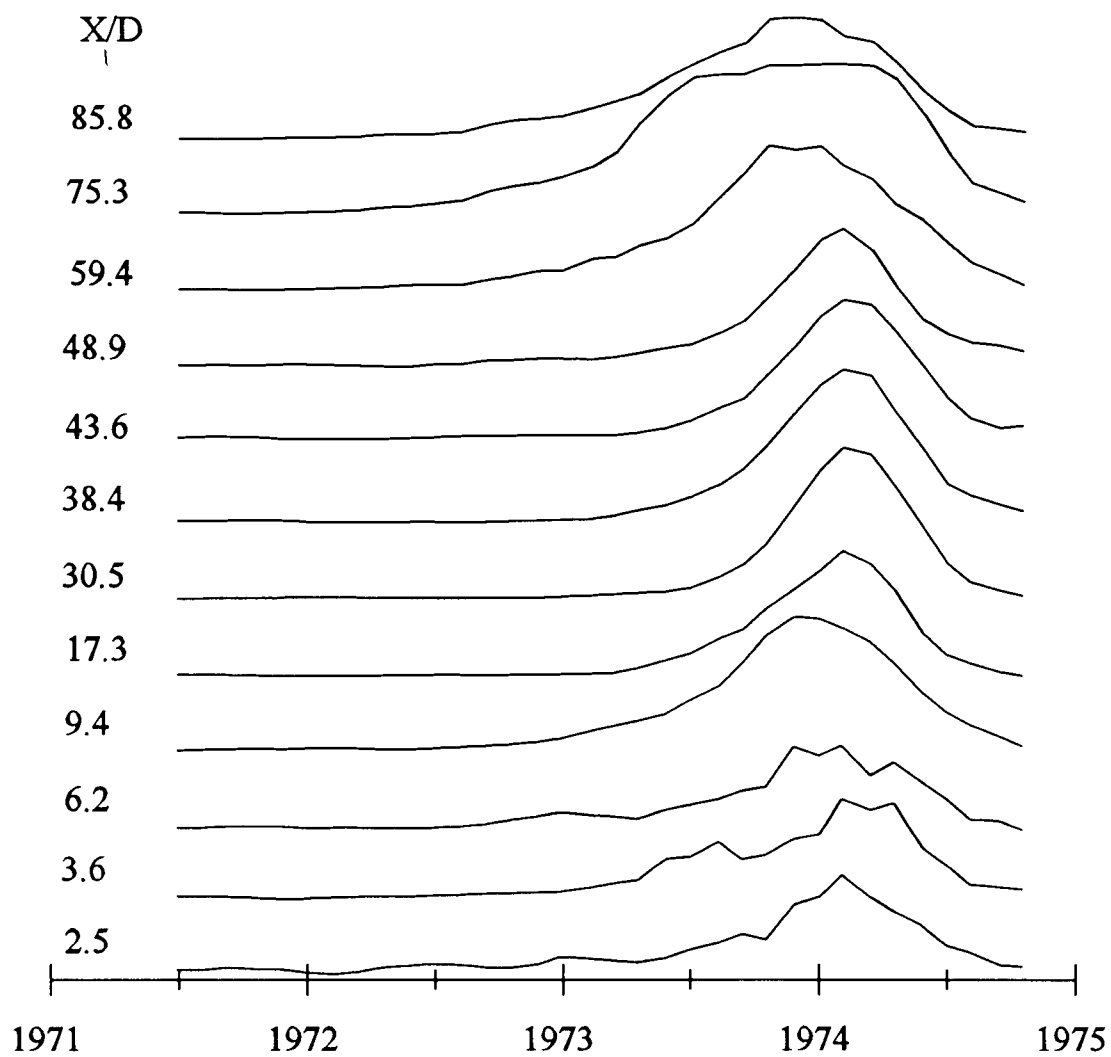


Fig. 5.2 Monomer Q-branch spectra for the first 85 X/D. Rotational warming is evident from the increased width above X/D = 60.

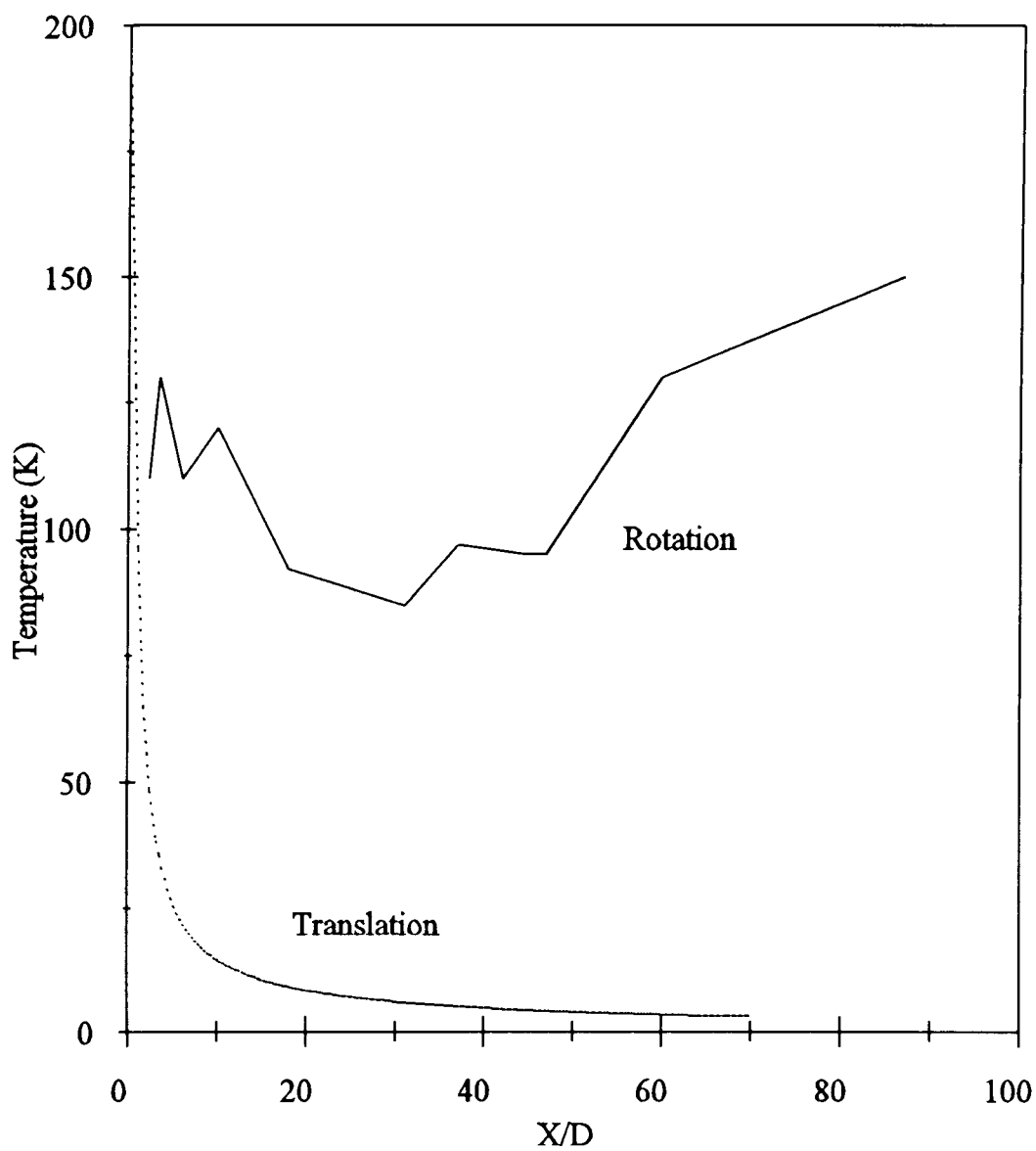


Fig. 5.3 Rotational temperature of the monomer is estimated in the jet spectra. The rise in temperature suggests the mach disk limit may occur at  $X/D = 60$ .

temperatures predicted for an isentropic expansion. Due to the heat of clustering, the latter serves only as a lower limit of the temperature.

Although the fitted rotational temperatures have a large uncertainty ( $\sim 20$  K) the trend suggests gradual rotational cooling out to about  $X/D = 60$ , at which point a temperature rise is indicated. This could be caused by entry into the mach disk region which signals the end of the free flow region of the expansion. Here collisions with background gas molecules would be expected to warm up the monomer and, to a lesser extent, the much more massive cluster. As seen below no appreciable rise in the cluster temperature is seen in this region. Moreover, most of the cluster phase changes occur below  $X/D = 60$  so that the assumption of free jet conditions in the consideration of cluster temperature is deemed valid in the following analysis.

### 5.1.3 Cluster Results

As one probes along the jet centerline away from the nozzle (increased  $X/D$  where  $D$  is nozzle diameter and  $X$  is distance from the nozzle), trends are also seen indicating cluster cooling and phase transitions. Figure 5.4 shows the  $X/D$  region in which liquid clusters transform into cubic solid and figure 5.5 shows the region of the cubic to orthorhombic transformation. In these two figures, the peaks shift to lower frequency as we probe further out in  $X/D$ , mirroring closely the trends for the cryostat samples as they were cooled. These peaks were fit using the CARS line shape program in the appendix to find peak centers, and the results are tabulated in table 5.1. The temperatures of the clusters are found from the peak frequencies and the  $T = f(\nu)$  relations of the bulk

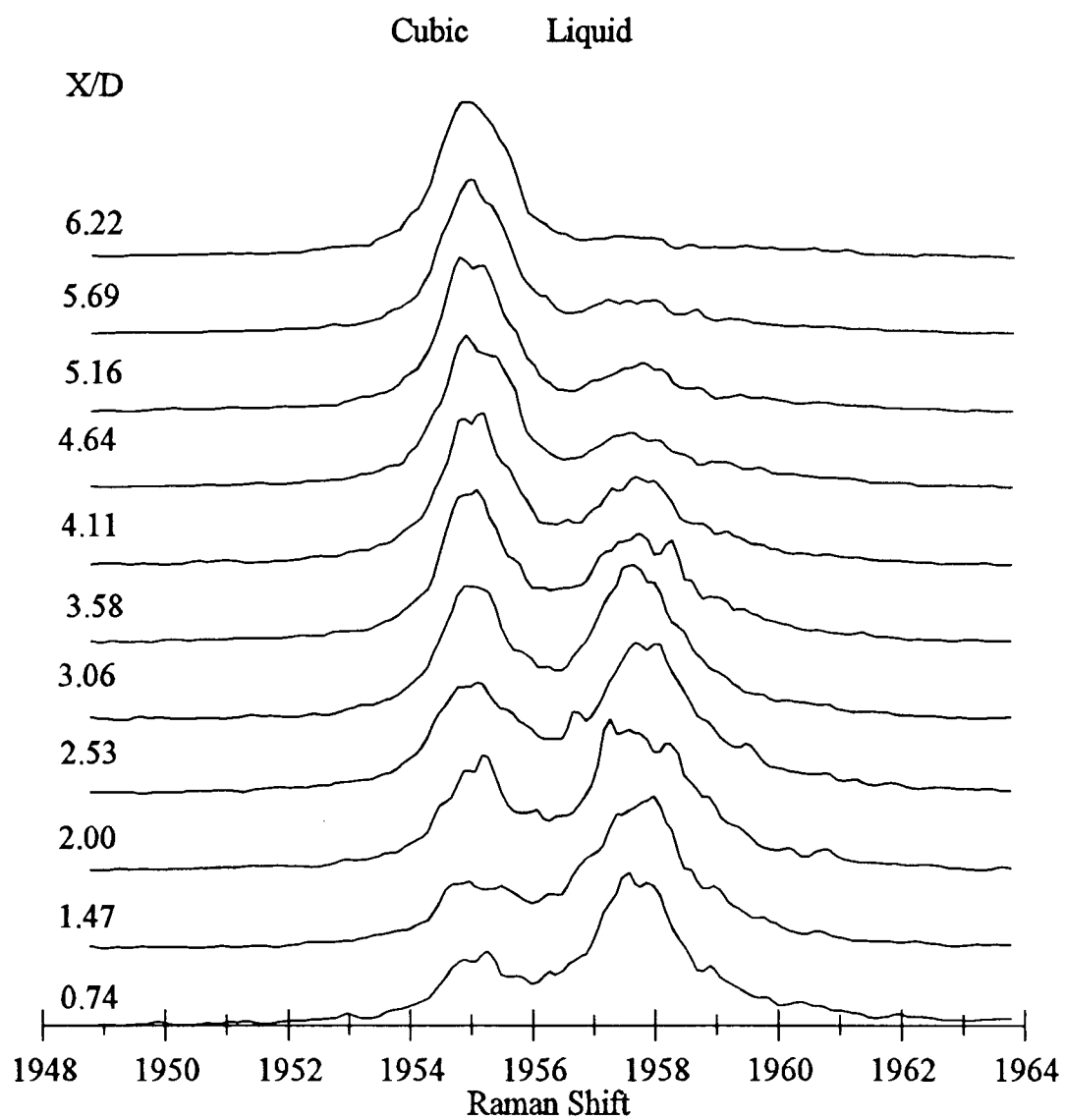


Fig. 5.4 The liquid to cubic solid transition can be seen in clusters very close to the nozzle.

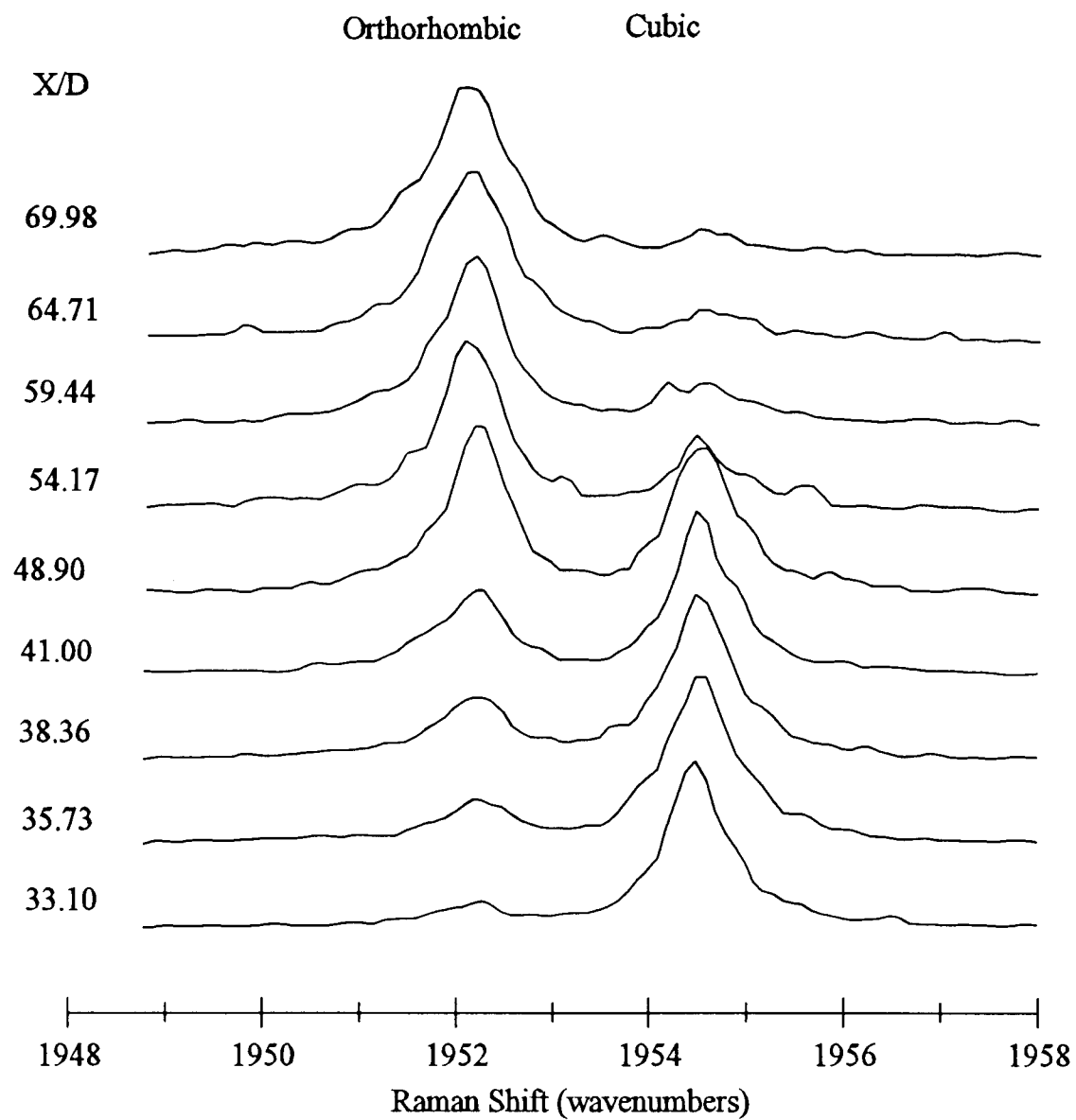


Fig. 5.5 The cubic solid to orthorhombic solid phase transition is seen late in the jet.

Table 5.1 Neat acetylene jet data; frequencies, temperatures, and percentages.

X/D	LIQUID			CUBIC			ORTHORHOMBIC		
	FREQ	TEMP (K)	%	FREQ	TEMP (K)	%	FREQ	TEMP (K)	%
0.74	1957.624	157.2	75.2	1955.402	198.9	24.7			
1.47	1957.668	158.2	69.2	1955.580	206.9	30.7			
2	1957.514	154.6	62.7	1955.341	196.1	37.3			
2.53	1957.675	158.3	61.8	1955.366	197.2	38.1			
3.06	1957.473	153.7	60.4	1955.266	192.4	39.6			
3.58	1957.512	154.6	59.5	1955.275	192.9	40.4			
4.11	1957.641	157.6	49.1	1955.254	191.9	50.8			
4.64	1957.455	153.3	44.2	1955.244	191.4	55.8			
5.16	1957.504	154.4	43.0	1955.250	191.7	57.0			
5.69	1957.435	152.8	43.1	1955.237	191.0	56.9			
6.22	1957.304	149.8	14.2	1955.053	181.5	85.8			
6.75				1954.973	177.0				
7.27				1954.983	177.6				
7.8				1955.007	179.0				
8.32				1954.932	174.7				
8.85				1954.898	172.7				
9.38				1954.900	172.8				
10.43				1954.869	170.9				
11.49				1954.814	167.5				
12.54				1954.753	163.6				
13.6				1954.723	161.5				
14.65				1954.722	161.5				
17.28				1954.645	156.0				
19.92				1954.600	152.7				
22.55				1954.601	152.7				
25.19				1954.683	151.3				
27.82				1954.562	149.7	91.0	1952.745	147.8	9.0
30.46				1954.532	147.2	82.7	1952.625	142.9	17.3
33.09				1954.405	144.9	75.5	1952.462	136.3	24.5
35.73				1954.533	147.3	74.5	1952.515	138.4	25.5
38.36				1954.534	147.4	65.2	1952.464	136.3	34.7
41				1954.510	145.3	54.9	1952.385	133.1	45.0
43.63				1954.474	142.2	48.1	1952.348	131.6	51.9
48.9				1954.435	138.5	34.8	1952.279	128.8	65.2
54.17				1954.369	141.7	30.1	1952.285	129.0	69.9
59.44				1954.456	140.5	24.7	1952.245	127.4	75.2
64.71							1952.263	128.1	76.3
69.98							1952.165	124.1	
75.25							1952.179	124.6	
80.5							1952.206	125.8	
85.79							1952.191	125.2	

This data can be found in the acetfit spreadsheet. The percentages are deduced from the area under the square root of the individually calculated peaks.

material. The absolute uncertainties in the frequencies is estimated to be less than  $\pm 0.1$   $\text{cm}^{-1}$  and the corresponding absolute temperature uncertainties are indicated by the error bars in fig. 5.6, where all of the cluster data is graphed as a function of  $X/D$ . The relative temperature changes are believed to be more accurate by about a factor of four.

The clusters are rapidly cooling as they travel out in the jet, and the regions where two types of clusters coexist are clearly evident. It is interesting that liquid clusters are present in the earliest spectra at  $X/D \sim 1$  and that these are about 40 K below the 192.7 K freezing point. It should be noted that this temperature estimate is based on an appreciable extrapolation of the equilibrium data, which only extended from 234 K to 193 K. Thus there is an unknown uncertainty due to this extrapolation which is not contained in the error bars indicated for the liquid clusters in fig. 5.6.

Cubic solid clusters appear in very low percentages in the earliest spectra (as can be seen in fig. 5.4) and gradually become the dominant phase as the liquid clusters freeze. We note that, within experimental error, the first cubic solid clusters appear to be at the melting temperature (192.7 K) for bulk acetylene.

Later in the expansion, the cubic clusters cool until at about  $X/D = 30$  they begin to change phase to orthorhombic solid. Here, the temperatures of the cubic solid clusters are calculated to be higher than the phase change temperatures of 137 K seen for equilibrium samples. Surprisingly, the temperatures deduced for the orthorhombic clusters lie slightly below those of the cubic solid. This is physically unreasonable since the heat of the phase transition should produce warmer orthorhombic clusters. Given the uncertainty estimates it seems probable that the two phases are nearly at the same temperature.

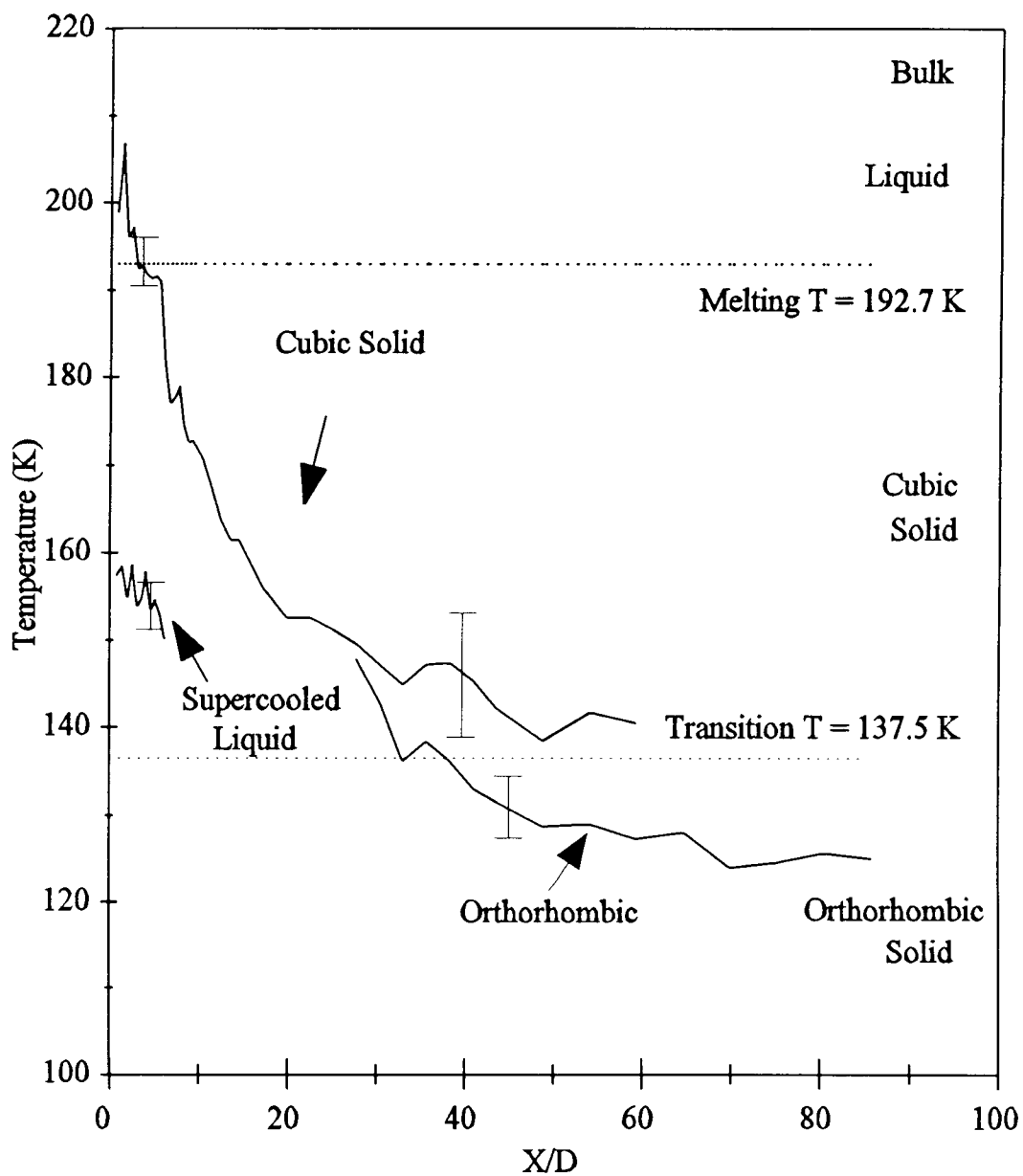


Fig. 5.6 Temperature of all phases of the clusters are graphed vs. X/D.

## 5.2 Mean Cluster Size

Richardson has described the use of a simple cooling curve model for the determination of mean cluster size and this method was applied in this work. Basically, the method accounts for heat transportation into and out of a cluster as condensation and evaporation occur during the cluster flight. This heat flux scales linearly with cluster surface area whereas the cooling depends upon the cluster heat capacity and therefore the volume. Thus the cooling curve is a function of cluster size. The calculation is done using the spreadsheet program Mixacetc.wb1 and the necessary input data including  $\Delta H_{\text{sub}}$ ,  $C_p$ ,  $P_{\text{vap}}$ , etc. are tabulated in table 5.2.

To avoid complications due to added heat release in phase transition regions, the region from  $X/D = 9$  to 30 is emphasized in the fitting process, since here one has essentially just cubic clusters. Figure 5.7 shows curves for several mean cluster diameters assumed to apply at  $X/D = 70$ . The best fit gives a diameter of about 20 nm but it should be noted that values from about 15 to 25 nm could be forced to give a comparable fit. The cooling model includes parameters to allow for a sticking fraction  $f$  less than one and some fractional cooling  $\alpha$  during non-condensing monomer-cluster collisions. The fits were done with  $f = 0.16$  and  $\alpha = 0.5$ , values found by Richardson to optimize his fit of  $\text{CO}_2$  cluster cooling curves. Variation in these from  $f = 0.15$  to 1 and  $\alpha = 0$  to 1 were explored and change the mean cluster size by no more than a factor of two.

Table 5.2 Physical constants for acetylene

Melting Point	191.7 K @ 85 torr	McIntosh <sup>61</sup>
Solid Transition Temp	133 K, 137.5 K, 142 K	McIntosh, <sup>61</sup> Richardson, <sup>50</sup> Miskewicz <sup>64</sup>
Boiling Point	189.6 K	McIntosh <sup>61</sup>
Vapor Pressure	0.1 torr @ 130 K (s) 4.6 torr @ 155 K 106 torr @ 190 K 146 torr @ 195 K 309 torr @ 210 K	71 st ed. CRC <sup>62</sup>
C <sub>p</sub> (l)	114.4 J/K mol	McIntosh <sup>61</sup>
(g)	44.3 J/K mol	Matheson <sup>63</sup>
C <sub>v</sub> (g)	35.915 J/K mol	
γ (C <sub>p</sub> /C <sub>v</sub> )	1.234	
ΔH <sub>vap</sub> (l)	21.21 kJ/ mol	McIntosh <sup>61</sup>
ΔH <sub>sub</sub> (s)	22.92 kJ/ mol	McIntosh <sup>61</sup>
ΔH <sub>fus</sub> (s-l)	3.785 kJ/ mol	Miskewicz <sup>63</sup>
ΔH <sub>ss</sub> (s-s)	2.54 kJ/ mol	Miskewicz <sup>64</sup>
ΔS <sub>fus</sub> (s-l)	19.6 J/ K mol	Miskewicz <sup>64</sup>
ΔS <sub>ss</sub> (s-s)	17.5 J/ K mol	Miskewicz <sup>64</sup>
Surface Tension (g-l)	16.4 mJ/m <sup>2</sup> (203 K)	CRC <sup>62</sup>
Collision Diameter	4.22 Å	Hirschfelder, Curtiss, Bird <sup>64</sup>
Viscosity	0.193 mN s / m <sup>2</sup>	Matheson <sup>63</sup>
Cubic lattice distance	6.195 Å	van Nes <sup>65</sup>
Density (l)	0.613 g/cm <sup>3</sup>	McIntosh <sup>61</sup>
Density (s)	0.73 g/cm <sup>3</sup>	McIntosh <sup>61</sup>

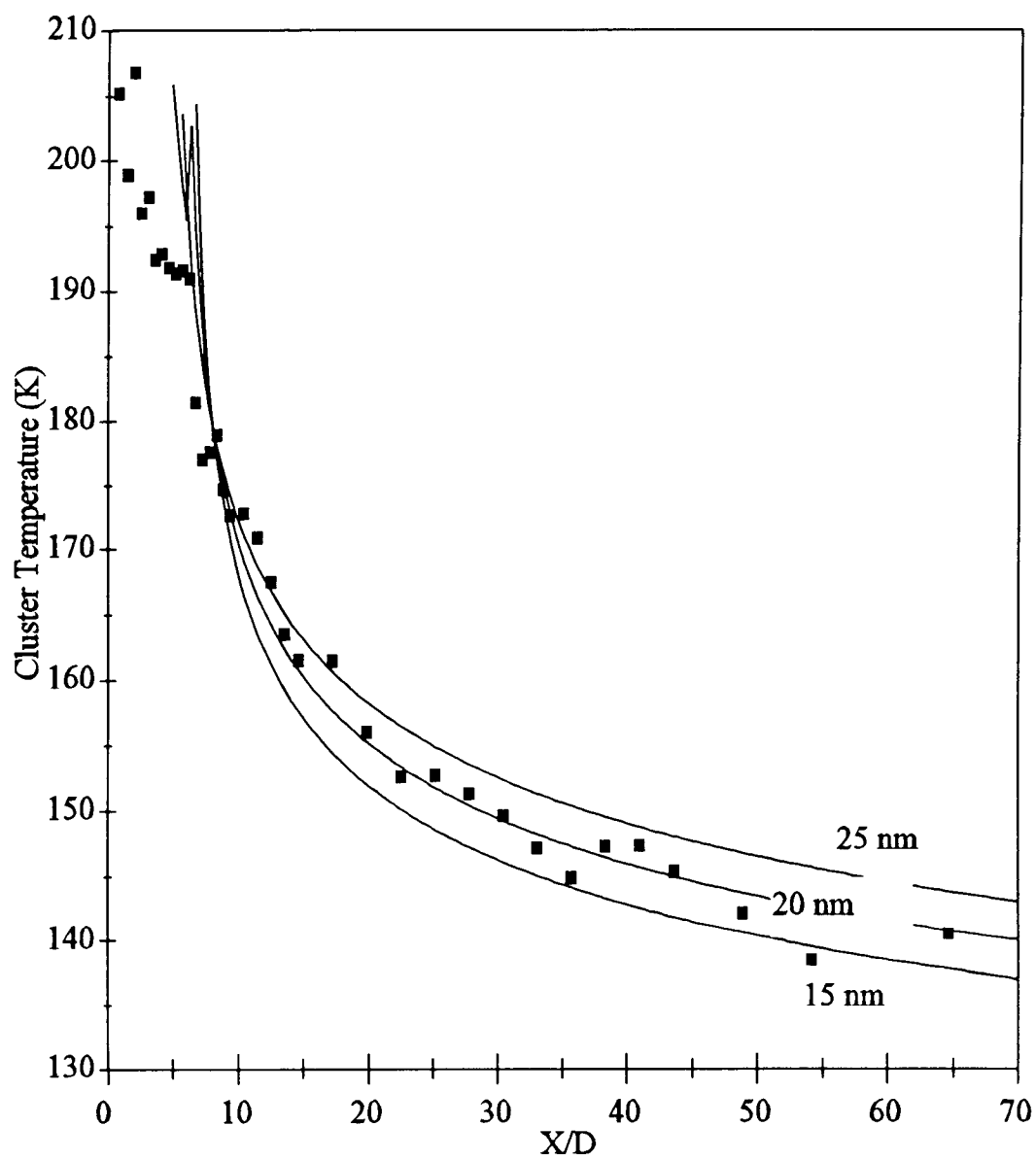


Fig. 5.7 Cubic solid cluster temperatures are fit with cooling curves by adjusting final temperature and cluster diameter.

## 5.3 Liquid - Solid Phase Transition

Cooling occurs in a supersonic jet which expands in a manner that, in the absence of clustering, follows the "dry isentrope" curve.<sup>66</sup> Our expansions deviate from these conditions, since the  $P_0$  and  $T_0$  conditions were chosen to favor the formation of liquid acetylene clusters very early in the jet to facilitate our study of the phase transition to cubic solid. This phase transition is triggered by small cubic solid nuclei which form in the liquid clusters. Once these nuclei are formed, the new phase can grow through the cluster. We consider here two limiting cases for this freezing process.

### 5.3.1 Isothermal Transition

A picture representing the slow freezing of the clusters in an isothermal phase transition model is given in fig. 5.8a. This model would suggest that the clusters are all at the melting point during a phase transition, and the rate at which they transform is completely governed by the rate at which they lose energy to the surroundings. It is assumed that the energy released in freezing exceeds that which can be taken up by the supercooled liquid. The cluster would be partially liquid and partially solid, with the latter presumably on the surface where cooling occurs. In this picture, the temperature of both phases would be expected to be the same since, for clusters of this size, it is estimated that the temperature gradient will be less than  $10^{-2}$  K.<sup>67</sup> Clearly our experimental data are not consistent with this isothermal model.

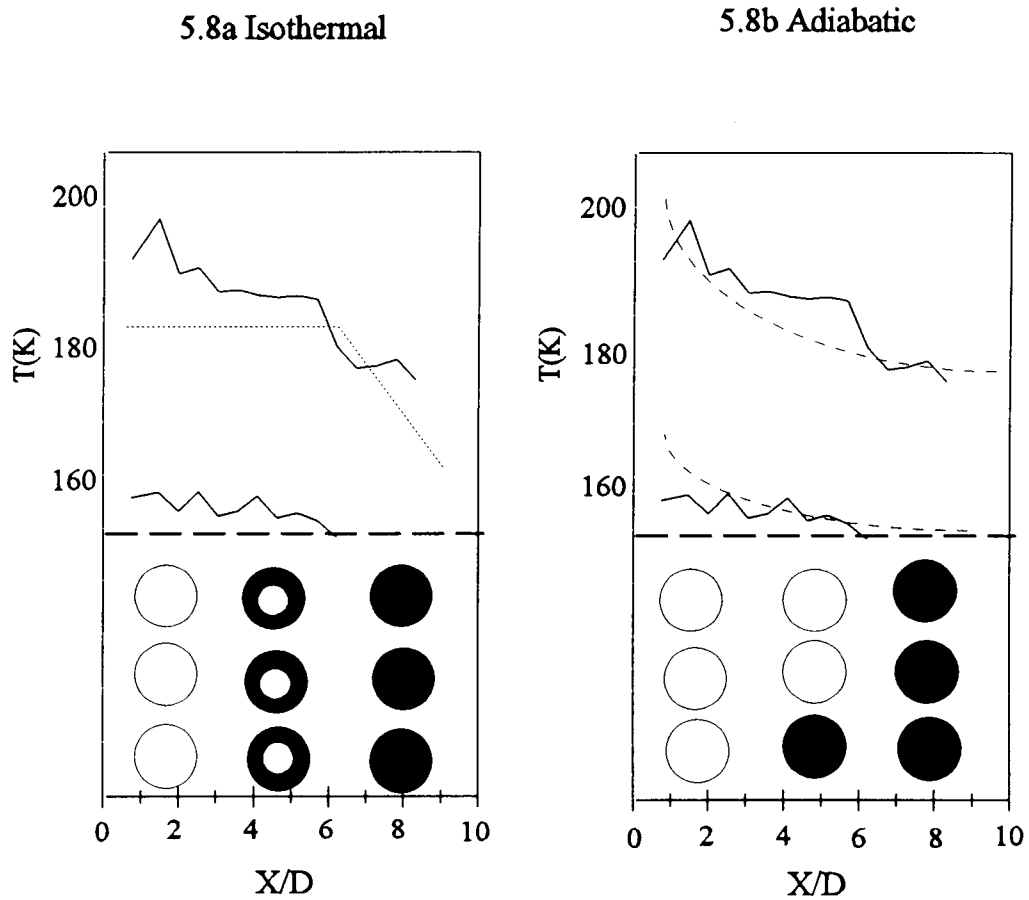


Fig. 5.8 Qualitative plots of the adiabatic and isothermal phase transition models are plotted with data. The data indicate a better match with the adiabatic model.

### 5.3.2 Adiabatic Transition

An adiabatic cooling model is shown in fig. 5.8b. Clusters which cool adiabatically would change phase rapidly relative to the rate at which they evolve heat to the surroundings. In this model a cluster is either entirely solid or entirely liquid and these will not be at the same temperature. The ratio of solid to liquid signal would represent the ratio of cubic clusters to liquid clusters at a point in the jet. Our data are in good accord with this adiabatic model. It is noteworthy that the temperature of the cubic clusters is essentially at 190 K, near the melting point of 192.7 K. Freezing at this temperature would release an amount of energy equal to  $\Delta H_{\text{fus}} = 3.785 \text{ kJ / mol}$ . This would cause a temperature change in the liquid of  $\Delta T = \Delta H_{\text{fus}} / C_{p(l)}$  of 33 K so that the supercooled temperature would be predicted to be 57 K, very close to our observed value of 55 K. This agreement offers support for the extrapolation of the bulk phase liquid  $T = f(v_2)$  relation into the supercooled region.

The data also bear on the question of how instantaneous is the adiabatic freezing of a small cluster, i.e. how rapid is it compared to the 3.5  $\mu\text{s}$  period of flight in which all liquid in our jet freezes to solid? In particular, if this process is slow on the measured time scale, then one would expect to have liquid and solid domains in the same cluster, with the temperature of both phases the same and rising from 155 K to 190 K as the freezing occurred. Again, there is no indication that this occurs at any point in the freezing zone of the expansion so that very rapid freezing is implied. This conclusion finds further support from an estimate of cluster growth rates outlined in the next section.

### 5.3.3 Crystal Growth Rate Calculation

Here we calculate the rate at which the solid grows through the liquid using the Wilson - Frenkel theory of diffusion limited flow rates as described by Bartell.<sup>68</sup> This theory gives a radial growth velocity of

$$Y = (D a / \Lambda^2) f_0 \exp(-\Delta S / R) (1 - \exp(-\Delta G / RT)) \quad (5.1)$$

where  $D$  is the diffusion coefficient,  $a$  is the distance between molecules,  $\Lambda$  is the mean free path in the liquid,  $f_0$  is a sticking fraction,  $\Delta S$  is the molar entropy change at the freezing point and  $\Delta G$  is the molar Gibbs energy of freezing at the supercooled temperature.  $D$  and  $\Lambda$  are given by

$$D = 3(\rho M k T)^{1/2} / 8\pi\rho d^2 M \quad (5.2)$$

$$\Lambda = 1 / (2^{1/2} \rho \pi d^2) \quad (5.3)$$

The difference in free energy is found through use of the relation  $(dG/dT)_p = -S$ . Solid and liquid acetylene have entropies which differ by 19.6 J / mol K at the freezing temperature. At this temperature, the difference in free energy between the two phases is zero. The difference in free energy between a supercooled liquid and a solid at the same temperature can be found from

$$\Delta G_v = \Delta S_{\text{fus}} \Delta T \quad (5.4)$$

where  $\Delta T$  is the difference between the supercooled transition temperature and the melting point.

To estimate the value of  $Y$ , we set the fraction of solid in the sample  $\alpha=1$  and use the cluster volume  $V$  calculated from the cooling curve. The growth rate  $Y$  calculated using the collision diameter and density from table 5.2 in equation 5.1 is 0.099 cm/s. According to Kaschiev's criterion for adiabatic phase transitions<sup>69</sup> the rate of nucleation must be far less than this rate of propagation

$$Y \gg J V^{4/3} \alpha^{1/3} \quad (5.5)$$

We compare this to 0.94 cm/s which was obtained from our experimental nucleation rates and equation 5.5. The estimate of the diffusion limited rate is one tenth the experimental rate, which suggests only a few nuclei may be formed when the liquid clusters freeze. This conclusion partially justifies our use of the relations we derive later that relate the nucleation rate to the interfacial free energy.

#### 5.3.4 Nucleation Rate

We assume here that the rate at which nuclei are formed  $J$  is the rate at which liquid clusters are transformed into solid. The best fit of the data yields  $J = 1.4 \times 10^{29} \text{ m}^{-3}\text{s}^{-1}$  at 155 K for 20 nm clusters. This rate is quite high but is in the range of  $J = 10^{27}$  to

$10^{30}$  observed by Bartell in electron diffraction measurements of freezing rates of other molecules. For example, Bartell found a nucleation rate of  $1.3 \times 10^{30} - 1.5 \times 10^{30} \text{ m}^{-3}\text{s}^{-1}$  for ammonia clusters<sup>60</sup> which were 8.6 nm in diameter.

The time it took to completely convert the liquid clusters into cubic solid clusters in the neat acetylene jet was 3.5  $\mu\text{s}$ . We can determine the amount of liquid and solid from the peak areas in the jet. We know approximately how fast the molecules are traveling from the free jet modeling, so we can measure the fraction of clusters in both phases as a function of time. The fraction of clusters which are in the cubic solid phase [ $1 - F(t)$ ] is plotted as a function of time in fig. 5.9. As shown by Bartell,<sup>60</sup>  $\ln[1 - F(t)]$  is a function of time  $(t - t_0)$ , nucleation rate  $J$ , and cluster volume  $V$

$$\ln(1-F(t)) = J V (t - t_0) \quad (5.6)$$

### 5.3.5 Interfacial Free Energy

Nucleation theory which was developed in ch. 2 can be extended to a study of the interfacial free energy between two phases in a cluster. To do this, the rate of phase transition and the free energy of the clusters are used to derive an expression which combines the rate at which the clusters are going through the phase transition with the energy required to overcome the interfacial tension between the host phase and the developing phase. The mean size of the clusters is also needed and for this we use the value of 20 nm obtained above from the cooling modeling.

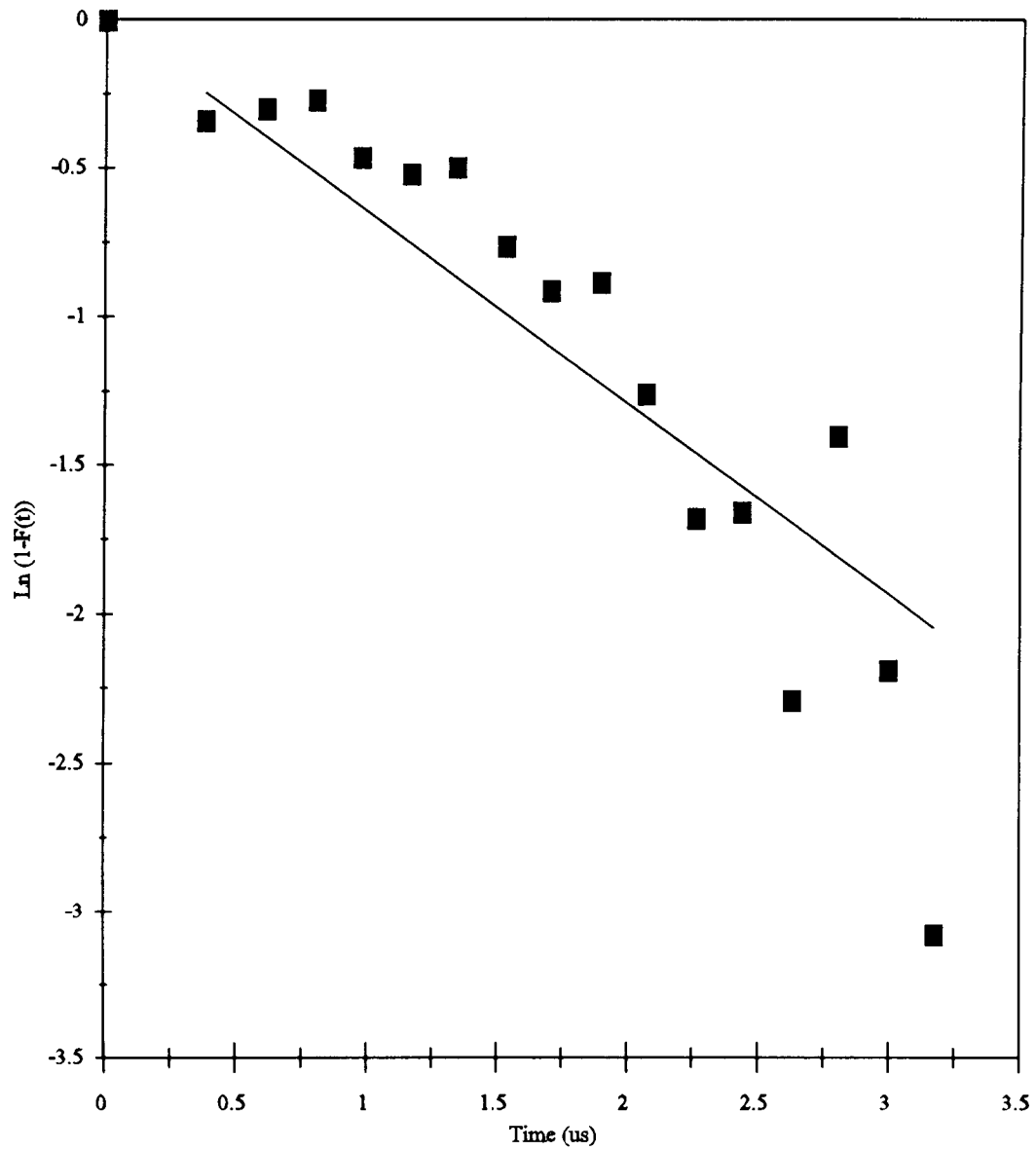


Fig. 5.9 The fraction of clusters frozen  $\ln(1-F(t))$  is fit with equation 5.6 using a cluster diameter of 20 nm to give a nucleation rate  $J$  of  $1.4 \times 10^{29} \text{ m}^{-3}\text{s}^{-1}$ .

The nucleation rate in a liquid host can be described classically<sup>70</sup>

$$J = [2(\sigma_{sl}kT)^{1/2} / (v_m^{5/3} \eta)] \exp(-\Delta G^*/kT) \quad (5.7)$$

where  $v_m$  is molecular volume,  $\eta$  is viscosity, and  $\sigma_{sl}$  is the liquid - solid interfacial free energy. A modified version of equation 2.26 based on thermodynamic aspects of nucleation theory is used to find the free energy barrier  $\Delta G^*$  to the formation of a critical nucleus this is written in terms of the free energy of freezing  $\Delta G_v$

$$\Delta G^* = 16 \pi \sigma_{sl}^3 / (3\Delta G_v^2) \quad (5.8)$$

One can determine the free energy of the interface  $\sigma_{sl}$  by using this expressions as described by Bartell and Huang.<sup>60</sup>  $\Delta G_v$  which is used in these calculations is found through the entropy of the transition and the temperature change as with  $\Delta G$  before. If the transition were isothermal,  $\Delta G_v$  would be zero, and we could not measure the interfacial free energy. We used  $\Delta S$  in table 5.2 to calculate  $\Delta G_v$  from

$$\Delta G_v = (T_m - T_2) \Delta S / V_m \quad (5.9)$$

where  $V_m$  is the molar volume of acetylene found from the density  $\rho = 0.613 \text{ g/cm}^3$  (l).<sup>61</sup>

When the experimental rate in 5.6 is found and used in 5.8,  $\sigma_{sl}$  can be found. The experimental rate of nucleation was found to be  $1.4 \times 10^{29} \text{ m}^{-3}\text{s}^{-1}$ . Our rate gives an

interfacial free energy of  $9.8 \text{ mJ/m}^2$  which we can compare to the known value for the liquid - gas surface tension of  $16.4 \text{ mJ/m}^2$  at  $193 \text{ K}$ , but it should be remembered that the liquid temperature is much lower.

We defer a comparison of this result to others until ch. 6, but we note here that Turnbull proposed a model for measuring the interfacial free energy between liquid and solid phases in non-metals<sup>71</sup>

$$\sigma_{sl} = k_T \Delta H / (v^2 N_a)^{1/3} \quad (5.10)$$

This equation uses the  $\Delta H$  and molecular volume  $v$  to determine the interfacial free energy. The constant  $k_T$  has a value of 0.32 for all non metals. From the known densities and  $\Delta H$  at the supercooled temperature for both the liquid - solid and solid - solid phase transition we get  $\sigma_{sl} = 11.9 \text{ mJ/m}^2$  and  $\sigma_{ss} = 8.7 \text{ mJ/m}^2$ .

It is interesting to consider the size of the critical nucleus which triggers the freezing in our clusters. From equation 2.25, we can find the critical radius in terms of the interfacial free energy and  $\Delta G_v$

$$r^* = 2\sigma / \Delta G_v \quad (5.11)$$

Using the free energy difference  $\Delta G_v$  at  $155 \text{ K}$  of  $1.74 \times 10^7 \text{ J / m}^3$  and our interfacial free energy value of  $9.8 \text{ mJ/m}^2$ , we get a critical nucleus radius of  $1.12 \text{ nm}$ . This corresponds to about 84 molecules or 21 unit cells.

### 5.3.6 Solid - Solid Interfacial Free energy

An attempt is made here to deduce the solid - solid interfacial free energy from the rate of transformation from cubic solid to orthorhombic solid. This procedure is similar to that done for the liquid-solid transition. From measured values of the fraction of orthorhombic clusters  $F(t)$ , the data was fit using eq. 5.6 and is plotted in fig. 5.10. The 20 nm diameter found from the cooling curves was used to deduce a  $J$  value of  $2.8 \times 10^{28} \text{ m}^{-3} \text{ s}^{-1}$ . This rate is 5 times smaller than the value deduced for the freezing process, presumably because of the much smaller deviation from the equilibrium temperature for the phase transition.

We would like to use this experimental value of  $J$  to calculate the surface tension  $\sigma_{ss}$  for the cubic - orthorhombic interface. However, the rate equation must be modified to eliminate viscosity for the solid host phase because the phase change does not involve translational movement in the lattice, but rather a simple reorientation and contraction. Accordingly we modify the equation to express the nucleation rate in terms which include librational frequencies of the molecules and energy barriers to rotation.

The kinetic model for nucleation presented in chapter 2 is essentially built around the basic equation for reaction dynamics

$$J = A \exp(-\Delta G^*/kT) \quad (5.12)$$

To apply this to nucleation in a solid, we must make sensible choices for the kinetic prefactor  $A$  and the energy barrier of the reaction  $\Delta G^*$ . Previous authors have related the

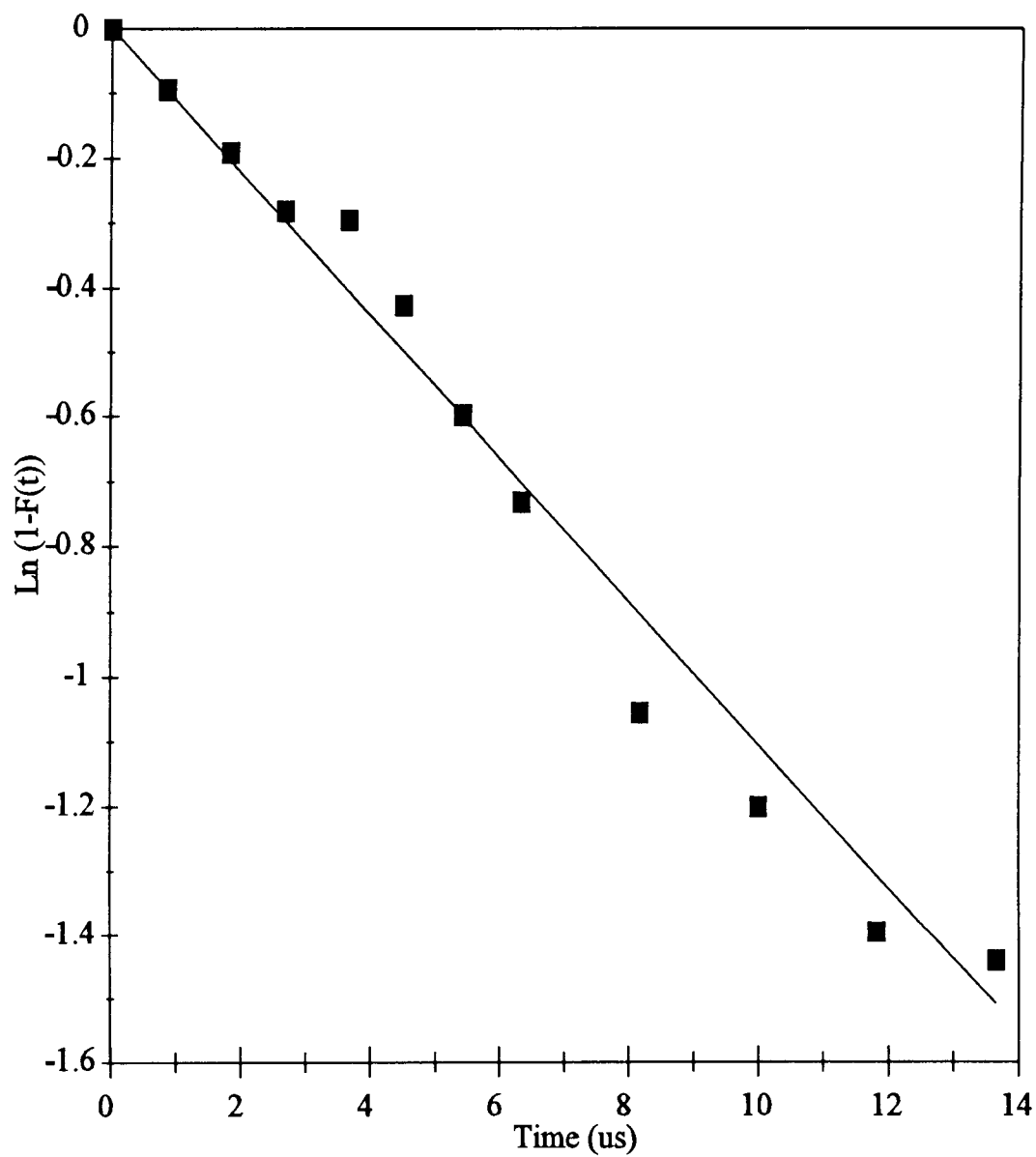


Fig. 5.10 The fraction of orthorhombic solid vs time is plotted and fit with eq. 5.6 to give a rate of  $2.8 \times 10^{28} \text{ m}^{-3} \text{ s}^{-1}$ .

prefactor to the interfacial free energy  $\sigma_{ss}$  and a frequency of interaction  $\nu$  (typically a librational mode of the crystal that promotes the phase transition).

$$A = (2(\sigma_{ss} / kT)^{1/2} / \nu^{2/3}) \nu \exp(-E / kT) \quad (5.13)$$

Here  $E$  is the energy barrier for motion which provides the phase change. This should be distinguished from the exponential term involving  $\Delta G^*$  which represents the energy necessary to form a critical nucleus of radius  $r^*$ . We take  $\Delta G^*$  to have the same form as previously (eq. 5.8) and, since the exact extent of cooling is unknown, we will consider a range of values.

To estimate  $E$ , the barrier for rotation of the  $C_2H_2$  molecule by  $45^\circ$  in going from the cubic to orthorhombic structure, we make use of the measured value of  $22 \text{ cm}^{-1}$  for the librational mode which promotes conversion. The energy  $E$  was estimated by assuming that the potential well of the molecule is a harmonic oscillator. The energy levels are found from

$$E = 1/2\pi(k/I)^{1/2} \quad (5.14)$$

$$E = (\nu + 1/2) h\nu \quad (5.15)$$

and the force constant was found from

$$k = (2 \pi \nu)^2 I \quad (5.16)$$

The moment of inertia  $I$  for acetylene was calculated from bond distances and masses to be  $3.19 \times 10^{-46} \text{ kg m}^2$ . For  $\nu = 1$ , a vibrational angular displacement of  $28^\circ$  was found. A total travel of  $45^\circ$  is needed to change the orientation from the cubic conformation to the orthorhombic, so we assume that rotating half this distance would be sufficient to cross into the orthorhombic potential well. This gives  $E = 3/2(22 \text{ cm}^{-1}) = 394 \text{ J/mole}$ . For values of  $\sigma$  of the order of  $1 - 10 \text{ mJ/m}^2$ ,  $A$  is about  $10^{38} \text{ m}^{-3}\text{s}^{-1}$ , a value about an order of magnitude lower than the corresponding factor in the case of the liquid to solid transition.

Using the experimental  $J$  value, equations 5.8 and 5.12 were then used to calculate the values for the interfacial free energy as a function of supercooling below the phase transition temperature. The results are plotted in fig. 5.11 where the range in  $r^*$  corresponds to a critical nucleus varying from 1300 to 60 unit cells. The nucleus size observed for the liquid is about 20 unit cells and for this size,  $\sigma_{ss}$  would be  $9 \text{ mJ/m}^2$ . Interestingly, this is the same value one obtains if one assumes Turnbull's empirical relation for  $\sigma_{sl}$  can also be applied for  $\sigma_{ss}$ . However this size would require an undercooling of about 30 K which greatly exceeds our estimate of  $\sim 5 \text{ K}$  for the maximum  $\Delta T$  that would be consistent with our temperature uncertainties. The latter corresponds to a value of  $\sigma_{ss}$  of  $2.6 \text{ mJ/m}^2$ . Although it is not possible to specify a definite value for  $\sigma_{ss}$ , from this analysis, a value near  $1 \text{ mJ/m}^2$  is deemed reasonable. It may be noted that this  $\sigma_{ss}$  value is comparable in size to values of  $3.2 \text{ mJ/m}^2$  and  $4.4 \text{ mJ/m}^2$  for  $\sigma_{ss}$  which were deduced by Bartell for  $(\text{CH}_3)_3\text{CCl}$  and  $\text{SeF}_6$  respectively.<sup>72</sup>

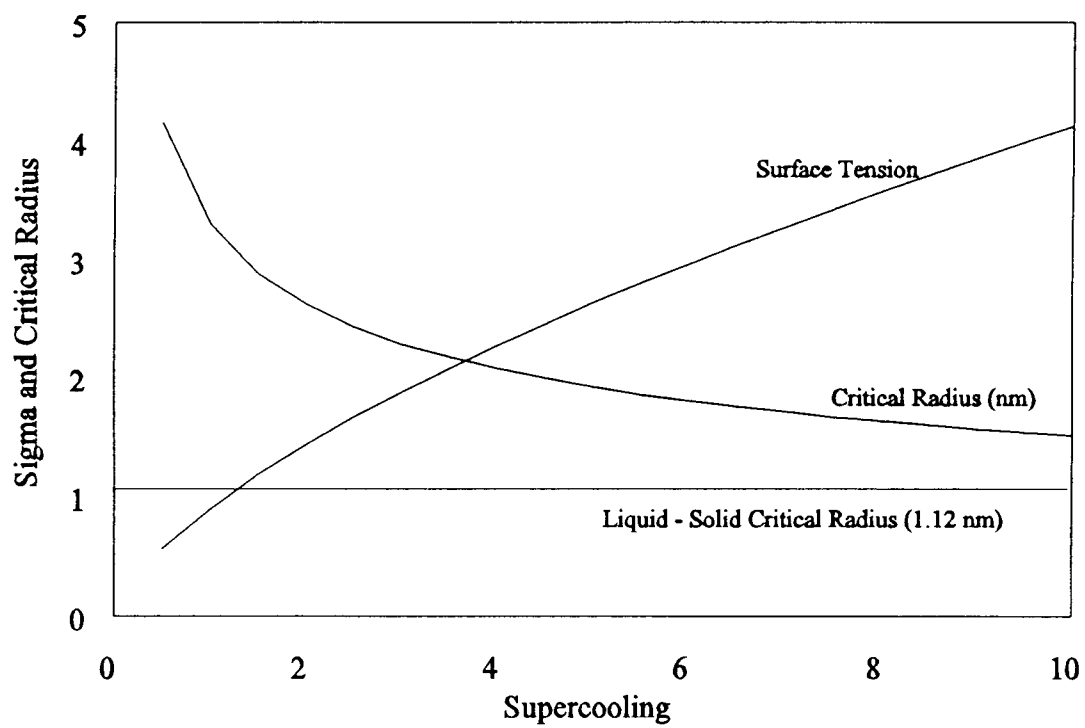


Fig. 5.11 Interfacial free energy is plotted as a function of the critical radius with  $v = 22 \text{ cm}^{-1}$ ,  $E = 394 \text{ J/mol}$  and  $J = 2.8 \times 10^{28} \text{ m}^{-3} \text{ s}^{-1}$ .

## 6. Acetylene Mixes

As part of this thesis work, we were also interested to find out if variation of the mean cluster size might influence the interfacial free energy or affect the temperature ranges in which the condensed phases exist. To achieve this, we used mixes of acetylene in helium to produce colder and smaller clusters for which similar properties could be measured as for neat expansions. In some studies initial jet expansion conditions were also selected to produce clusters which were going through the solid - solid phase transition immediately after leaving the jet. By producing cubic solid as the initial phase, we were able to measure the solid - solid interfacial free energy for smaller clusters in the first part of the jet. We also found it possible to measure cluster diameters from newly discovered peaks attributed to surface layers in small clusters of acetylene. The contribution of these layers are most pronounced in clusters which have diameters less than 10 nm. Also, we explored the possibility of detecting very small clusters such as dimers and trimers, etc. or larger aggregates in new metastable solid phases.

### 6.1 Mix Data

#### 6.1.1 Experimental Conditions

Five sets of data were collected from jets of acetylene mixed in helium; a 50% mix at 7 atm and 220 K, 12% mixes at 27 and 29 atm at 200 K, a 10% mix at 27 atm and 213

K, and a 4% mix at 31 atm and 185 K. Corresponding spectra are presented in figs. 6.1 - 6.5 and the peak frequency and temperature data for all mixes are presented in tables 6.1 - 6.5. The 50% mix produced about 80% clustering, and the extent of clustering is listed for the 4%, 12% and 10% mixes in table 6.6. A summary of temperatures for each phase is provided in table 6.7.

### 6.1.2 First Phases Formed for All Conditions

The nascent phase of acetylene produced in the jet varies according to the initial conditions. The spectrum of each expansion taken closest to the nozzle is shown in fig. 6.6. The neat and 50% mix show very similar spectra, which include a large liquid peak and a small cubic solid peak. The 10% and 12% spectra at 27 atm show cubic solid as the first phase. The colder of the two (at 200 K) shows a trace of all three condensed phases present. The 29 atm 12% and the 31 atm 4% expansions show only orthorhombic solid in relatively small clusters formed in these more rapidly cooling conditions. All of the peaks in the mix spectra can be assigned to known condensed phases except for the large peak which appears at  $\sim 1960 \text{ cm}^{-1}$  in the 4 - 12% mixes. Although this peak is close to the position of the  $B_{3g}$  peak of the orthorhombic solid, it is far more intense than one would expect for such a mode, a point considered later. There is also an intriguing new broad feature on the high frequency side of the  $1960 \text{ cm}^{-1}$  peak which is particularly apparent in the spectra of the 4% mix (fig. 6.5). Possible sources for this feature are also discussed.

Table 6.1 Amix: 50% acetylene in He, 220 K, 7 atm

X/D	Liquid T liquid(K)	Cubic T cubic (K)	% cubic
0.8	1955.641	152.1 1953.185	177.7 0.287
1.2	1955.327	146.5 1953.295	187.8 0.176
2	1955.333	146.3 1953.428	192.5 0.263
3	1955.105	141.2 1953.115	176.1 0.367
3.5	1955.086	139.4 1953.169	180.3 0.375
4	1954.989	139.2 1952.884	167.4 0.489
4.4	1955.121	141.9 1953.207	183.8 0.385
4.8	1955.025	140.2 1952.932	166.2 0.354
5.2	1955.167	140.3 1952.938	166.2 0.601
5.6	1954.929	137.6 1952.845	160.0 0.685
6	1954.843	135.3 1952.955	165.9 0.687
6.4	1954.717	133.7 1952.817	157.5 0.907
6.8		1952.822	158.5 1
7.2		1952.724	151.1 1

Table 6.2 Emix: 12% acetylene in He, 200 K, 29 atm

X/D	New	Ortho.	Cubic	New - Ag	T Cub	T Orth	T New	A Ag/A New
0.7	1958.2	1950.0	1952.8	8.2	158	110	109	1.63
0.8	1958.5	1950.2	1953.3	8.2	189	119	108	1.55
1	1958.1	1949.9		8.2		105	109	2.53
1.2	1958.1	1950.0	1952.6	8.0	147	110	124	2.84
1.6	1957.9	1949.7	1951.5	8.1		97	115	2.41
2.4	1958.0	1949.6		8.3		95	94	3.12
3.2	1958.0	1949.5		8.4		92	89	2.69
4	1957.7	1949.2		8.4		77	84	4.12
6	1957.8	1949.1		8.6		75	69	1.85

Table 6.3 Imix: 4% acetylene in He, 185 K, 31 atm

X/D	Ortho.	New	New - Ag	T Ag	T B3g	A Ag	A New
0.4	1949.0	1958.0	9.0	68	32	19.88	13.1
0.5	1948.8	1957.9	9.0	63	28	31.46	29.0
0.6	1949.4	1957.8	8.4	86	90	38.79	31.6
0.7	1949.4	1958.2	8.7	88	61	41.41	19.8
0.8	1952.1	1958.3	6.2	195	307	0.664	2.88

Table 6.4 Gmix: 12% acetylene in He, 200 K, 27 atm.

X/D	New	Ortho.	Cubic	New - Ag	A Orth	A Cub	A New	T orth	T cub	T New	A Ag/A New
0.4		1950.5	1952.7		1.05	3.95	1.50	129	151		0.69
0.5	1958.5	1950.3	1952.8	8.1	3.15	3.97	1.59	124	159	117	1.98
0.6	1958.4	1950.7	1952.7	7.6	2.38	5.88	1.65	141	152	162	1.44
0.8	1958.3	1950.2	1952.7	8.1	5.08	5.49	1.82	118	148	118	2.78
1	1958.1	1950.1	1952.7	7.9	4.59	5.47	1.34	114	150	133	3.40
1.2	1958.1	1950.2	1952.6	7.9	4.88	3.23	0.82	117	146	137	5.91
1.6	1958.2	1950.3	1952.6	7.8	5.42	4.01	1.41	124	147	146	3.84
2	1958.2	1950.0		8.2	6.31		0.91	109		112	6.89
2	1958.1	1950.2	1952.3	7.8	4.87	4.06	1.59	119		142	3.05
2.8	1957.9	1949.7		8.1	5.21		0.50	99		113	10.2
4	1957.8	1949.7		8.1	5.30		0.67	97		117	7.84
6	1957.9	1949.4		8.4	4.79		1.16	85		85	4.10
8	1957.7	1949.1		8.6	3.32		0.49	71		66	6.73
10	1957.5	1949.0		8.5	4.8		1.01	70		80	4.76

Table 6.5 Hmix: 10% acetylene in He, 213 K, 27 atm.

X/D	New	Ortho.	Cubic	New - Ag	A New	A Orth	A Cub	T Orth	T Cub	T New	A Ag/A New
0.4	1958.2		1953.1		1.08		2.45		175		
0.6			1952.8				5.37		158		
0.8		1950.4	1952.8			0.49	6.12	125	158		
1	1958.9	1950.5	1953.1	8.3	0.97	0.75	3.94	133	178	100	0.77
1.2	1958.5	1950.5	1953.1	8.0	0.90	0.46	3.64	130	177	127	0.51
1.4		1950.0	1952.8			2.02	5.96	111	155		
1.6	1958.3	1950.2	1953.1	8.0	5.42	1.57	5.44	120	178	129	0.29
2	1958.6	1950.3	1953.2	8.3	2.83	2.34	4.12	120	180	96	0.82
2.4	1958.1	1950.3	1953.3	7.8	2.21	2.78	2.03	120	185	143	1.25
2.8	1958.4	1950.3	1952.9	8.0	2.91	4.32	5.94	123	166	128	1.48
3.2	1958.1	1950.1	1952.0	8.0	2.1	3.73	6.33	114		126	1.77
3.6	1958.1	1949.9	1952.0	8.1	1.43	4.13	3.23	106		116	2.89
4	1958.0	1949.8	1951.5	8.2	1.70	4.61	3.32	100		106	2.71
4.4	1957.9	1949.8	1954.0	8.1	1.49	5.16	3.60	100		113	3.46
4.8	1958.0	1949.8	1952.1	8.2	1.31	5.67	3.17	100		112	4.33
6	1958.0	1949.5	1952.2	8.4	1.73	4.21	3.19	91		90	2.43

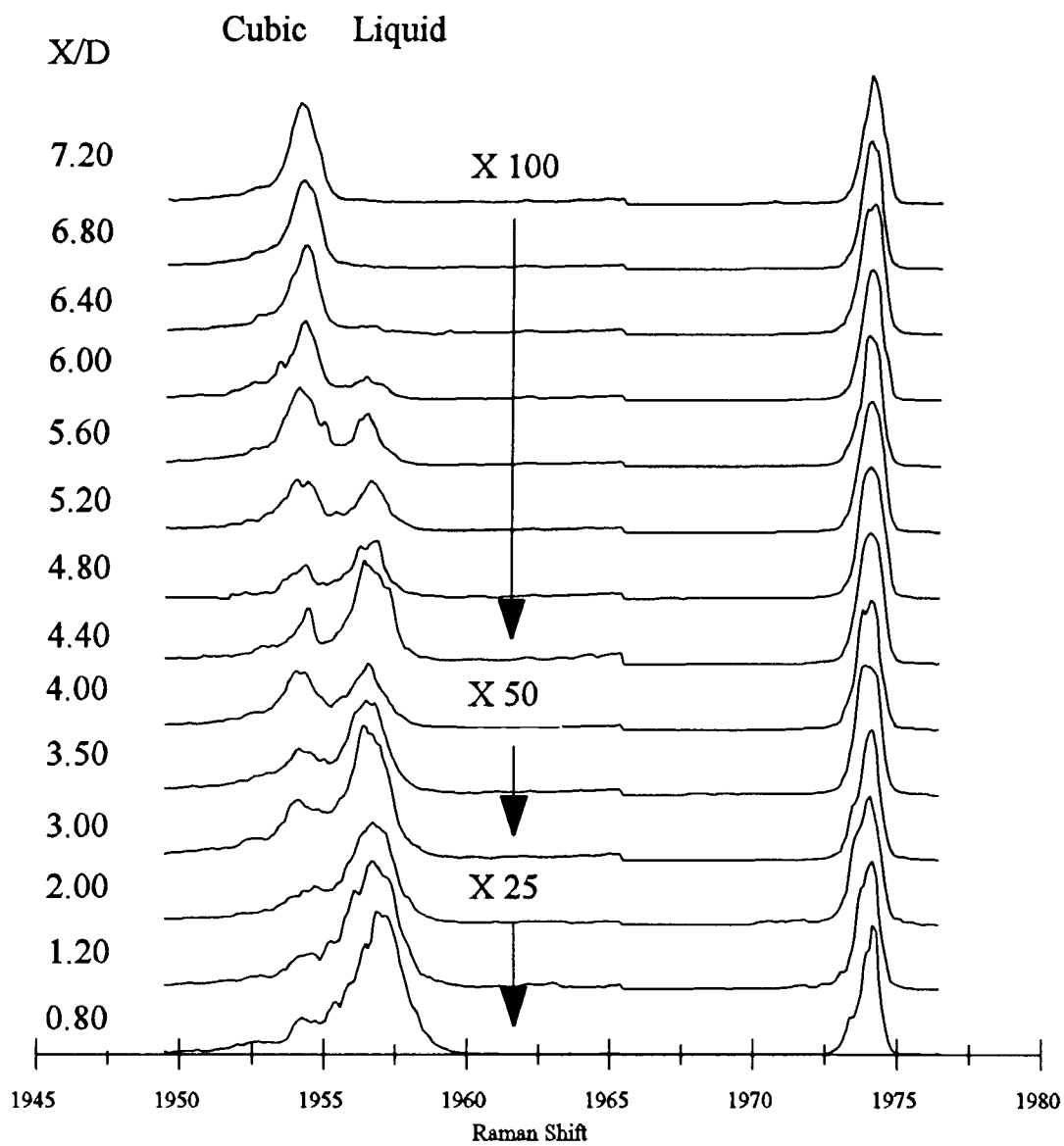


Fig. 6.1 50% acetylene in He, 220 K, 7 atm. showing the complete liquid to solid transition in  $\sim 18$  nm clusters.

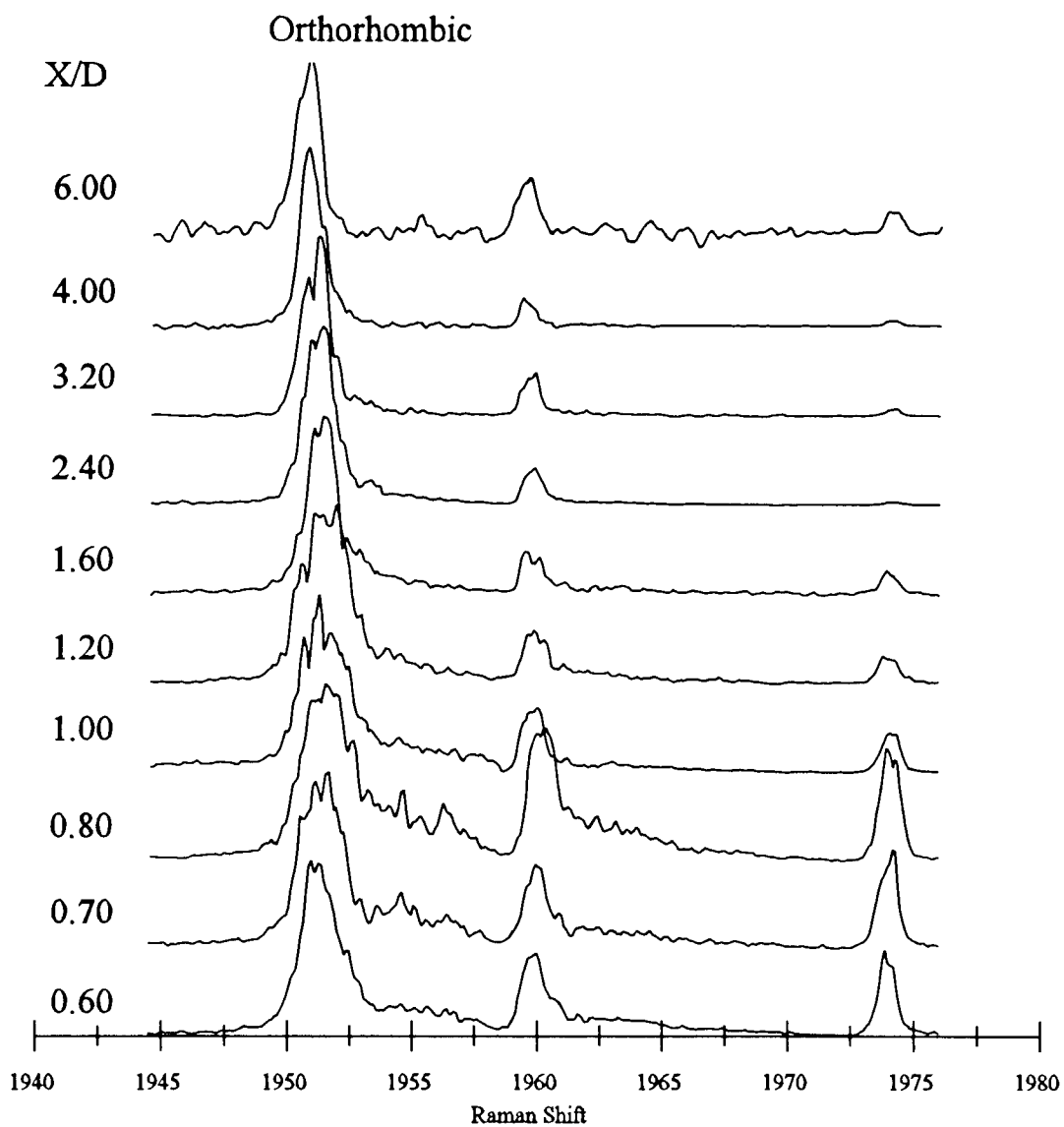


Fig. 6.2 12% acetylene in He, 200 K, 29 atm. showing a large new feature.

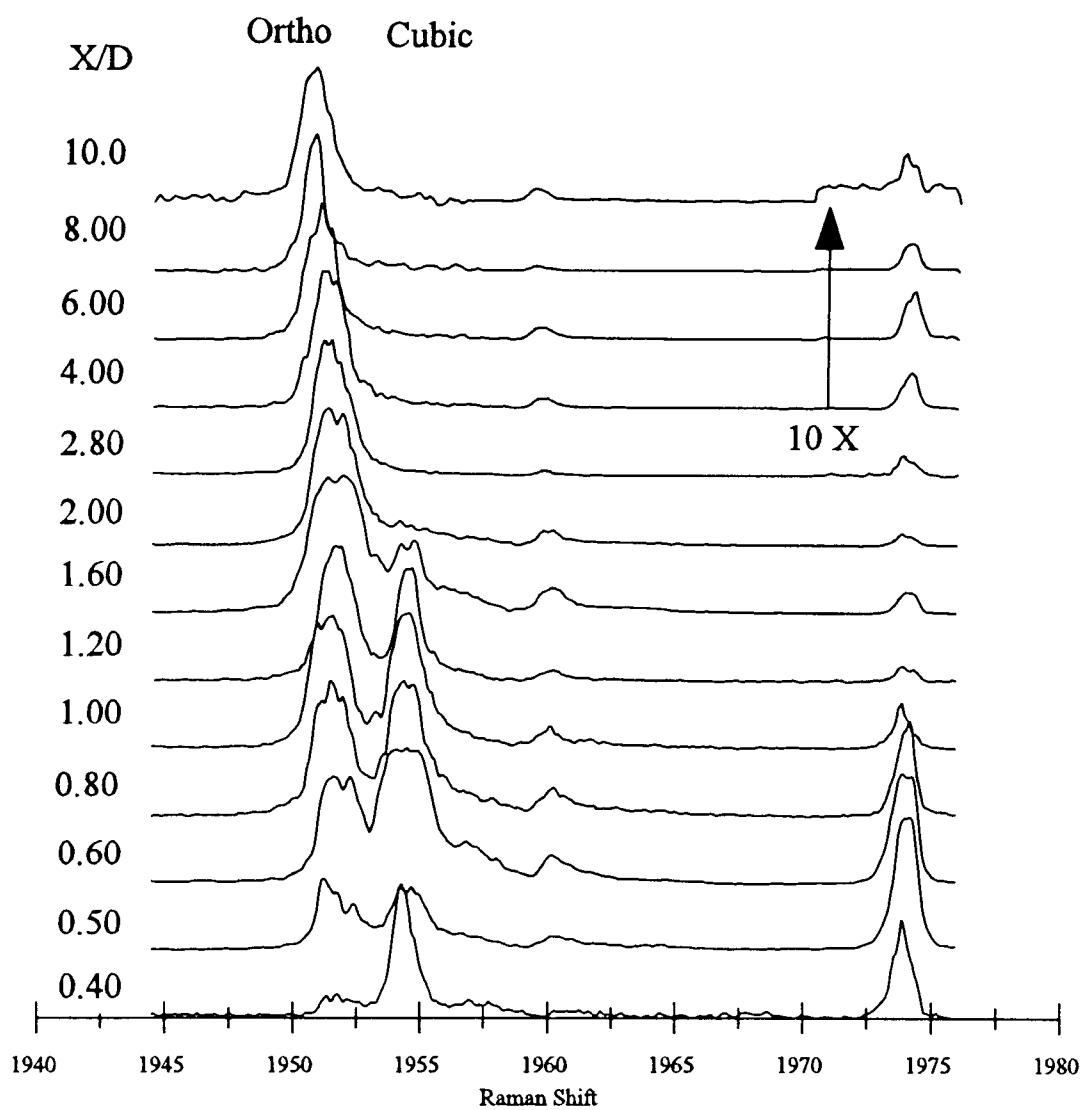


Fig. 6.3 12% acetylene in He, 200 K, 27 atm. showing the complete transition from cubic solid to orthorhombic solid, and a new feature at  $1960 \text{ cm}^{-1}$ .

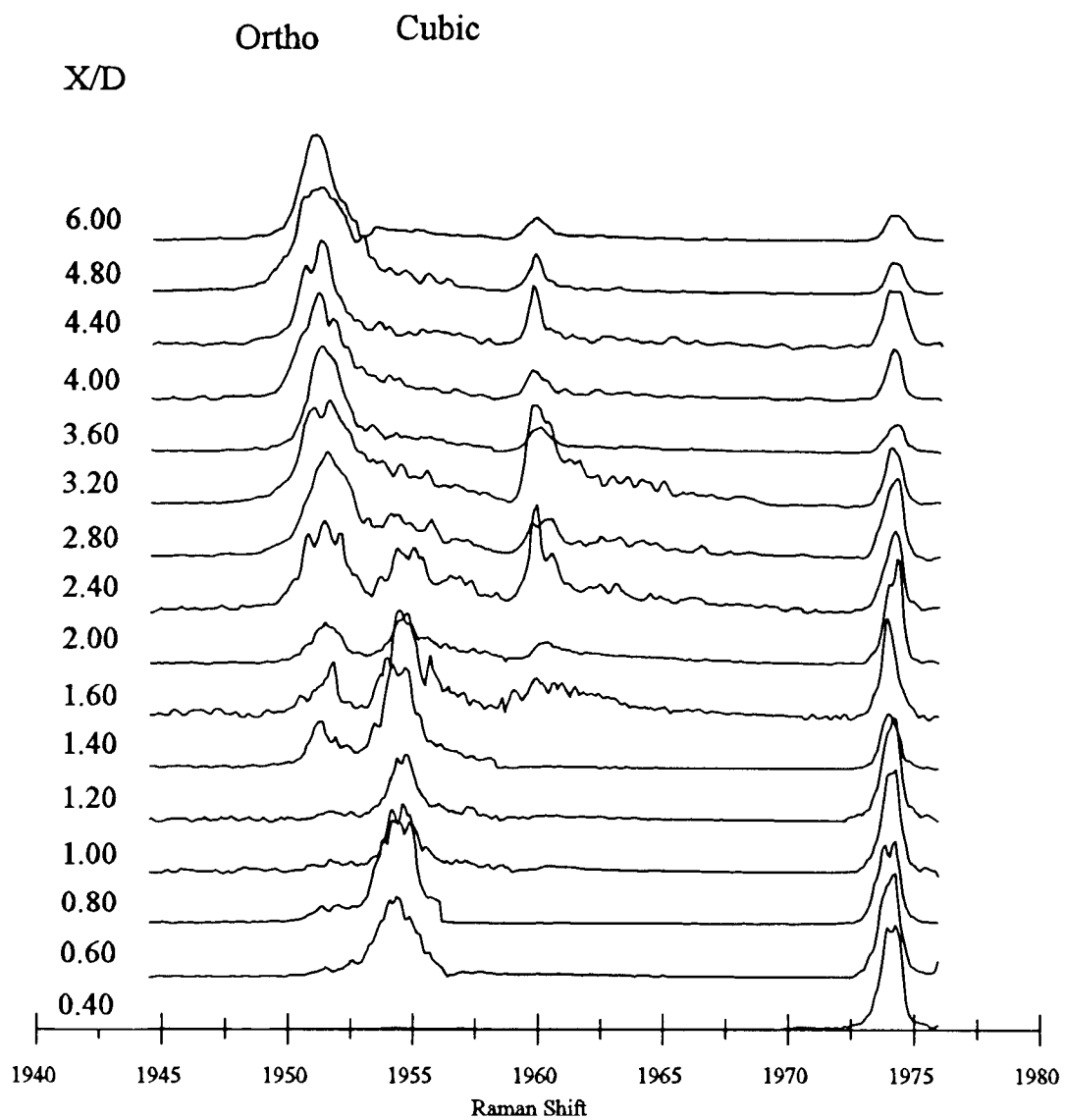


Fig. 6.4 10% acetylene in He, 213 K, 27 atm. showing the complete cubic solid to orthorhombic solid transition.

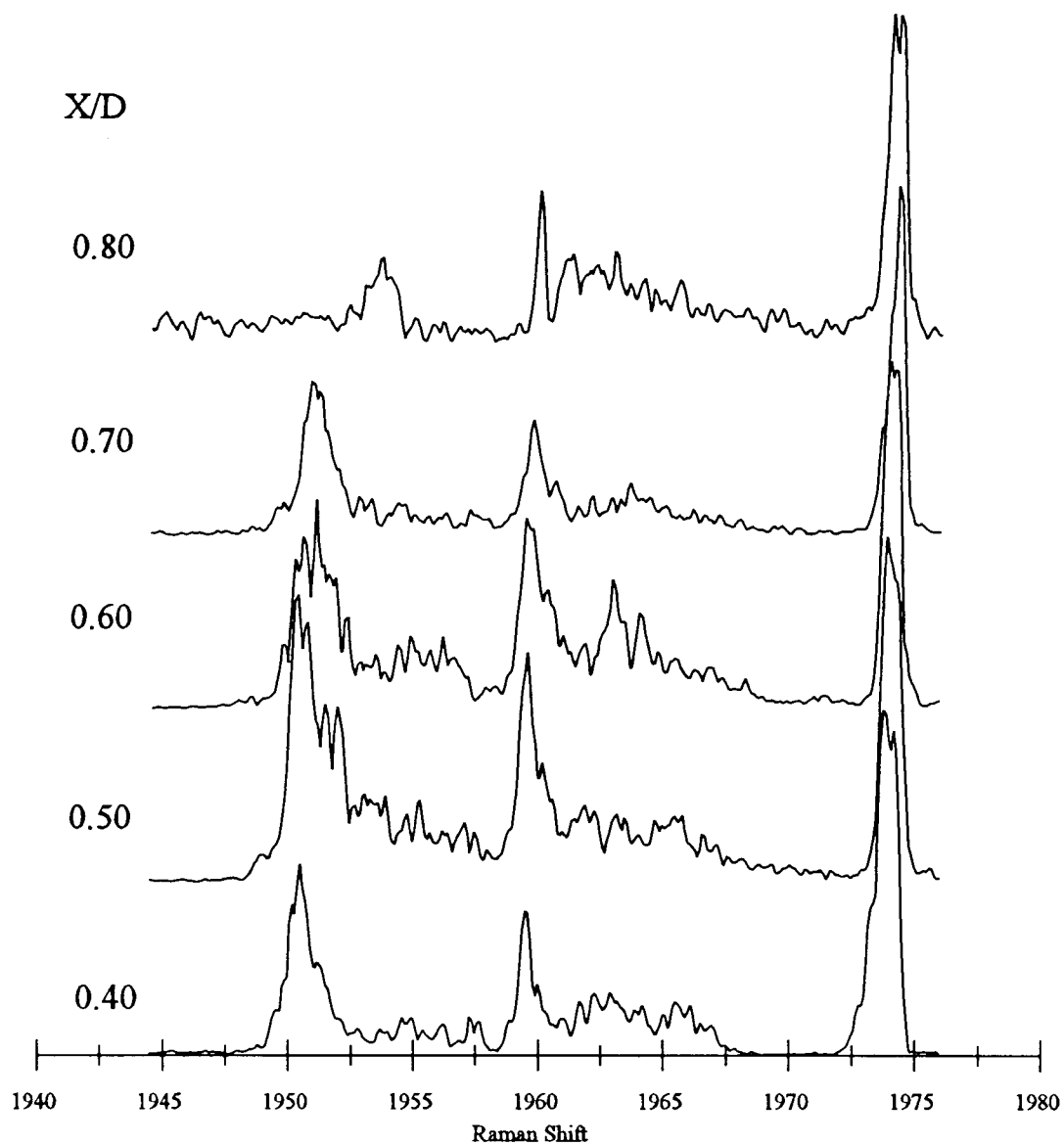


Fig. 6.5 4% acetylene in He, 185 K, 31 atm. showing a new feature at 1960  $\text{cm}^{-1}$ .

Table 6.6 Percent clustering for acetylene mixes

X/D	12% 29 atm 200 K	12% 27 atm 200 K	10% 27 atm 213 K	4% 31 atm 185 K
0.4		0.76	0.51	0.82
0.5		0.71		0.84
0.6	0.86	0.8	0.64	0.82
0.7	0.82			0.8
0.8	0.86	0.85	0.7	0.74
1	0.86	0.89	0.64	
1.2	0.88	0.9	0.63	
1.4			0.8	
1.6	0.88	0.91	0.82	
2		0.9	0.75	
2.4	0.96		0.7	
2.8		0.98	0.84	
3				
3.2	0.9		0.91	
3.5				
3.6			0.85	
4	0.92	0.93	0.86	
4.4			0.8	
4.8			0.88	
5.2				
5.6				
6	0.84	0.92	0.91	
6.4				
6.8				
7.2				
8		0.92		
10		0.9		

Table 6.7 Temperature of acetylene condensed phases

X/D	50% 7atm 220 K		12% 29atm 200 K		12% 27atm 200 K		10% 27atm 213 K		4% 31 atm 185 K
	Liquid	Cubic	Cubic	Ortho	Cubic	Ortho	Cubic	Ortho	Ortho
0.4					151	130	175		68
0.5					159	124			63
0.6				97	152	141	159		86
0.7			159	111					88
0.8	152	177	190	120	148	119	158	126	195
1				106	150	114	179	133	
1.2	146	187	147	110	146	117	177	131	
1.4							155	111	
1.6				98	147	124	179	120	
2	147	192				110	181	120	
2.4				95			185	120	
2.8						100	167	124	
3	142	176							
3.2				92				114	
3.5	140	180							
3.6								106	
4	140	167		78		97		101	
4.4	141	183						100	
4.8	140	165						100	
5.2	141	166							
5.6	138	160							
6	136	165		75		86		91	
6.4	133	157							
6.8		158							
7.2		151							
8						72			
10						70			

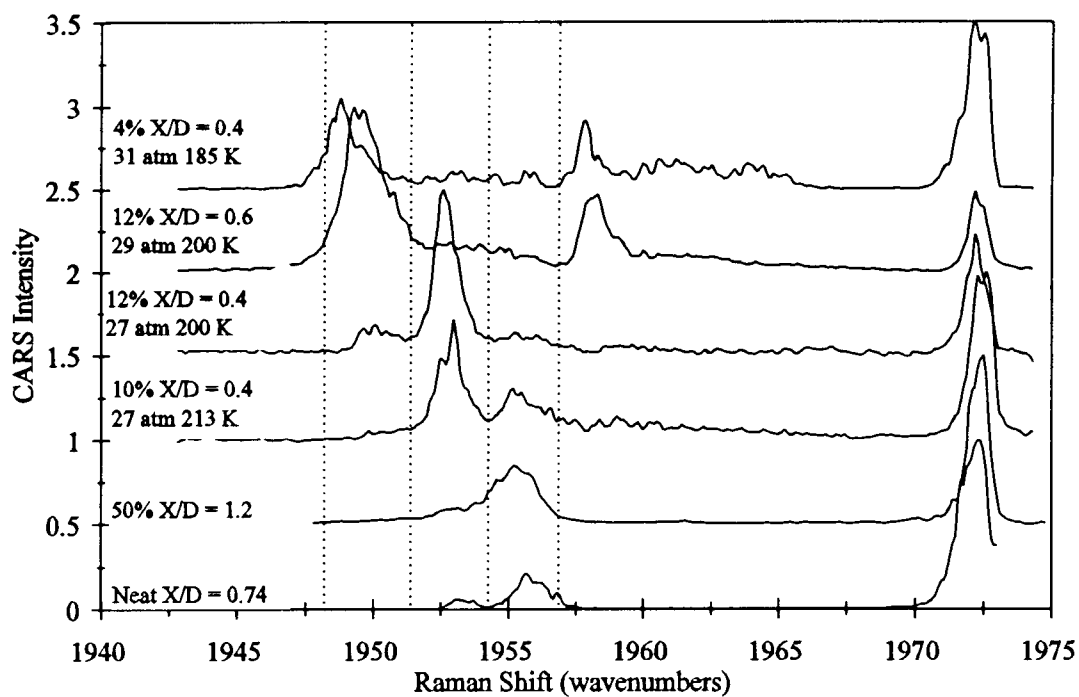


Fig. 6.6 The first condensed phase of acetylene which is seen depends on the mix and the initial conditions.

## 6.2 Cooling Curves and Phase Transitions

### 6.2.1 Adiabatic Nature of Cooling

As noted in the last chapter, for an adiabatic transition, the temperature difference between the liquid and solid in the T vs. X/D curves for clusters in a jet should be  $\Delta H_{\text{fus}}/C_p$  (33 K). Liquid and solid temperatures for clusters in the 50% mix are graphed with those for the neat data in fig. 6.7. It is clear that more extensive supercooling is obtained for the mix expansion the temperature difference between the cubic and the liquid clusters in the neat sample is an average of 41 K, the average difference between liquid and solid in the mix data is 31 K. Since these are near the calculated 33 K, the heat of fusion can be considered to be stored entirely in the cluster. By assuming that the phase transition is completely adiabatic and is limited by the nucleation rate, we can deduce the nucleation rate from the measured rate of freezing.

### 6.2.2 Liquid - Solid Interfacial Free Energy

The interfacial free energy for the phase transition from liquid to solid acetylene was studied in the neat jet in the previous chapter and an analogous treatment is done here. The entire liquid to solid phase transition is present only in the 50% mix data set, so it alone will be compared to the neat data set. The total time it took to convert the liquid clusters into solid clusters was 2.2  $\mu\text{s}$  for the 50% mix as compared to 3.5  $\mu\text{s}$  in the neat data. We check the assumption that the nucleation is the rate limiting step by using Kaschiev's criterion eq. 5.5. We find that the growth rate must be in excess of 0.80 cm/s

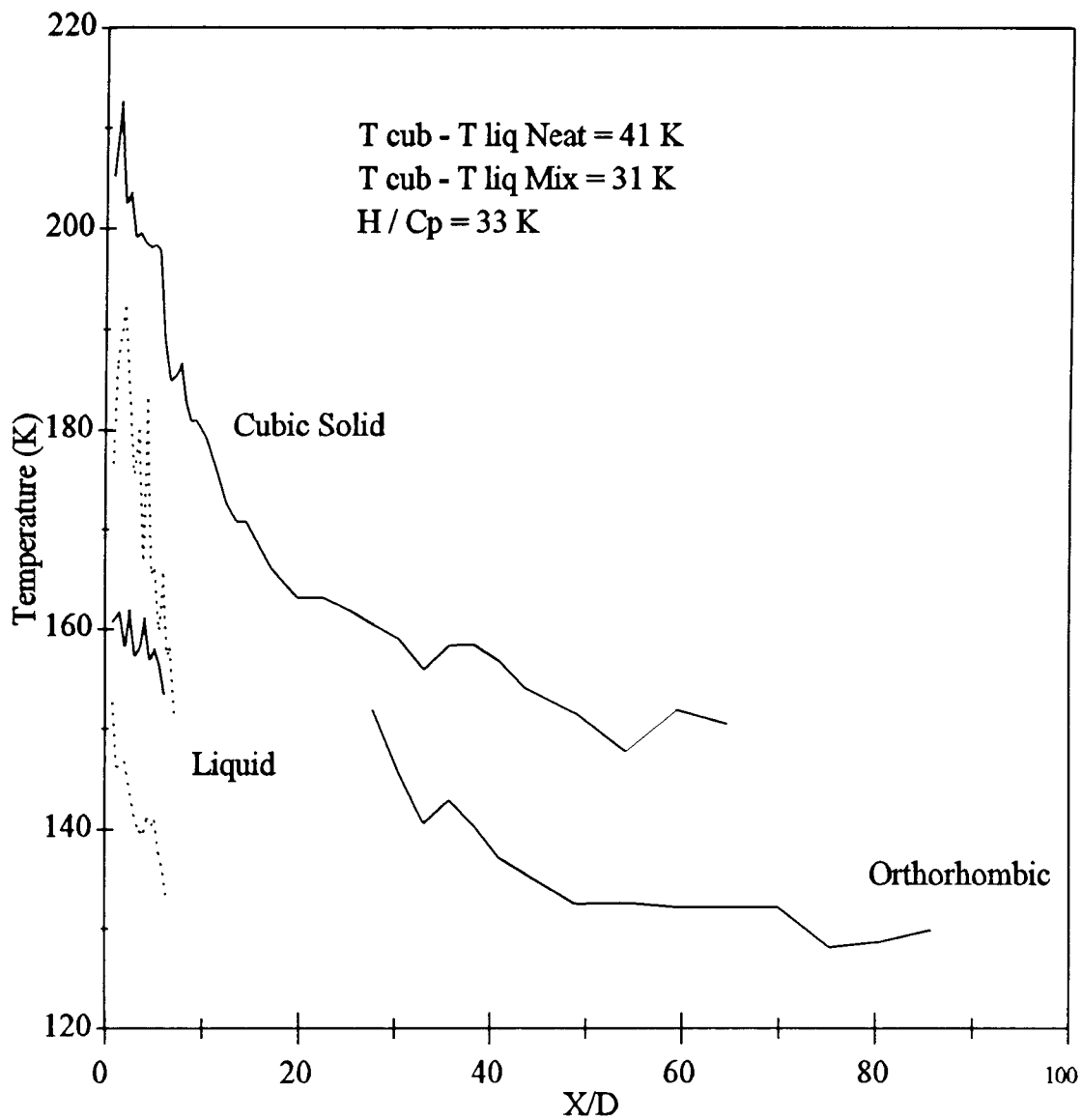


Fig. 6.7 Temperature vs. X/D curves for the 50% mix (dashed lines) and the neat (solid lines) jets, both have the liquid to cubic solid phase transition.

to satisfy the criterion. The calculated growth rate is 0.13 cm/s so once again the growth rate is greater than the transition rate and nucleation is the rate limiting step. From the data presented in fig. 6.1, the square-rooted peak areas can be used to determine the fraction of the clusters which are in each phase and this is graphed in fig. 6.8. A cluster diameter of 18 nm is found from the cooling curve (fig 6.9), and the rate of nucleation can be calculated for the mix clusters of this size from  $F(t)$  (eq. 5.6). The result is  $1.8 \times 10^{29}$  mol/m<sup>3</sup>s, whereas the rate for the neat data was  $1.4 \times 10^{29}$  mol/m<sup>3</sup>s.

By substituting the nucleation rate calculated from eq. 5.6 into eq. 5.8, an interfacial free energy of 11.6 mJ/m<sup>2</sup> is obtained. This is slightly higher than 10.1 mJ/m<sup>2</sup> that the neat spectra gave, a fact which can be attributed to the colder temperature of the supercooled liquid in the mix (140 K) compared to that of the neat liquid (155 K). Similarly, the critical radius for this colder liquid is somewhat smaller, 0.97 nm, corresponding to about 54 molecules.

### 6.2.3 Solid - Solid Interfacial Energy

In the previous chapter we concluded that the transition from cubic solid to orthorhombic solid was also an adiabatic transition and we make the same assumption in this chapter for the mix data. The time it takes to complete a transition from cubic solid to orthorhombic is much shorter than that for the neat clusters. The 12% mix at 27 atm and 200 K finished the transition in 0.43 μs, while the 10% mix at 213 K and 27 atm finished in 0.57 μs. To measure the cluster diameters, cooling curves were not used because the scans did not have very many points and the temperature data was not very accurate due

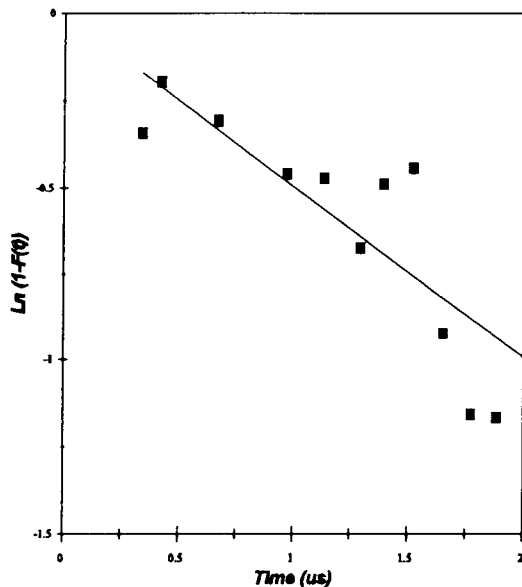


Fig. 6.8 Fraction of clusters frozen in the 50% mix fit with equation 5.6 giving a nucleation rate of  $1.8 \times 10^{29} \text{ m}^{-3}\text{s}^{-1}$ .

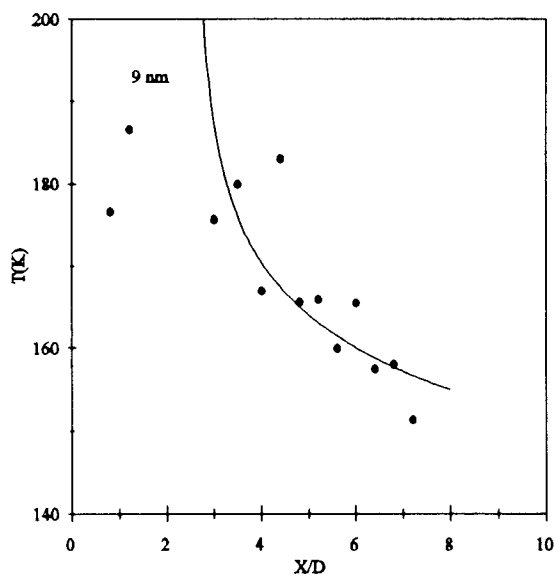


Fig. 6.9 Cooling curve fit to the cubic temperature data of the 50% mix jet gives an 18 nm diameter for the clusters.

to the width of the peaks. Instead a size was deduced from areas of peaks attributed to core and surface layers of the small clusters. In the next section we discuss surface to volume ratio measurements which were used to deduce a cluster diameter of 10 nm for the 10% and 12% mixes. The same method that we used for calculating  $\sigma_{ss}$  in the previous chapter was then employed in this chapter. We calculated a nucleation rate from fitting our data in a  $\ln(1-F(t))$  vs.  $J$  plot to equation 5.6 (figs. 6.10 - 6.11). Values of  $3.8 \times 10^{31}$  and  $1.4 \times 10^{31} \text{ m}^{-3}\text{s}^{-1}$  were obtained for 12% and 10% mixes. These rates were used with a librational frequency of  $22 \text{ cm}^{-1}$  and an energy barrier of  $394 \text{ J/mole}$  to give a range of possible free energies as a function of supercooling. The calculated values for  $\sigma_{ss}$  range from  $4 \text{ J/m}^2$  to  $1 \text{ mJ/m}^2$  in a fashion nearly identical to the curves shown for the neat studies. All of the values which were calculated for the neat and mix data sets in the evaluation of  $\sigma$  are tabulated in table 6.8.

### 6.3 New Features in the Acetylene Spectrum

#### 6.3.1 1960 $\text{cm}^{-1}$ Feature

Spectra of acetylene mixtures in helium all yielded previously unseen spectral features in the region between the monomer peak and the bulk solid peaks. Graphed in fig. 6.12 is a spectrum taken of a 12% mix along with a spectrum of clusters in a neat jet. The clusters are in similar stages of the cubic to orthorhombic phase transition as both spectra display a large orthorhombic peak, and a slight shoulder due to the existence of

Table 6.8 Results for all data.

	Neat (ls)	50% (ls)		Neat (ss)	12% (ss)	10% (ss)
Dc (nm)	20	18	Dc (nm)	20	10	10
Tc (K)	152	140	Tc (K)	~135	~135	~135
V(m <sup>3</sup> )	4.19x10 <sup>-24</sup>	3.568x10 <sup>-25</sup>	V(m <sup>3</sup> )	4.19x10 <sup>-24</sup>	8.181x10 <sup>-27</sup>	8.181x10 <sup>-27</sup>
(t-t <sub>0</sub> )(μs)	3.45	2.44	(t-t <sub>0</sub> )(μs)	15.49	0.4301	0.57
J <sub>exp</sub> (m <sup>-3</sup> s <sup>-1</sup> )	1.4x10 <sup>29</sup>	1.8x10 <sup>29</sup>	J <sub>exp</sub> (m <sup>-3</sup> s <sup>-1</sup> )	2.8x10 <sup>28</sup>	3.8x10 <sup>31</sup>	1.4x10 <sup>31</sup>
V(m <sup>3</sup> /mol)	4.241x10 <sup>-5</sup>	4.241x10 <sup>-5</sup>	V(m <sup>3</sup> /mol)	3.562x10 <sup>-5</sup>	3.562x10 <sup>-5</sup>	3.562x10 <sup>-5</sup>
η(mNs/m <sup>2</sup> )	0.195	0.195	v(cm <sup>-1</sup> )	22	22	22
v(m/s)	0.318	0.318	E (J/mol)	394	394	394
D(m <sup>2</sup> /s)	1.21x10 <sup>-8</sup>	1.15x10 <sup>-8</sup>	σ <sub>sl</sub> (mJ/m <sup>2</sup> )	4	3.2	3.2
Λ(m)	8.9x10 <sup>-11</sup>	8.9x10 <sup>-11</sup>				
a(m)	6.1x10 <sup>-9</sup>	6.1x10 <sup>-9</sup>				
σ <sub>sl</sub> (mJ/m <sup>2</sup> )	9.8	11.8				

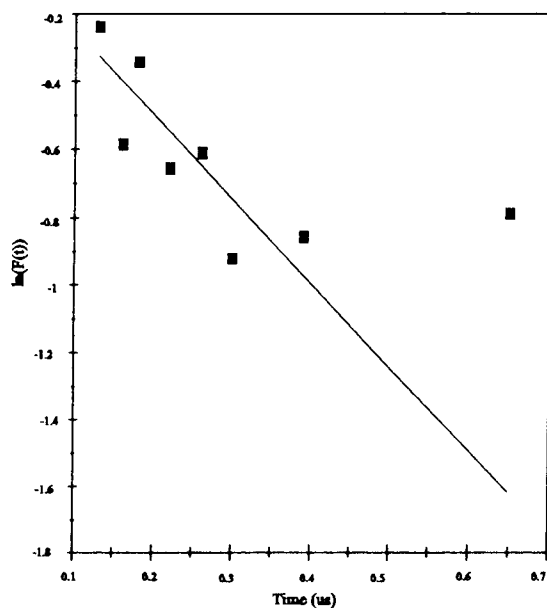


Fig. 6.10 The fraction of orthorhombic solid present vs. time in a 12% 27 atm. jet is fit with eq. 5.6 to give a nucleation rate of  $3.8 \times 10^{31} \text{ m}^{-3}\text{s}^{-1}$ .

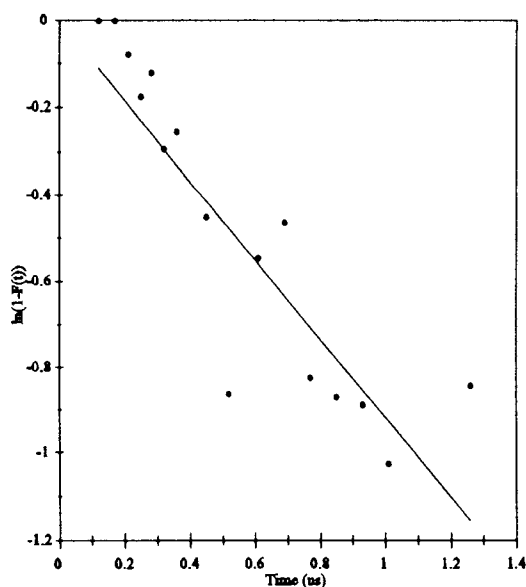


Fig. 6.11 The fraction of orthorhombic acetylene present in the 10 % 213 K jet is plotted and fit with eq. 5.6 to give a nucleation rate of  $1.4 \times 10^{31} \text{ m}^{-3}\text{s}^{-1}$ .

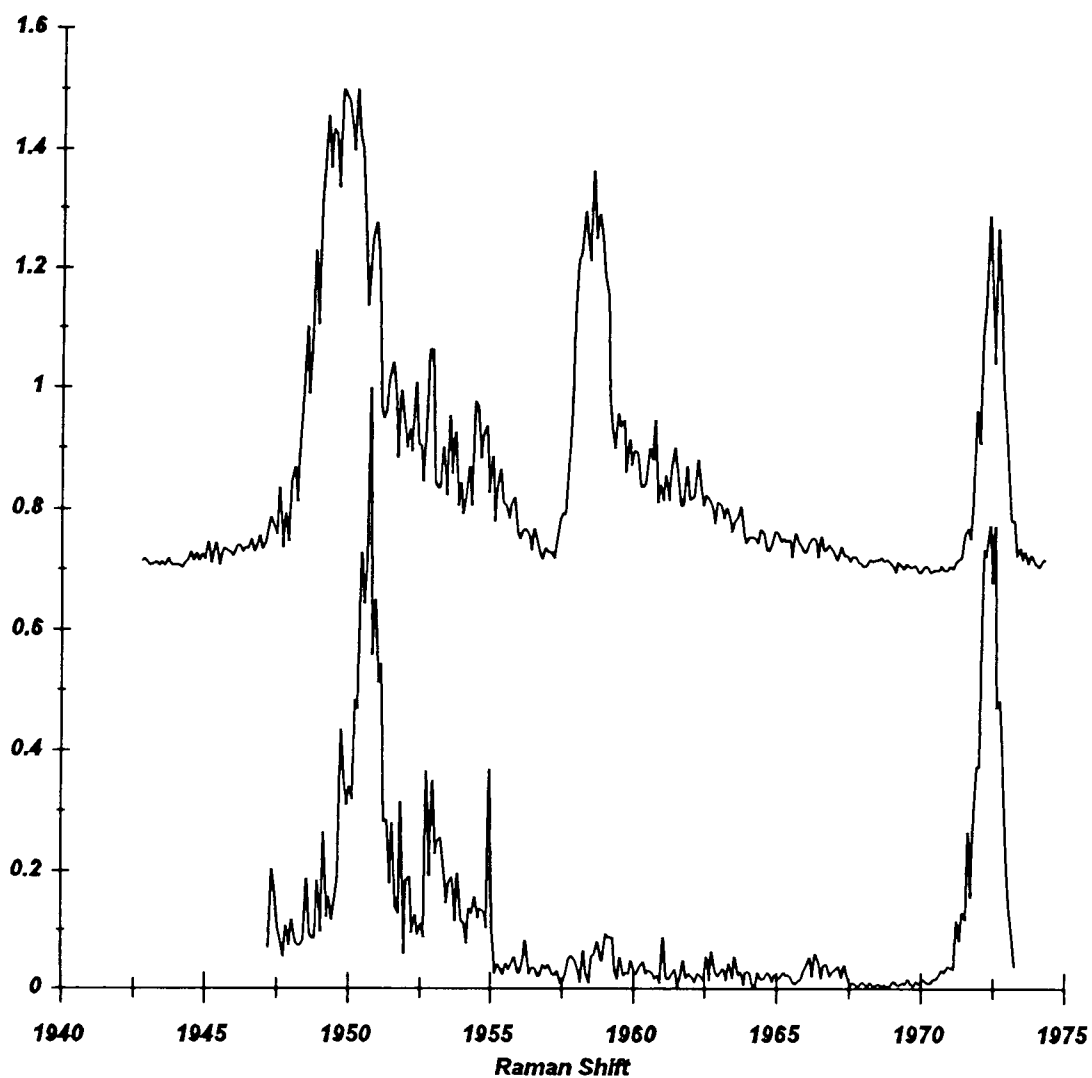


Fig. 6.12 A spectrum from a 12% mix at 29 atm (top) is compared to a similar neat acetylene spectrum. The mix spectrum shows a strong new peak at  $1960\text{ cm}^{-1}$ .

cubic phase clusters. The striking new feature at  $1960\text{ cm}^{-1}$  is strongest in the spectrum taken of the 12% mix. Peak centers for the new peak are tabulated in tables 6.1 - 6.5 for all of the mix data sets. The possibility that this peak is simply a large contribution of the  $B_{3g}$  component of the orthorhombic mode is considered below.

### 6.3.2 Assignment of the New Feature as the $B_{3g}$ Peak:

The proximity of the new feature to the  $B_{3g}$  component of the orthorhombic crystal leads us to consider its intensity. It should be noted that these  $A_g$  and  $B_{3g}$  features correspond to in - phase and out-of-phase combinations of the  $C\equiv C$  stretch of the two molecules in the unit cell. Since populations contributing to the  $A_g$  peak are always the same as those contributing to the  $B_{3g}$  peak, the intensity ratio is dependent on the bond polarizability derivatives and the way they combine due to the regularity of the crystal. Acetylene bulk solid data show the  $B_{3g}$  peak at intensity levels of  $1/6^{\text{th}}$  to  $1/30^{\text{th}}$  that of the  $A_g$  peak<sup>73</sup> with the higher value corresponding to well annealed cryostat samples. The spectra of the 12% mix show that the peak at this new position is usually a good fraction of the  $A_g$  peak (from 20% upward) and many times the intensities are equivalent to those of the  $A_g$  peak. This strongly suggests that the peak is not the  $B_{3g}$  peak since the crystal formed in the rapidly cooling jets always have line widths  $\sim 50\%$  larger than the equilibrium samples and hence are likely to be less crystalline.

### 6.3.3 Assignment as Surface Layer of Acetylene Clusters:

An alternate assignment of the  $1960\text{ cm}^{-1}$  peak is to vibrations of molecules on the

surface layer of the clusters. For small clusters in the size range below 10 nm, new features have also been seen in spectra of CO<sub>2</sub> clusters. These features, which occur in the spectral region between the monomer peak and the bulk solid peak, are reasonably interpreted as signal from surface molecules since there is no doubt that these reside in a different environment than the core molecules. Infrared work on small ammonia clusters revealed peaks which were thought to be due to molecules vibrating on the surface of a cluster.<sup>74</sup>

If the new feature is indeed due to the surface of the cluster, the relative intensities can be used to calculate the size of the cluster. The size of the cluster should then follow some reasonable trend as clusters go out in X/D and be of the correct magnitude based on what we expect from the initial conditions. The conditions which give the largest relative signals for the surface feature should produce clusters which are smallest; i.e. the clusters produced in the 4% mix should be the smallest, with the 12% mix at 29 atm being the next smallest, followed by the 10% mix and then the other 12% mix.

#### 6.3.4 Cluster Diameter Calculation:

Cluster sizes are calculated from the surface to core peak ratio using a simple spherical model which assumes that there is a one molecule thick surface layer generating all of the surface signal. The thickness of the surface layer is assumed to be 0.376 nm, which is deduced as the molecular diameter from the density of the orthorhombic phase. If the signals are compared, the ratio of surface volume to total can be represented by

$$V_s/V_T = (3r\Delta^2 - 3r^2\Delta - \Delta^3)/r^3 \quad (6.1)$$

if the total radius is  $r$  and the thickness of the surface layer is  $\Delta$ . Using this, the radius can be found.

The experimental ratios were taken assuming that the entire  $1960 \text{ cm}^{-1}$  peak was from the surface. Figure 6.13 shows the sizes of clusters that were calculated from the surface to volume ratio. Although there is appreciable variation in size the average cluster diameter in the most dilute expansions is about 10 nm. This value was used in the interfacial free energy calculation of the last section. The 10 nm value is sensibly smaller than the larger values of 20 and 18 nm deduced from cooling curves for the neat and 50% expansions.

### 6.3.5 Diffuse Feature near $1963 \text{ cm}^{-1}$

In further diluted samples of acetylene, a diffuse band in the region between  $1960 \text{ cm}^{-1}$  and  $1965 \text{ cm}^{-1}$  is observed. This is easily seen in the 4% mix, (fig. 6.5) and is also somewhat in the warmer 10% mix (fig. 6.4). The 4% mix spectra are compared to a 12% spectrum in fig. 6.14 to show the enhancement of relative intensity of this broad feature for smaller clusters expected in the 4% mix. The origin of this peak is unknown, but two possibilities seem reasonable. The first is that it is due to very small clusters such as dimers, trimers and tetramers, etc. In support of this the feature is found about  $10 \text{ cm}^{-1}$  lower than the monomer Q-branch and shifts of this magnitude have been reported for the

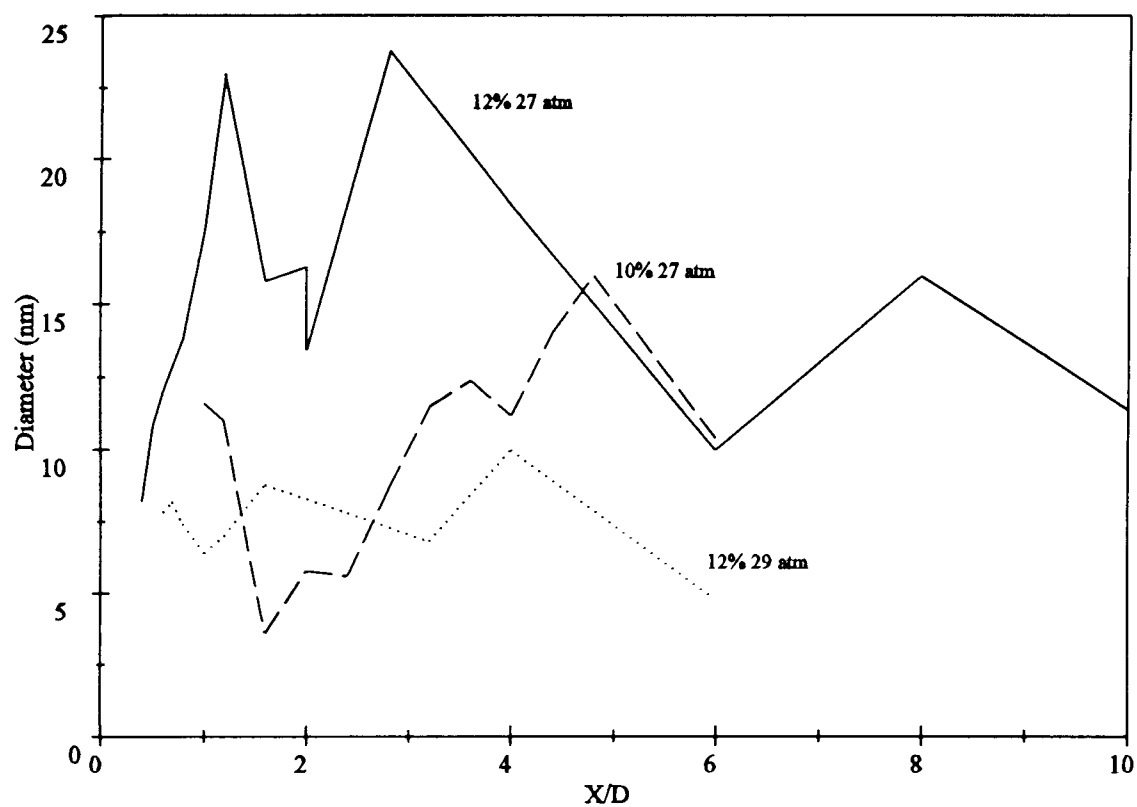


Fig. 6.13 Cluster sizes are calculated from the surface to volume ratio yielding cluster diameters of around 10 nm.

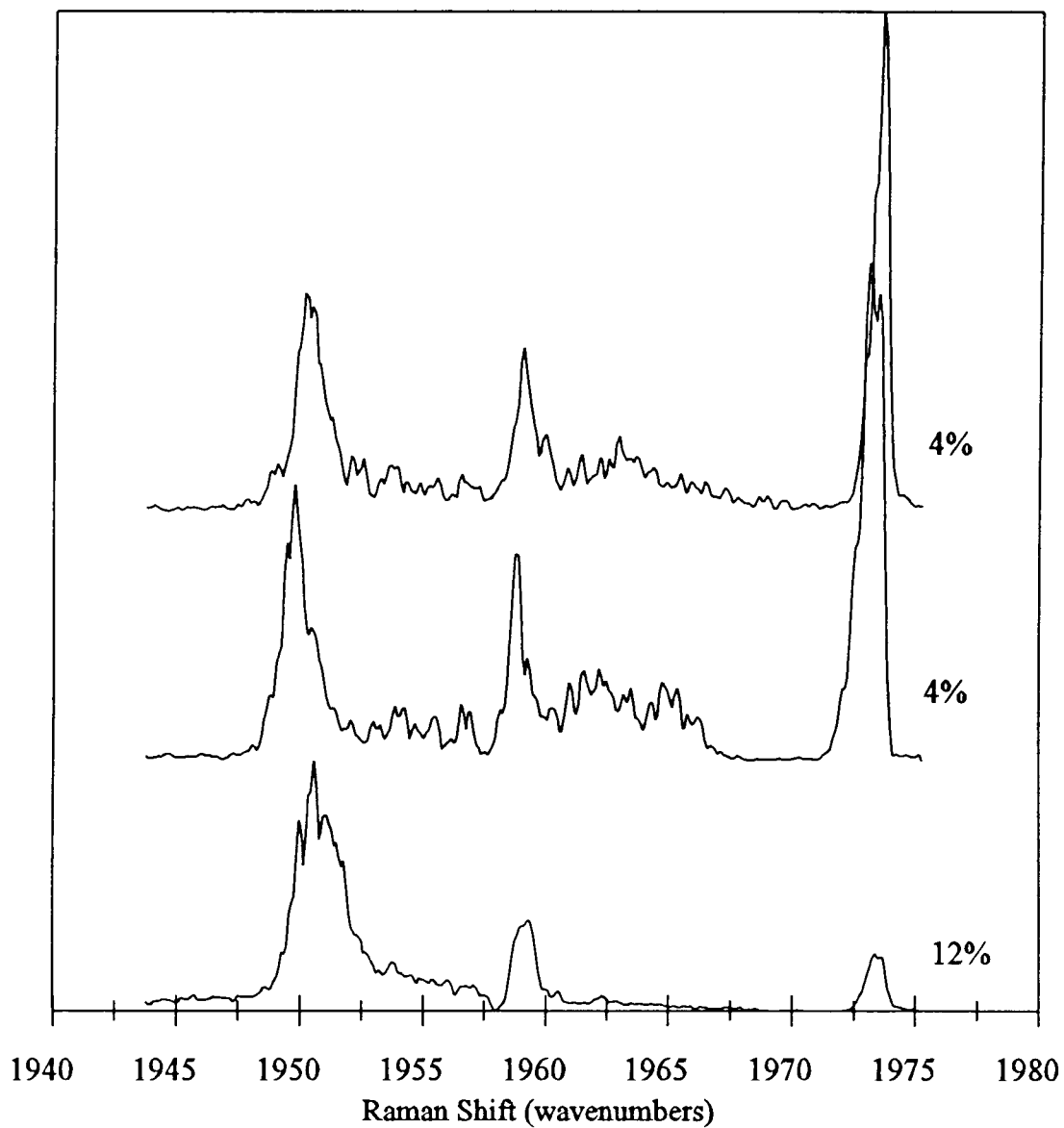


Fig. 6.14 A graph of a 12% spectrum and two 4% spectra. The latter cases show the increased contribution from a broad surface feature in the region of 1963 cm<sup>-1</sup>.

antisymmetric CH stretching mode of acetylene dimer<sup>75</sup> and trimer<sup>76</sup>. Higher resolution studies in this region would be useful.

The second possibility is that one or more metastable structures may exist for the smaller (perhaps  $n < 50$ ) clusters formed under the rapidly cooling condition of these expansions. In particular, theoretical molecular dynamics calculation by Van de Waal for  $\text{CO}_2$  predict stable forms corresponding to a pentagonal bipyramidal structure of units and to an icosohedral arrangement of 13 units. The bulk phase cubic structure can be assembled from a similar cubo-octahedral arrangement of 13 units which ultimately aggregate together. The speculation here is that the diffuse feature corresponds to clusters assembled on pentagonal bipyramidal or icosohedral core units rather than on the cubo-octahedral structure.

Regardless of which of the two above possibilities is correct, it is clear that some structural element unknown in the equilibrium phases of acetylene must be responsible for this intriguing diffuse feature. Future studies of the band at increased sensitivities which are possible in the Raman - ionization apparatus in our lab might be fruitful.

## 6.4 Discussion

This work has given the following values for interfacial free energies (surface tensions) of acetylene;  $\sigma_{sl} = 10.1 \text{ mJ/m}^2$  for 20 nm clusters at 152 K,  $\sigma_{sl} = 11.6 \text{ mJ/m}^2$  for 18 nm clusters at 140 K, and  $\sigma_{ss} = 2 \text{ mJ/m}^2$  for 20 and 10 nm clusters at  $\sim 136 \text{ K}$ . It is interesting to compare these results with other values reported in the literature but they

are very limited and consist mainly of  $\sigma_{sl}$  values for metals at their melting points. A few values for nonmetals have been obtained by Bartell using the same approach employed here but with the freezing rates deduced from diffraction studies rather than from Raman spectroscopy. Table 6.9 summarizes what, to the best of our knowledge, is available for  $\sigma_{sl}$  values for nonmetals.

When we compare the  $\sigma_{sl}$  to  $\sigma_{lg}$  we notice that  $\sigma_{lg}$  for  $\text{CCl}_4$  and  $\text{NH}_3$  data decreases as temperature increases, a general feature of all liquid - gas interfaces. It is seen that  $\sigma_{sl}$  is much lower than  $\sigma_{lg}$  if the latter is extrapolated to the transition temperature of the supercooled sample. This result is physically reasonable since it seems that the energy necessary to create a surface of liquid interacting with a vapor must be greater than that for the liquid interacting with a solid of nearly the same density and intermolecular separation. Indeed our values for  $\sigma_{sl}$  for acetylene are clearly lower than a value of about  $\sigma_{lg} = 27 \text{ mJ/m}^2$  which we obtain by extrapolating known values of  $\sigma_{lg}$  as a function of temperature. However, these values are in accord with Turnbull's empirical relationship  $\sigma_{sl} = k \Delta H_{fus} / (V^{2/3} N_a^{1/3})$ . Here  $k$  evaluated for metalloids is the value at the melting point. This relationship yields  $\sigma_{sl} = 11.9 \text{ mJ/m}^2$ .

Finally, few comparisons can be made of our approximate  $\sigma_{ss}$  value of  $2 \text{ mJ/m}^2$  for the solid - solid phase transitions of acetylene. The only two other values for a solid - solid phase transition are those of Bartell for  $(\text{CH}_3)_3\text{CCl}$  ( $\sigma_{ss} = 3.2 \text{ mJ/m}^2$ ) and for  $\text{SeF}_6$  ( $\sigma_{ss} = 4.4 \text{ mJ/m}^2$ ). The small magnitudes of these numbers are consistent with the nature of the phase transition in all these cases. That is, the conversion essentially involves purely reorientational movement of the molecules in the lattice, with no need for extensive

Table 6.9 Interfacial Free Energies

	$\sigma_{gl}$ (mJ/m <sup>2</sup> )	$\sigma_{sl}$ (mJ/m <sup>2</sup> )	$\sigma_{ss}$ (mJ/m <sup>2</sup> )
(CH <sub>3</sub> ) <sub>3</sub> C Cl			3.2 <sup>74</sup>
CH <sub>3</sub> CCl <sub>3</sub>		4.7 (165 K) <sup>77</sup>	
C Cl <sub>4</sub>	26.95 (20 K) <sup>62</sup>	5.46 (175 K) <sup>78</sup>	
	17.26 (100 K) <sup>62</sup>		
	6.95 (200 K) <sup>62</sup>		
SeF <sub>6</sub>			4.4 (105 K) <sup>74</sup>
NH <sub>3</sub>	44.5 (233 K) <sup>64</sup>	23 (128 K) <sup>79</sup>	
	23.4 (284 K) <sup>62</sup>		
	18.1 (307 K) <sup>62</sup>		
C <sub>2</sub> H <sub>2</sub>	16.4 (203 K) <sup>62</sup>	10.1 (155 K)	4 (~135 K)
	18.8 (193 K) <sup>64</sup>	11.6 (140 K)	

translational disruption. Thus the interfacial free energy would be expected to be much less than for  $\sigma_{sl}$  or  $\sigma_{lg}$  as observed.

## 6.5 Conclusions

As a part of this work, accurate frequency temperature relations were obtained for the  $\nu_2$  vibrational mode of liquid, cubic solid, and orthorhombic solid acetylene. The phase transitions for acetylene clusters were viewed in a condensing supersonic jet. The method by which these cooling clusters went through the phase transitions was modeled and both transitions were found to be essentially adiabatic. We then used the measured rate of transition to determine the rate of nucleation. This was then used in the framework of homogeneous nucleation theory to obtain the interfacial free energy for clusters containing liquid - solid and solid - solid interfaces. For clusters going through the liquid to solid transition,  $\sigma_{sl}$  was found to be 10.1 mJ/m<sup>2</sup> for 155 K, 20 nm clusters and 11.6 mJ/m<sup>2</sup> for colder, 140 K, smaller, 18 nm, clusters produced in a 50% mix.

Similarly, the solid - solid interfacial free energies were found through relating the vibrational frequencies of the crystal to the nucleation rate. The frequency of crystal libration for the  $A_g$  mode of 22 cm<sup>-1</sup> was used to deduce interfacial free energy of about 2 mJ/m<sup>2</sup> for both the 20 nm 135 K neat sample clusters and the aggregate formed in mixes.

For the very small clusters formed in dilute mixes, spectra were taken which show new features for acetylene. One of these is believed to be due to molecules on the outer layer of the cluster. From its relative intensity, we were able to deduce a diameter for the

clusters of about 10 nm. A second diffuse feature was also seen which could be due to dimers and trimers or to metastable structures for acetylene and further studies of this band are suggested.

## Bibliography

1. Bernstein, E. R., Law, K. and Schauer, M.; *J. Chem. Phys.*, 80(2), (1984) 634 - 44
2. Schauer, M., Law, K. and Bernstein, E. R.; *J. Chem. Phys.*, 81(1), (1984) 49 - 56
3. Nowak, U., Menapace, J. A. and Bernstein, E. R.; *J. Chem. Phys.*, 89(3), (1988) 1309 - 21
4. Law, K. S., Schauer, M., and Bernstein, E. R.; *J. Chem. Phys.*, 81(11), (1984) 4871 - 82
5. Dao, P. D., Morgan, S. and Castleman, A. W., Jr.; *Chem. Phys. Letters*, 113 (2) (1985) 219 - 24
6. Furlan, A., Troxler, T. and Leutwyler, S.; *J. Phys. Chem.*, 97(51), (1993) 13527 - 13534
7. Nesbitt, D. J.; *Ann. Rev. Phys. Chem*, 45, (1994) 367 - 99
8. Lovejoy, C. M. and Nesbitt, D. J.; *J. Chem. Phys.* 86(6), (1987) 3151 - 65
9. Shum, M. A.; *Ber. Bunsen-Ges.* 99(10), (1995) 1159 - 67
10. Liu, K., Fellers, R. S., Viant, M. R., McLaughlin, R. P., Brown, M. G. and Saykally, R. J.; *Rev. Sci. Instrum.* 67(2), (1996) 410 - 16
11. Hwang, H. J., Van Orden, A., Tanaka, K., Kuo, E. W., Heath, J. R. and Saykally, R. J.; *Mol. Phys.*, 79(4), (1993) 769 - 76
12. Van Orden, A., Hwang, H. J., Kuo, E. W. and Saykally, R. J.; *J. Chem. Phys.*, 98(9), (1993) 6678 - 6683
13. Barth, H. D. and Huisken, F.; *Chem. Phys. Lett.*, 169(3), (1990) 198 - 203
14. Richardson, A.; *Coherent Anti-Stokes Raman Spectroscopy of Solid Acetylene and Carbon Dioxide*, Thesis Oregon State University (1993)
15. Goyal, S., Schutt, D. L. and Scoles, G.; *J. Phys. Chem.*, 102(6), (1995) 2302 - 14
16. Barth, H. D., Huisken, F., Ilyukhin, A. A.; *Appl. Phys. B*, B52(2), (1991) 84 - 9

17. Beck, R. D., Hineman, M. F. and Nibler, J. W.; *J. Chem. Phys.*, 92(12), (1990) 7068 - 78
18. Lee, K. H., Triggs, N. E. and Nibler, J. W.; *J. Phys. Chem.*, 98, (1994) 4382 - 8
19. Bartell, L. S., Laszlo, H. and Valente, E. J.; *J. Phys. Chem.*, 93, (1989) 6201 - 5
20. Bartell, L. S., Harsanyi, L. Dibble, T. S. and Lennon, P. J.; *J. Phys. Chem.*, 94, (1990) 6009 - 12
21. Bartell, L. S.; *Z. Phys. D*, 26, (1993) 101 - 4
22. Bartell, L. S.; *J. Phys. Chem.*, 94, (1990) 5102 - 9
23. McKeller, A. Robert W.; *Faraday discuss.* 97, (1994) 69 - 80
24. Bauerecker, S., Taucher, J., Weitkamp, C., Michaelis, W. and Cammenga, H. K.; *J. Mol. Struct.* 348, (1995) 237 - 42
25. Abraham, Kim, Stein; *J. Chem. Phys.*, 75(1), (1981) 403 - 10
26. Goyal, S., Schutt, D. L., and Scoles, G.; *J. Phys. Chem.*, 97, (1993) 2236 - 45
27. Fischer, G., Miller, R. E., Watts, R. O.; *Chem. Phys.* 80(1-2), (1983) 147 - 55
28. Kim, S. S. and Stein, G. D.; *Rev. Sci. Instr.*, 53, (1982) 838
29. Bartell, L. S.; *Chem. Rev.*, 86, (1986) 492
30. Levy, D. H.; *J. Chem. Soc., Faraday Trans.*, 82(8), (1986) 1123 - 35
31. Lipert, R. J., Colson, S. D.; *J. Phys. Chem.*, 93(10), (1989) 3894 - 6
32. Wittmeyer, S. A., Topp, M. R.; *J. Phys. Chem.*, 95(12), (1991) 4627 - 35
33. Bumburger, R. E., Blake, G. A.; *Chem. Phys. Lett.*, 161(4-5), (1989) 308 - 14
34. Ohshima, Y., Endo, Y., Ogata, T.; *J. Chem. Phys.*, 102(4), (1995) 1493 - 500
35. Schmuttenmaer, C. A., Cohen, R. C., Pugliano, N., Heath, J. R., Cooksy, A. L., Busarow, K., L. and Saykally, R. J.; *Science*, 294(4971), (1990) 897 - 900
36. Bueger, H., Rahner, A., Amrein, A., Hollenstein, H. and Quack, M.; *Chem. Phys. Lett.*, 156(6), (1989) 557 - 63

37. Gough, T. E., Mengel, N., Rowntree, P. A. and Scoles, G.; *J. Chem. Phys.*, 83(10), (1985) 4958 - 61
38. Pine, A. S.; *J. Opt. Soc. Am.*, 64, (1974) 1683 - 90
39. Lovejoy, C. M., Nesbitt, D. J.; *Rev. Sci. Instr.*, 58, (1987) 807 - 11
40. Huber - Wälchli, P., Guthals, D. M. and Nibler, J. W.; *Chem. Phys. Lett.*, 67, (1979) 233
41. Barth, H. D. and Huisken, F.; *Springer Proc. Phys.*, 63, (1992) 242 - 54
42. Beck, R. and Nibler, J. W.; *Chem. Phys. Lett.*, 148, (1988) 271
43. Lee, K. H.: *Coherent Anti-Stokes Raman Spectroscopy of Acetylene Clusters*, Thesis, Oregon State University, 1991
44. Tolles, W. M. and Harvey, A. B.; *Introduction to Nonlinear Phenomena in: Chemical Applications of Nonlinear Raman Spectroscopy* 1981 Academic Press
45. Goyot - Sionnest, P. and Shen, Y. R.; *Phys Rev. B* 38 12, 7985 (1988)
46. Tolles, W. M., Nibler, J. W., McDonald, J. R. and Harvey A. B.; *Applied Spectroscopy* 31, 4, 253
47. Miller, D. R.; in: *Atomic and Molecular Beam Methods*, Vol 1, ed. G. Scoles (Oxford University Press, New York, 1988).
48. McDonald, J. E.; *Am. J. Phys.* 30, 870 (1962)
49. McDonald, J. E.; *Am. J. Phys.* 31, 31 (1963)
50. Richardson, A.; *Coherent Anti-Stokes Raman Spectroscopy of Solid Acetylene and Carbon Dioxide*, Thesis Oregon State University, 1993
51. Gerstenkorn, S. and Luc, P.; *Atlas du spectre d'absorption de la molécule de l'iode* (14800-20000  $\text{cm}^{-1}$ ) (Editions du C.N.R.S. ) 1978
56. Brodenson, S.; *High-Resolution Rotational Vibrational Raman Spectroscopy: in Raman Spectroscopy of Gases and Liquids*, edited by A. Weber (Weiley International New York, 1979) Vol. 11
57. Aoki, K., Kakudate, Y., Yoshida, M., Usuba, S., Tanaka, K., and Fujiwara, S.; *Solid State Communications* v. 64, 10 1329 - 1331 1987
58. van Nes, Gerhard J. H. and van Bolhuis, Fre; *Acta Cryst.* (1979) B35, 2580

59. Anderson, A., Andrews, B. and Torrie, B. H.; *Journal of Raman Spec.* 16, (3) 203 (1985)
60. Broderson, S.; *High Resolution Rotation Vibrational Raman Spectroscopy in Raman Spectroscopy of Gases and Liquids* edited by A. Weber (Weiley Internaitonal 1979) vol. 11
61. McIntosh, C. J.; *Phys. Chem.*, 11, (1907) 306
62. CRC 71<sup>st</sup> ed. CRC Press, Inc.
63. Miskiewicz, S., Reiser, K., and Dforfmuller, T.; *Ber. Bunsenges. Phys Chem.*, 80, (5), (1976) 395
64. Hirschfelder, J. O., Curtiss, C. F., and Bird, R. B.; *Molecular theory of Gases and Liquids* (John Weiley and Sons, 1967)
65. van Nes, G. J. H., and Bolhius, F.; *Acta Cryst.*, B 35, (1979) 2580 - 2593
66. Lee, K., Triggs, N., and Nibler, J. W.; *J. Phys. Chem.*, 98, (1994) 4382 - 8
67. Beck, R. D., Hineman, M. F., and Nibler, J. W.; *J. Chem. Phys.*, 92 (12), (1990) 7068
68. Bartell, L. S.; *Z. Phys. D* 26, (1993) 101-104
69. Kaschiev, D., Verdoes, D., van Rosmaalen, G. M.; *J. Crystal Growth*, 110, (1991) 373
70. Buckle, E. R.; *Proc. R. Soc. London*, a261, (1961) 189
71. Turnbull, D.; *J. Appl. Phys* 21, (1950) 1022
72. Dibble, T. S., and Bartell, L. S.; *J. Phys. Chem.*, 96, (1992) 21, 8603 - 10
73. Lee, K. H., Triggs, N. E., and Nibler, J. W.; *J. Phys. Chem.*, 98, (1994) 4382 - 88
74. Barth, H. D., Huisken, F.; *J. Chem. Phys.* 87 (5) (1987)
75. Prichard, D. C., Nandi, R. N., and Muentner, J. S.; *J. Chem. Phys.*, 89 (1988) 115.
76. Prichard, D. C., and Muentner, J. S.; *Chem Phys Lett.* 135 (1,2) (1987) 9 - 15
77. Dibble, T.S., Bartell, L. S.; *J. Phys. Chem.*, 96, (1992) 2317 - 22
78. Bartell, L. S., and Dibble, T. S.; *J. Phys. Chem.* 95, (1991), 1159
79. Huang, J. and Bartell, L. S.; *J. Phys. Chem.* 98, (1994), 4543

APPENDIX

## AI. CARS Fitting Program

### AI.1 To Fit a Spectrum

#### AI.1.1 CARS Spectra of Neighboring Peaks

To obtain the correct information on peak widths, centers and amplitudes, one must be able to fit the spectra taken with the functions that most closely describe the way the signal was generated. CARS spectra have line shapes which are unique to the nonlinear interactions the light has with molecules. When two spectral features are close together in a CARS spectrum (as in rotational features in a Q-branch) such that their separation is on the order of their line width, they will interact to give a spectrum which is not the same as one which two neighboring peaks would in a linear spectroscopy. Neighboring peaks will tend to move the apparent centers of both the peaks away from the true position.

CARS spectra of acetylene in the jet provides an example of a spectrum which has two close peaks where the peaks effect each other. Each peak seen has it's own line center, width and characteristic shape. In a typical spectrum which shows the liquid - solid transition, we see two peaks which are separated by roughly  $2.5 \text{ cm}^{-1}$  which have widths of  $\sim 2 \text{ cm}^{-1}$ . These peaks will move each other in the CARS spectra, so we must fit them with the correct function to find the correct center.

### AI.1.2 CARS Spectra Models

In a Raman spectrum, the signal comes about through addition of the susceptibilities of all the transitions. In CARS, the peaks are created through addition of the square of the susceptibility. The susceptibility for a third order process is

$$\chi^{(3)} = P^3 N / (\Delta W^2 - i\Gamma^2) \quad (\text{A.1})$$

The total CARS susceptibility can be produced from the addition of the above susceptibilities for each vibrational transition.

$$\chi_{\text{tot}} = \chi_1' + \chi_2' + \chi_1'' + \chi_2'' + \chi^{\text{NR}} \quad (\text{A.2})$$

where  $\chi'$  is the real,  $\chi''$  is the imaginary and  $\chi^{\text{NR}}$  is the non-resonant portion of the susceptibility. Adding and squaring of the above susceptibility can be done to give

$$\chi_{\text{tot}}^2 = \chi_1'^2 + \chi_2'^2 + 2\chi_1'\chi_2' + \chi_1''^2 + \chi_2''^2 + 2\chi_1''\chi_2'' + 2\chi_1'\chi^{\text{NR}} + 2\chi_2'\chi^{\text{NR}} + \chi^{\text{NR}^2} \quad (\text{A.3})$$

Addition of squared susceptibilities will produce a different spectrum than will squaring added susceptibilities. The cross terms in the susceptibility involving a contribution from both the first and second peaks will give a different h\shape than it would have if there were a linear interaction. When fitting a CARS spectrum, this set of cross terms must be accounted for.

## AI.2 The Program

A spectrum is calculated from the total susceptibility because we consider laser power not to fluctuate over the course of taking a spectrum. This spectrum is compared to the data and a point by point difference is taken between the data and the calculated spectrum and squared to give the sum of the square of the differences  $\chi$  (not to be confused with the susceptibility  $\chi$ ). The program uses simple functions for the real and imaginary parts to  $\chi$ :

$$\chi' = 2 \Delta\omega I / (4\Delta\omega^2 + \Gamma^2) \quad (\text{A.4})$$

and

$$\chi'' = 2\Gamma I / (4\Delta\omega^2 + \Gamma^2) \quad (\text{A.5})$$

$I$  is the intensity of the transition,  $\Delta\omega$  is the difference between the peak center frequency and the CARS frequency, and  $\Gamma$  is the line width of the transition. The real contributions from all peaks in the spectrum are summed to give a  $\chi'_{\text{tot}}$  as the imaginary parts are to give a  $\chi''_{\text{tot}}$ . The total susceptibility is then calculated from these real and imaginary parts along with a constant  $\chi^{\text{NR}}$  at each point in the spectrum. Peak centers and widths can be adjusted by the user to minimize  $\chi$  which is displayed.

FITFORM.FRM - 1

```

Sub SaveFit_Click ()
CmdOut.CancelError = True
CmdOut.DefaultExt = ".tbl"
CmdOut.Filename = "Default.tbl"
CmdOut.Filter = "Data Files (*.dat)|*.DAT|Table Files (*.TBL)|*.tbl|Print Files (*.PRN)|*.prn|All Files (*.*)|*.*"
CmdOut.FilterIndex = 2
CmdOut.Flags = OFN_OVERWRITEPROMPT Or OFN_PATHMUSTEXIST
CmdOut.Action = 2
Open CmdOut.Filename For Output As #1
For H = 1 To Peak
Print #1, "Center "; H, A(H * 4 - 3)
Print #1, "Amplitude "; H, A(H * 4 - 2)
Print #1, "Width "; H, A(H * 4 - 1)
Next H
Close #1
MsgBox "Writing to File " + CmdOut.Filename
End Sub
Sub AmplitudeMinus_MouseDown (Button As Integer, Shift As Integer, X As Single, Y As Single)
If (Button + LEFT_BUTTON) <> 0 Then PeakDown = 1
DrawDown
LeastSquares
End Sub
Sub AmplitudeMinus_MouseUp (Button As Integer, Shift As Integer, X As Single, Y As Single)
If (Button + LEFT_BUTTON) <> 0 Then PeakDown = 0
DrawDown
End Sub
Sub AmplitudePlus_MouseDown (Button As Integer, Shift As Integer, X As Single, Y As Single)
If (Button + LEFT_BUTTON) <> 0 Then PeakUp = 1
DrawUp
LeastSquares
End Sub
Sub AmplitudePlus_MouseUp (Button As Integer, Shift As Integer, X As Single, Y As Single)
If (Button + LEFT_BUTTON) <> 0 Then PeakUp = 0
DrawUp
End Sub
Sub Fit_Click ()
AmplitudePlus.Enabled = False
AmplitudePlus.Visible = False
AmplitudeMinus.Enabled = False
AmplitudeMinus.Visible = False
MoveLeft.Enabled = False
MoveLeft.Visible = False
MoveRight.Enabled = False
MoveRight.Visible = False
WidthMinus.Enabled = False
WidthMinus.Visible = False
WidthPlus.Enabled = flase
WidthPlus.Visible = False
FitRoutine

```

End Sub

FITFORM.FRM - 2

Sub FitEnd\_Click ()

For H = 1 To Peak \* 4

A(H) = 0

Next H

SelectBox.Clear

RemoveBox.Clear

Peak = 0

PeakSelect = 0

FitForm.Enabled = False

FitForm.Visible = False

GraphForm.Visible = True

GraphForm.Enabled = True

Plot

End Sub

Sub Form\_MouseDown (Button As Integer, Shift As Integer, X As Single, Y As Single)

Peak = Peak + 1

PeakSelect = Peak

K = Peak \* 4

A(K - 3) = X

A(K - 2) = Y

If Y > ychi Then ychi = Y

A(K - 1) = .02 \* (xmax - xmin)

A(K) = 200000

Peaks = Str\$(Peak)

SelectBox.AddItem "Peak" + Peaks

RemoveBox.AddItem "Peak" + Peaks

AmplitudeMinus.Visible = True

AmplitudeMinus.Enabled = True

AmplitudePlus.Visible = True

AmplitudePlus.Enabled = True

MoveLeft.Visible = True

MoveLeft.Enabled = True

MoveRight.Visible = True

MoveRight.Enabled = True

WidthMinus.Visible = True

WidthMinus.Enabled = True

WidthPlus.Visible = True

WidthPlus.Enabled = True

Nterms = Peak \* 4 + 2

A(Nterms - 1) = .01

Form.Enabled = False

Draw

End Sub

Sub MoveLeft\_MouseDown (Button As Integer, Shift As Integer, X As Single, Y As Single)

If (Button + LEFT\_BUTTON) <> 0 Then PeakLeft = 1

DrawLeft

LeastSquares

End Sub

```

Sub MoveLeft_MouseUp (Button As Integer, Shift As Integer, X As Single, Y As Single)
If (Button + LEFT_BUTTON) <> 0 Then PeakLeft = 0
DrawLeft
End Sub
Sub MoveRight_MouseDown (Button As Integer, Shift As Integer, X As Single, Y As Single)
If (Button + LEFT_BUTTON) <> 0 Then PeakRight = 1
DrawRight
LeastSquares
End Sub

```

FITFORM.FRM - 3

```

Sub MoveRight_MouseUp (Button As Integer, Shift As Integer, X As Single, Y As Single)
If (Button + LEFT_BUTTON) <> 0 Then PeakRight = 0
DrawRight
End Sub
Sub NewFit_Click ()
For H = 1 To Peak * 4
A(H) = 0
Next H
SelectBox.Clear
RemoveBox.Clear
Peak = 0
PeakSelect = 0
ychi = 0
Draw
End Sub
Sub RemoveBox_Click ()
RemoveBtn.Enabled = True
End Sub
Sub RemoveBox_LostFocus ()
PeakSelect = Val(Mid$(RemoveBox.Text, 6, Len(RemoveBox.Text) - 5))
End Sub
Sub RemoveBtn_Click ()
RemoveBtn.Visible = False
RemoveBox.Visible = False
RemoveBtn.Enabled = False
RemoveBox.Enabled = False
If PeakSelect < Peak Then
For H = PeakSelect To Peak - 1
A(H * 4) = A((H * 4) + 4): A((H * 4) - 1) = A((H * 4) + 3): A((H * 4) - 2) = A((H * 4) + 2): A((H * 4) - 3) =
A((H * 4) + 1)
Next H
End If
H = Peak * 4
A(H - 3) = 0: A(H - 2) = 0: A(H - 1) = 0: A(H) = 0
Peak = Peak - 1
RemoveBox.Clear
SelectBox.Clear
For H = 1 To Peak
hs = Str$(H)
SelectBox.AddItem "Peak" + hs

```

```

RemoveBox.AddItem "Peak" + hs
Next H
Peaks = Str$(Peak)
SelectBox.Text = "Peak" + Peaks
RemoveBox.Text = "Peak" + Peaks
Draw
End Sub
Sub RemovePeak_Click ()
RemoveBox.Visible = True
RemoveBox.Enabled = True
RemoveBtn.Visible = True
Peaks = Str$(Peak)
RemoveBox.Text = "Peak " + Peaks
If Peak = 0 Then RemoveBox.Text = "No Peak Selected"
End Sub
Sub SaveFunctions_Click ()
CmdOut.CancelError = True

```

FITFORM.FRM - 4

```

On Error GoTo ed
CmdOut.DefaultExt = TBL
CmdOut.Filename = Left$(InputFile, (Len(InputFile) - 4)) + ".TBL"
CmdOut.Filter = "Data Files (*.DAT)|*.dat|Table Files (*.TBL)|*.tbl|Print Files(*.PRN)|*.prn|Text Files (*.TXT)|*.txt|All Files (*.*)|*.*"
CmdOut.FilterIndex = 2
CmdOut.Flags = OFN_OVERWRITEPROMPT Or OFN_PATHMUSTEXIST
CmdOut.Action = 2
Open CmdOut.Filename For Output As #1
  For H = 1 To Peak * 4
    b(H) = A(H)
    A(H) = 0
  Next H
For H = 1 To Peak
  A(1) = 0
  A(2) = 0
  A(3) = 0
  A(4) = 0
  A(1) = b(H * 4 - 3)
  A(2) = b(H * 4 - 2)
  A(3) = b(H * 4 - 1)
  A(4) = b(H * 4)
  SinglePeak
  Print #1, "Peak "; H
  For I = 1 To Pts
    Print #1, X(I), YF(I), Sqr(YF(I))
  Next I
Next H
Close #1
ed:
Resume edd
edd:

```

```

End Sub
Sub SavePeaks_Click ()
CmdOut.CancelError = True
On Error GoTo ee
CmdOut.DefaultExt = TBL
CmdOut.FileName = Left$(InputFile, (Len(InputFile) - 4)) + ".TBL"
CmdOut.Filter = "Data Files (*.DAT)|*.dat|Table Files (*.TBL)|*.tbl|Print Files(*.PRN)|*.prn|Text Files
(*.TXT)|*.txt|All Files (*.*)|*.*"
CmdOut.FilterIndex = 2
CmdOut.Flags = OFN_OVERWRITEPROMPT Or OFN_PATHMUSTEXIST
CmdOut.Action = 2
Open CmdOut.FileName For Output As #1
For H = 1 To Peak
Print #1, "CENTER ", H, A(H * 4 - 3)
Print #1, "AMPLITUDE ", H, A(H * 4 - 2)
Print #1, "WIDTH ", H, A(H * 4 - 1)
Next H
  For H = 1 To Peak * 4
  b(H) = A(H)
  A(H) = 0
  Next H
For H = 1 To Peak
  A(1) = 0
  A(2) = 0
  A(3) = 0
  A(4) = 0
  A(1) = b(H * 4 - 3)

FITFORM.FRM - 5

  A(2) = b(H * 4 - 2)
  A(3) = b(H * 4 - 1)
  A(4) = b(H * 4)
  SinglePeak
  Print #1, "Peak ", H
  peaksum = 0
  For I = 1 To Pts
  peaksum = peaksum + Sqr(YF(I))
  Next I
  peaksum = peaksum * Abs(Del)
  Print #1, "Square Root Area", peaksum
  Next H
  For H = 1 To Peak * 4
  A(H) = b(H)
  Next H
Close #1
ee:
Resume eee
eee:
End Sub
Sub ScaleDown_MouseDown (Button As Integer, Shift As Integer, X As Single, Y As Single)
If (Button + LEFT_BUTTON) <> 0 Then ScalDown = 1

```

```

ScalesDown
LeastSquares
End Sub
Sub ScaleDown_MouseUp (Button As Integer, Shift As Integer, X As Single, Y As Single)
If (Button + LEFT_BUTTON) <> 0 Then ScalDown = 0
ScalesDown
End Sub
Sub ScaleReset_Click ()
AmplitudeMinus.Visible = False
AmplitudePlus.Visible = False
WidthMinus.Visible = False
WidthPlus.Visible = False
MoveLeft.Visible = False
MoveRight.Visible = False
ScaleUp.Visible = True
ScaleDown.Visible = True
End Sub
Sub ScaleUp_MouseDown (Button As Integer, Shift As Integer, X As Single, Y As Single)
If (Button + LEFT_BUTTON) <> 0 Then ScalUp = 1
ScalesUp
LeastSquares
End Sub
Sub ScaleUp_MouseUp (Button As Integer, Shift As Integer, X As Single, Y As Single)
If (Button + LEFT_BUTTON) <> 0 Then ScalUp = 0
ScalesUp
End Sub
Sub SelectBox_Click ()
SelectBtn.Enabled = True
End Sub

```

FITFORM.FRM - 6

```

Sub SelectBox_LostFocus ()
PeakSelect = Val(Mid$(SelectBox.Text, 6, Len(SelectBox.Text) - 5))
End Sub
Sub SelectBtn_Click ()
SelectBtn.Visible = False
SelectBox.Visible = False
SelectBtn.Enabled = False
SelectBox.Enabled = False
AmplitudePlus.Visible = True
AmplitudePlus.Enabled = True
AmplitudeMinus.Visible = True
AmplitudeMinus.Enabled = True
MoveLeft.Enabled = True
MoveLeft.Visible = True
MoveRight.Visible = True
MoveRight.Enabled = True
WidthPlus.Enabled = True
WidthMinus.Visible = True
WidthPlus.Visible = True
WidthMinus.Enabled = True

```

```

End Sub
Sub SelectPeak_Click ()
SelectBox.Visible = True
SelectBox.Enabled = True
SelectBtn.Visible = True
SelectBox.Text = "Peak " & PeakSelect
If Peak = 0 Then SelectBox.Text = "No Peak Selected"
End Sub
Sub WidthMinus_MouseDown (Button As Integer, Shift As Integer, X As Single, Y As Single)
If (Button + LEFT_BUTTON) <> 0 Then PeakThin = 1
DrawThin
LeastSquares
End Sub
Sub WidthMinus_MouseUp (Button As Integer, Shift As Integer, X As Single, Y As Single)
If (Button + LEFT_BUTTON) <> 0 Then PeakThin = 0
DrawThin
End Sub
Sub WidthPlus_MouseDown (Button As Integer, Shift As Integer, X As Single, Y As Single)
If (Button + LEFT_BUTTON) <> 0 Then PeakFat = 1
DrawFat
LeastSquares
End Sub
Sub WidthPlus_MouseUp (Button As Integer, Shift As Integer, X As Single, Y As Single)
If (Button + LEFT_BUTTON) <> 0 Then PeakFat = 0
DrawFat
End Sub
Sub XnrDown_MouseDown (Button As Integer, Shift As Integer, X As Single, Y As Single)
If (Button + LEFT_BUTTON) <> 0 Then xneg = 1
DrawXneg
LeastSquares
End Sub

```

FITFORM.FRM - 7

```

Sub XnrDown_MouseUp (Button As Integer, Shift As Integer, X As Single, Y As Single)
If (Button + LEFT_BUTTON) <> 0 Then xneg = 0
DrawXneg
End Sub
Sub XnrUp_MouseDown (Button As Integer, Shift As Integer, X As Single, Y As Single)
If (Button + LEFT_BUTTON) <> 0 Then xpos = 1
DrawXpos
LeastSquares
End Sub
Sub XnrUp_MouseUp (Button As Integer, Shift As Integer, X As Single, Y As Single)
If (Button + LEFT_BUTTON) <> 0 Then xpos = 0
DrawXpos
End Sub

```

GRAPHFOR.FRM - 1

```

Sub Command1_Click ()
Open CmdOut.FileName For Output As #1

```

```

For h = 2 To pts - 1
  Y(h) = (Y(h - 1) + Y(h) + Y(h + 1)) / 3
Next h
Plot
End Sub
Sub AcceptGraphBtn_Click ()
If StartPointReal = 0 Then GoTo PL
For h = StartPointReal To EndPointReal
Y(h) = yc(h)
Next h
PL: Plot
End Sub
Sub ExitGraphBtn_Click ()
'hide
Form1.Enabled = True
Form1.Visible = True
Form1.SelectMainFormBtn.Enabled = True
Form1.ExitMainFormBtn.Enabled = True
Form1.DataTypeFrame.Visible = False
Form1.DataTypeFrame.Enabled = False
GraphForm.Enabled = False
GraphForm.Visible = False
End Sub
Sub FilterBox_DblClick ()
FilterFac = FilterBox.Text
For h = StartPointReal To EndPointReal
yc(h) = (Y(h) + Offset) / FilterFac
Next h
  replot
End Sub
Sub FilterBox_KeyPress (KeyAscii As Integer)
If KeyAscii = 13 Then
FilterFac = FilterBox.Text
For h = StartPointReal To EndPointReal
yc(h) = (Y(h) + Offset) / FilterFac
Next h
  replot
End If
End Sub
Sub FitBtn_Click ()
GraphForm.Visible = False
GraphForm.Enabled = False
FitForm.Visible = True
FitForm.Enabled = True
FitForm.Left = 0
FitForm.Top = 0
FitForm.Height = 9000
FitForm.Width = 12000
Ychi = 0
Draw
End Sub
Sub Form_Load ()

```

```
FilterFac = 1
```

```
GRAPHFOR.FRM - 2
```

```
'Offset = 0
```

```
'StartPoint = 0
```

```
'EndPoint = 0
```

```
'StartPointReal = 0
```

```
'EndPointReal = 0
```

```
End Sub
```

```
Sub Form_MouseDown (Button As Integer, Shift As Integer, x As Single, Y As Single)
```

```
StartGraph = x
```

```
End Sub
```

```
Sub Form_MouseUp (Button As Integer, Shift As Integer, x As Single, Y As Single)
```

```
EndGraph = x
```

```
End Sub
```

```
Sub OffsetMinus_MouseDown (Button As Integer, Shift As Integer, x As Single, yy As Single)
```

```
If (Button + LEFT_BUTTON) <> 0 Then BringDown = 1
```

```
OffsetDown
```

```
End Sub
```

```
Sub OffsetMinus_MouseUp (Button As Integer, Shift As Integer, x As Single, Y As Single)
```

```
If (Button + LEFT_BUTTON) <> 0 Then BringDown = 0
```

```
OffsetDown
```

```
End Sub
```

```
Sub OffsetPlus_MouseDown (Button As Integer, Shift As Integer, x As Single, yy As Single)
```

```
If (Button + LEFT_BUTTON) <> 0 Then BringUp = 1
```

```
OffsetUp
```

```
End Sub
```

```
Sub OffsetPlus_MouseUp (Button As Integer, Shift As Integer, x As Single, Y As Single)
```

```
If (Button + LEFT_BUTTON) <> 0 Then BringUp = 0
```

```
OffsetUp
```

```
End Sub
```

```
Sub RestartGraphBtn_Click ()
```

```
For h = StartPointReal To EndPointReal
```

```
yc(h) = Y(h)
```

```
Next h
```

```
FilterBox.Text = 1
```

```
FilterFac = 1
```

```
Offset = 0
```

```
replot
```

```
End Sub
```

```
Sub SaveGraphBtn_Click ()
```

```
CmdOut.CancelError = True
```

```
On Error GoTo en
```

```
CmdOut.DefaultExt = ".tbl"
```

```
CmdOut.FileName = Left$(InputFile, (Len(InputFile) - 4)) + ".smo"
```

```
CmdOut.Filter = "Data Files (*.dat)|*.DAT|Table Files (*.TBL)|*.tbl|Print Files (*.PRN)|*.prn|All Files  
(*.*)*.*"
```

```
CmdOut.FilterIndex = 2
```

```
CmdOut.Flags = OFN_OVERWRITEPROMPT Or OFN_PATHMUSTEXIST
```

```
CmdOut.Action = 2
```

```
MsgBox "Writing to File " + CmdOut.FileName
```

```

Open CmdOut.FileName For Output As #1
For h = 1 To pts
Print #1, x(h), Y(h)
Next h

```

GRAPHFOR.FRM - 3

```

Close #1
en:
Resume enn
enn:
End Sub
Sub SelectGraphBtn_Click ()
If StartGraph > EndGraph Then 'make StartGraph
  Holde = StartGraph 'a lower value
  StartGraph = EndGraph 'than EndGraph
  EndGraph = Holde
End If
ReDim yc(pts)
If x(1) < x(pts) Then GoTo foreward
  If StartGraph < x(pts) Then StartGraph = x(pts)
  If EndGraph > x(1) Then EndGraph = x(1)
For h = 1 To pts
If x(h) > StartGraph Then GoTo mork
StartPoint = h
h = pts
mork: Next h
For h = 1 To pts
If x(h) > EndGraph Then GoTo muck
EndPoint = h
h = pts
muck: Next h
GoTo skip
foreward:
  If StartGraph < x(1) Then StartGraph = x(1)
  If EndGraph > x(pts) Then EndGraph = x(pts)
For h = 1 To pts
If x(h) < StartGraph Then GoTo dork
StartPoint = h
h = pts
dork: Next h
For h = 1 To pts
If x(h) < EndGraph Then GoTo duck
EndPoint = h
h = pts
duck: Next h
skip:
If StartPoint > EndPoint Then
  Holder = StartPoint
  StartPoint = EndPoint
  EndPoint = Holder
End If

```

```

StartPointReal = StartPoint
EndPointReal = EndPoint
StartPoint = StartPointReal - 10
EndPoint = EndPointReal + 10
If StartPoint < 1 Then StartPoint = 1
If EndPoint > pts - 9 Then EndPoint = pts
For h = StartPoint To EndPoint
yc(h) = Y(h)
Next h
replot
OffsetPlus.Enabled = True
OffsetPlus.Visible = True
OffsetMinus.Enabled = True
OffsetMinus.Visible = True
FilterBox.Enabled = True
FilterBox.Visible = True
FilterLabel.Visible = True
FilterFac = 1

```

GRAPHFOR.FRM - 4

```

FilterBox.Text = 1
Offset = 0
End Sub
Sub sommtheBox_Click ()
For h = 2 To pts - 1
Y(h) = (Y(h - 1) + Y(h) + Y(h + 1)) / 3
Next h
Plot
End Sub
Sub SqrtBox_Click ()
CmdOut.CancelError = True
On Error GoTo ebn
CmdOut.DefaultExt = ".tbl"
CmdOut.Filename = "Default.tbl"
CmdOut.Filter = "Data Files (*.dat)|*.DAT|Table Files (*.TBL)|*.tbl|Print Files (*.PRN)|*.prn|All Files (*.*)|*.*"
CmdOut.FilterIndex = 2
CmdOut.Flags = OFN_OVERWRITEPROMPT Or OFN_PATHMUSTEXIST
CmdOut.Action = 2
ReDim gg(pts)
MsgBox "Writing to File " + CmdOut.Filename
Open CmdOut.Filename For Output As #1
For h = 1 To pts
If Y(h) < 0 Then
Y(h) = -Y(h)
gg(h) = -(Sqr(Y(h)))
Else gg(h) = Y(h) ^ .5
End If
Print #1, x(h), gg(h)
Next h
Close #1

```

```

ebn:
Resume ebnn
ebnn:
End Sub

```

PHILS3RD.FRM - 1

```

Sub Option3_Click ()
ray = 3
End Sub
Sub CarsOnly_Click ()
ray = 1
ProceedBtn.Enabled = True
End Sub
Sub CarsPlus1_Click ()
ray = 2
ProceedBtn.Enabled = True
End Sub
Sub CarsPlus2_Click ()
ray = 3
ProceedBtn.Enabled = True
End Sub
Sub ExitMainFormBtn_Click ()
End
End Sub
Sub Old_Click ()
ray = 6
ProceedBtn.Enabled = True
End Sub
Sub OldI_Click ()
ray = 5
ProceedBtn.Enabled = True
End Sub
Sub ProceedBtn_Click ()
InputFile = CmdIn.FileName
Open InputFile For Input As #1
charlie = 0
chas = 0
charles = 0
chuck = 0
head = 0
Pts = 0
If ray = 4 Then GoTo nko
If ray = 5 Then GoTo onk
If ray = 6 Then GoTo kon
Do Until charlie = 1
Input #1, chuck
chip = charles + chuck
If charles <> 0 Then
If chuck <> 0 Then
If chip = 18787.804 Then charlie = 1
If chip = 18787.805 Then charlie = 1

```

```
End If
End If
charles = chuck
head = head + 1
Loop
head = head - 2
Close #1
Open InputFile For Input As #1
nko:
If ray = 4 Then
```

PHILS3RD.FRM - 2

```
Pts = 0
Do Until EOF(1)
  Pts = Pts + 1
  Input #1, xx, yy
Loop
Close #1
ReDim x(Pts), Y(Pts)
Open InputFile For Input As #1
For h = 1 To Pts
  Input #1, x(h), Y(h)
Next h
Close #1
End If
onk:
If ray = 5 Then
  Pts = 0
  For h = 1 To 6
    Input #1, garbage
  Next h
  Do Until EOF(1)
    Pts = Pts + 1
    Input #1, xx, yy, rr
  Loop
  Close #1
  ReDim x(Pts), Y(Pts), R(Pts)
  Open InputFile For Input As #1
  For h = 1 To 6
    Input #1, garbage
  Next h
  For h = 1 To Pts
    Input #1, x(h), Y(h), R(h)
    x(h) = 18787.804 - x(h)
  Next h
  Close #1
End If
kon:
If ray = 6 Then
  Pts = 0
  For h = 1 To 6
```

```

Input #1, garbage
Next h
Do Until EOF(1)
  Pts = Pts + 1
  Input #1, xx, yy
Loop
Close #1
ReDim x(Pts), Y(Pts)
Open InputFile For Input As #1
For h = 1 To 6
Input #1, garbage
Next h
For h = 1 To Pts
Input #1, x(h), Y(h)
x(h) = 18787.804 - x(h)
Next h
Close #1
End If
If ray = 1 Then
For h = 1 To head
Input #1, garbage
Next h
Do Until EOF(1)
  Pts = Pts + 1
  Input #1, dyey, xx, yy

```

PHILS3RD.FRM - 3

```

Loop
Close #1
ReDim x(Pts), Y(Pts), dye(Pts)
Open InputFile For Input As #1
For h = 1 To head
Input #1, garbage
Next h
For h = 1 To Pts
Input #1, dye(h), x(h), Y(h)
Next h
Close #1
End If
If ray = 2 Then
For h = 1 To head
Input #1, garbage
Next h
Do Until EOF(1)
  Pts = Pts + 1
  Input #1, dyey, xx, yy, rr
Loop
Close #1
ReDim x(Pts), Y(Pts), dye(Pts), R(Pts)
Open InputFile For Input As #1
For h = 1 To head

```

```

Input #1, garbage
Next h
For h = 1 To Pts
Input #1, dye(h), x(h), Y(h), R(h)
Next h
Close #1
End If
If ray = 3 Then
For h = 1 To head
Input #1, garbage
Next h
Do Until EOF(1)
Pts = Pts + 1
Input #1, dyey, xx, yy, rr, qq
Loop
Close #1
ReDim x(Pts), Y(Pts), dye(Pts), R(Pts), q(Pts)
Open InputFile For Input As #1
For h = 1 To head
Input #1, garbage
Next h
For h = 1 To Pts
Input #1, dye(h), x(h), Y(h), R(Pts), q(Pts)
Next h
Close #1
End If
Form1.Enabled = False
Form1.Visible = False
GraphForm.Show
GraphForm.Enabled = True
Plot
End Sub
Sub SelectMainFormBtn_Click ()
CmdIn.FileName = ""
CmdIn.Filter = "Print Files (*.PRN)|*.prn|Table Files (*.TBL)|*.tbl|Data Files (*.DAT)|*.dat|Text Files (*.TXT)|*.txt|AllFiles (*.*)|*.*"
CmdIn.FilterIndex = 1
CmdIn.Flags = OFN_FILEMUSTEXIST Or OFN_PATHMUSTEXIST

```

PHILS3RD.FRM - 4

```

CmdIn.Action = 1
If CmdIn.FileName = "" Then MsgBox "No File Selected You Turkey"
DataTypeFrame.Enabled = True
DataTypeFrame.Visible = True
End Sub
Sub XYData_Click ()
ray = 4
ProceedBtn.Enabled = True
End Sub

```

P3MOD.BAS - 1

```

Global X!(), Y!(), gg!(), Startgraph!, EndGraph!, dye!(), R!(), q!(), yc!()
Global garbage!, Pts%, ray%, xx!, yy!, dyey!, rr!, qq!
Global InputFile$
Global xmin!, xmax!, xminn!, xmaxx!, ymax!, ymaxx!, yminn!, diffx!, diffy!
Global StartPoint%, EndPoint%, Holde%, FilterFac!, Offset!, StartPointReal%, EndPoint
Real%
Global BringUp%, BringDown%
Global WF!, W0!, Del!, Peaks$, Peak%, hs$, K%, L%, A!(400), W!, C11#, C12#, XR#, XI#,
CHIRL#, CHIIM#
Global CHI2#(4000), CHI2MAX#, SQTPI!, ALPD#, XV#, YV#, AC#, T#(6), C#(6), S#(6), Y1#,
Y2#, R1#, R2#
Global D#, D1#, D2#, D3#, D4#, YRI#, YII#, YF#(4000), MS!, V%, Nterms%
Global PeakUp%, PeakDown%, PeakLeft%, PeakRight%, PeakThin%, PeakFat%
Global PeakSelect%, LL%
Global DD!(400), Alpha#(400, 400), Beta#(400), Nfree%, DA#(400), sum#, sum1#, sum2#,
sum3#, sum4#, sum7#, sum8#, sum9#
Global AJ#, AK#, J%, I%, Delta#, Sigma#(400), B!(400)
Global Bray#(400, 800), IK#(400), JK#(400), Det#, G%, xpos!, xneg!
Global it#, Solv%, TI#, Row%, Col%, save#, amax#, Holder#
Global Charlie!, Chuck!, Charles!, Chip!, ychi!, ScalUp!, ScalDown!
Sub Draw ()
V = 0: MS = 26
If Peak = 0 Then
  For h = 1 To Pts
    YF(h) = 0
  Next h
GoTo ES
End If
WF = X(Pts)
W0 = X(1)
Del = (WF - W0) / Pts
W = W0 - Del
For h = 1 To Pts
W = W + Del
YRI = 0
YII = 0
CHIRL = 0
CHIIM = 0
CHI2(h) = 0
  For L = 1 To Peak
    K = L * 4
    WJ = A(K - 3) - W
    If V = 1 Then GoSub VGTPFL
    C11 = WJ
    C12 = (A(K - 2) / (4 * C11 * C11 + A(K - 1) * A(K - 1)))
    XR = 2 * C11 * C12
    XI = A(K - 1) * C12
    CHIRL = CHIRL + XR
    CHIIM = CHIIM + XI
    'CHI2(h) = CHI2(h) + (A(K - 2) * A(K - 2)) / ((WJ + A(Nterms - 1)) ^ 2 + (A(K - 1)) ^ 2)
  Next L

```

```

    Debug.Print WJ, CHIIM, CHIRL, CHI2(h)
    CHI2(h) = (CHIRL + A(Nterms - 1)) ^ 2 + CHIIM * CHIIM
    Next h
    CHI2MAX = CHI2(1)
    For h = 1 To Pts
    If CHI2(h) > CHI2MAX Then CHI2MAX = CHI2(h)
    Next h
    For h = 1 To Pts
    CHI2(h) = CHI2(h) / CHI2MAX
    YF(h) = CHI2(h)
    Next h

```

P3MOD.BAS - 2

```

GoTo ES
VGTPFL:
    SQTPI = 1.772453851
    ALPD = .00000043014 * A(K - 3) * Sqr(A(K) / MS)
    XV = WJ / ALPD
    YV = A(K - 1) / (2 * ALPD)
    GoSub CPF
    AC = SQTPI / (2 * ALPD)
    XR = A(K - 2) * WI * AC
    XI = A(K - 2) * WR * AC
Return
CPF:
    T(1) = .314240376
    T(2) = .947788341
    T(3) = 1.59768264
    T(4) = 2.27950708
    T(5) = 3.02063703
    T(6) = 3.8897249
    C(1) = 1.01172805
    C(2) = -.75187147
    C(3) = .012557727
    C(4) = .0100220082
    C(5) = -.000242068135
    C(6) = .000000500848061
    S(1) = 1.393237
    S(2) = .231152406
    S(3) = -.155351466
    S(4) = .00621836624
    S(5) = .0000919082906
    S(6) = -.000000627525958
    WR = 0
    WI = 0
    Y1 = YV + 1.5
    Y2 = Y1 ^ 2
    If YV > .85 Then GoTo TWO
    If Abs(XV) < 18.1 * YV + 1.65 Then GoTo TWO
    If Abs(XV) < 12 Then WR = Exp(-XV * XV)
    Y3 = YV + 3

```

```

For I = 1 To 6
  R1 = XV - T(I)
  R2 = R1 ^ 2
  D = 1 / (R2 + Y2)
  D1 = Y1 * D
  D2 = R1 * D
  WR = WR = TV * (C(I) * (R1 * D2 - 1.5 * D1) + S(I) * Y3 * D2) / (R2 + 2.25)
  R1 = XV = T(I)
  R2 = R1 ^ 2
  D = 1 / (R2 + Y2)
  D3 = Y1 * D
  D4 = R1 * D
  WR = WR + YV * (C(I) * (R1 * D4 - 1.5 * D3) - S(I) * Y3 * D4) / (R2 + 2.25)
  WI = WI + C(I) * (D2 + D4) + S(I) * (D1 - D3)

```

```
Next I
```

```
Return
```

```
TWO:
```

```

For I = 1 To 6
  R1 = XV - T(I)
  D = 1 / (R1 ^ 2 + Y2)
  D1 = Y1 * D
  D2 = R1 * D
  R1 = XV + T(I)
  D = 1 / (R1 ^ 2 + Y2)
  D3 = Y1 * D
  D4 = R1 * D

```

```
P3MOD.BAS - 3
```

```

  WR = WR + C(I) * (D1 + D3) - S(I) * (D2 - D4)
  WI = WI + C(I) * (D2 + D4) + S(I) * (D1 - D3)

```

```
Next I
```

```
Return
```

```
ES:
```

```
FitForm.Cls
```

```
FitForm.Left = 0
```

```
FitForm.Top = 0
```

```
FitForm.visible = True
```

```
FitForm.Enabled = True
```

```
FitForm.Height = 8300
```

```
FitForm.Width = 12000
```

```
'GraphForm.visible = False
```

```
'GraphForm.Enabled = False
```

```
FitForm.ScaleMode = 0
```

```
xmax = 0: xmin = 40000: ymax = 0
```

```
For h = 1 To Pts
```

```
  If X(h) > xmax Then xmax = X(h)
```

```
  If X(h) < xmin Then xmin = X(h)
```

```
  If Y(h) > ymax Then ymax = Y(h)
```

```
Next h
```

```
For h = 1 To Pts
```

```
  YF(h) = YF(h) * ychi
```

```

Next h
xmaxx = xmax + (xmax - xmin) * .05
xminn = xmin - (xmax - xmin) * .05
ymaxx = ymax + ymax * .05
yminn = 0 - ymax * .05
FitForm.Scale (xminn, ymaxx)-(xmaxx, yminn)
FitForm.Line (xmin, ymax)-(xmin, 0), RGB(200, 0, 0)
FitForm.Line -(xmax, 0), RGB(200, 0, 0)
diffx = (xmax - xmin) / 4
diffy = ymax / 100
FitForm.Line (xmin + diffx, -diffy)-(xmin + diffx, diffy), RGB(200, 0, 0)
FitForm.Line (xmin + 2 * diffx, -diffy)-(xmin + 2 * diffx, diffy), RGB(200, 0, 0)
FitForm.Line (xmin + 3 * diffx, -diffy)-(xmin + 3 * diffx, diffy), RGB(200, 0, 0)
For h = 2 To Pts
FitForm.Line (X(h - 1), Y(h - 1))-(X(h), Y(h)), RGB(200, 200, 0)
FitForm.Line (X(h - 1), YF(h - 1))-(X(h), YF(h)), RGB(200, 0, 0)
Next h
GraphForm.MousePointer = 3
End Sub
Sub DrawDown ()
LL = PeakSelect * 4
'Debug.Print A(LL - 2)
Do While PeakDown = 1
A(LL - 2) = A(LL - 2) - .005 * ymax
Draw
DoEvents
Loop
End Sub
Sub DrawFat ()
LL = PeakSelect * 4
'Debug.Print A(LL - 1)
Do While PeakFat = 1
A(LL - 1) = A(LL - 1) + .02
Draw
DoEvents
Loop

```

P3MOD.BAS - 4

```

End Sub
Sub DrawLeft ()
LL = PeakSelect * 4
'Debug.Print A(LL - 3)
Do While PeakLeft = 1
A(LL - 3) = A(LL - 3) - .005
Draw
DoEvents
Loop
End Sub
Sub DrawRight ()
LL = PeakSelect * 4
'Debug.Print A(LL - 3)

```

```

Do While PeakRight = 1
A(LL - 3) = A(LL - 3) + .005
Draw
DoEvents
Loop
End Sub
Sub Draws ()
V = 0: MS = 26
If Peak = 0 Then
For h = 1 To Pts
YF(h) = 0
Next h
GoTo ESs
End If
WF = X(Pts)
W0 = X(1)
Del = (WF - W0) / Pts
W = W0 - Del
For h = 1 To Pts
W = W + Del
YRI = 0
YII = 0
CHIRL = 0
CHIIM = 0
CHI2(h) = 0
For L = 1 To Peak
K = L * 4
WJ = A(K - 3) - W
If V = 1 Then GoSub VGTPFLs
C11 = WJ
C12 = (A(K - 2) / (4 * C11 * C11 + A(K - 1) * A(K - 1)))
XR = 2 * C11 * C12
XI = A(K - 1) * C12
CHIRL = CHIRL + XR
CHIIM = CHIIM + XI
'CHI2(h) = CHI2(h) + (A(K - 2)) ^ 2 / ((WJ + A(Nterms - 1)) ^ 2 + (A(K - 1)) ^ 2)
Next L
CHI2(h) = (CHIRL + A(Nterms - 1)) ^ 2 + CHIIM * CHIIM
Next h
CHI2MAX = CHI2(1)
For h = 1 To Pts
If CHI2(h) > CHI2MAX Then CHI2MAX = CHI2(h)
Next h
For h = 1 To Pts
CHI2(h) = CHI2(h) / CHI2MAX

P3MOD.BAS - 5

YF(h) = CHI2(h)
Next h
GoTo ESs
VGTPFLs:

```

```

SQTPI = 1.772453851
ALPD = .00000043014 * A(K - 3) * Sqr(A(K) / MS)
XV = WJ / ALPD
YV = A(K - 1) / (2 * ALPD)
GoSub CPFs
AC = SQTPI / (2 * ALPD)
XR = A(K - 2) * WI * AC
XI = A(K - 2) * WR * AC
Return
CPFs:
T(1) = .314240376
T(2) = .947788341
T(3) = 1.59768264
T(4) = 2.27950708
T(5) = 3.02063703
T(6) = 3.8897249
C(1) = 1.01172805
C(2) = -.75187147
C(3) = .012557727
C(4) = .0100220082
C(5) = -.000242068135
C(6) = .000000500848061
S(1) = 1.393237
S(2) = .231152406
S(3) = -.155351466
S(4) = .00621836624
S(5) = .0000919082906
S(6) = -.000000627525958
WR = 0
WI = 0
Y1 = YV + 1.5
Y2 = Y1 ^ 2
If YV > .85 Then GoTo TWOo
If Abs(XV) < 18.1 * YV + 1.65 Then GoTo TWOo
If Abs(XV) < 12 Then WR = Exp(-XV * XV)
Y3 = YV + 3
For I = 1 To 6
  R1 = XV - T(I)
  R2 = R1 ^ 2
  D = 1 / (R2 + Y2)
  D1 = Y1 * D
  D2 = R1 * D
  WR = WR + TV * (C(I) * (R1 * D2 - 1.5 * D1) + S(I) * Y3 * D2) / (R2 + 2.25)
  R1 = XV - T(I)
  R2 = R1 ^ 2
  D = 1 / (R2 + Y2)
  D3 = Y1 * D
  D4 = R1 * D
  WR = WR + YV * (C(I) * (R1 * D4 - 1.5 * D3) - S(I) * Y3 * D4) / (R2 + 2.25)
  WI = WI + C(I) * (D2 + D4) + S(I) * (D1 - D3)
Next I
Return

```

TWOo:

```

For I = 1 To 6
  R1 = XV - T(I)
  D = 1 / (R1 ^ 2 + Y2)
  D1 = Y1 * D
  D2 = R1 * D
  R1 = XV + T(I)
  D = 1 / (R1 ^ 2 + Y2)

```

P3MOD.BAS - 6

```

  D3 = Y1 * D
  D4 = R1 * D
  WR = WR + C(I) * (D1 + D3) - S(I) * (D2 - D4)
  WI = WI + C(I) * (D2 + D4) + S(I) * (D1 - D3)
Next I
Return
ESs:
For h = 1 To Pts
  YF(h) = YF(h) * ychi
Next h
GraphForm.MousePointer = 3
  End Sub
  Sub DrawThin ()
LL = PeakSelect * 4
'Debug.Print A(LL - 1)
Do While PeakThin = 1
A(LL - 1) = A(LL - 1) - .02
Draw
DoEvents
Loop
  End Sub
  Sub DrawUp ()
LL = PeakSelect * 4
'Debug.Print A(LL - 2)
Do While PeakUp = 1
A(LL - 2) = A(LL - 2) + .005 * ymax
Draw
DoEvents
Loop
  End Sub
  Sub DrawXneg ()
Do While xneg = 1
A(Nterms - 1) = A(Nterms - 1) - .01
Draw
DoEvents
Loop
  End Sub
  Sub DrawXpos ()
Do While xpos = 1
A(Nterms - 1) = A(Nterms - 1) + .01
Draw

```

```

DoEvents
Loop
End Sub
Sub FitRoutine ()
'sum8 = 0
'sum7 = sum
'sum9 = 1
For I = 1 To 3
' For J = 1 To Pts
' K = I * J

```

P3MOD.BAS - 7

```

' Do Until sum9 < 0
' sum8 = sum7
' If I = 1 Then A(K) = A(K) + .005
' If I = 2 Then A(K) = A(K) + .01 * ymax
' If I = 3 Then A(K) = A(K) + .05
' LeastSquares
' sum7 = sum
' sum9 = sum8 - sum7
' Loop
' sum8 = 0
' sum7 = sum
' sum9 = 1
' Do Until sum9 < 0
' sum8 = sum7
' If I = 1 Then A(K) = A(K) - .005
' If I = 2 Then A(K) = A(K) - .01 * ymax
' If I = 3 Then A(K) = A(K) - .05
' LeastSquares
' sum7 = sum
' sum9 = sum8 - sum7
' If I = 1 Then A(K) = A(K) + .005
' If I = 2 Then A(K) = A(K) + .01 * ymax
' If I = 3 Then A(K) = A(K) + .05
' Loop
' Next J
Next I
Nterms = Peak * 4 + 2
For h = 1 To Peak
J = 4 * h
DD(J - 3) = .1: DD(J - 2) = .05 * A(J - 2): DD(J - 1) = .2 * A(J - 1): DD(J) = 10
00
Next h
A(Nterms) = ychi: DD(Nterms) = .01 * ychi
A(Nterms - 1) = .01: DD(Nterms - 1) = .01
Nfree = Pts - Nterms
Draws
red:
If Nfree <= 0 Then End
sum = 0

```

```

Draws
LeastSquares
  sum1 = sum          'sum1 is the original chi^2
  For J = 1 To Nterms
    AJ = A(J)         'add to each term a delta
    A(J) = AJ + DD(J)
    ychi = A(Nterms)
Draws
LeastSquares
  sum2 = sum          'sum2 is the chi^2 for delta J
  Alpha(J, J) = sum2 - (sum1 * 2) 'diagonals get d2X/dJ2
  Beta(J) = -sum2
  For I = 1 To Nterms
    If I = J Then GoTo ka      'not diagonals
    If I > J Then GoTo here    'only I's > J get A() + DD()
    Alpha(I, J) = (Alpha(I, J) - sum2) / 2 'second finish offs
    Alpha(J, I) = Alpha(I, J): GoTo ka
here: Alpha(J, I) = sum1 - sum2 'set up off diagonals
    AK = A(I)                'd2X/dIdJ first
    A(I) = AK + DD(I)
    ychi = A(Nterms)
Draws
LeastSquares
  sum3 = sum          'sum3 is dIdJ
  Alpha(J, I) = Alpha(J, I) + sum3*sum1 - sum2 - sum3

P3MOD.BAS - 8

  A(I) = AK
      'reset A(I)
ka: Next I
ychi = A(Nterms)      'Change next I
  A(J) = AJ - DD(J)
  ychi = A(Nterms)    'Step Back
Draws                  'this completes curvature measure
LeastSquares
  sum4 = sum
  A(J) = AJ

  Alpha(J, J) = (Alpha(J, J) + sum4) / 2 'diagonals = sum2-sum1+sum4-sum1
  Beta(J) = (Beta(J) + sum4) / 4      'first derivative (sum4-sum2)/4
Next J
ychi = A(Nterms)
  For J = 1 To Nterms
    'Debug.Print Alpha(J, J)
    If Alpha(J, J) > 0 Then GoTo jj
    If Alpha(J, J) = 0 Then GoTo there
    Alpha(J, J) = -Alpha(J, J): GoTo over
there: Alpha(J, J) = .001
over: For I = 1 To Nterms
  If I = J Then GoTo kk
  Alpha(J, I) = 0: Alpha(I, J) = 0

```

```

kk: Next I
jj: Next J
MatrixInvert
  For J = 1 To Nterms
    DA(J) = 0
    For I = 1 To Nterms
      DA(J) = DA(J) + Beta(I) + Alpha(J, I)
    Next I
    DA(J) = .2 * DA(J) * DD(J)
  Next J
  For J = 1 To Nterms
    A(J) = A(J) + DA(J): Next J

up: ychi = A(Nterms)
Draws
LeastSquares
  sum2 = sum
If sum2 = Holder Then GoTo ox
  If sum1 < sum2 Then
    For J = 1 To Nterms
      DA(J) = DA(J) / 2
      A(J) = A(J) - DA(J)
    Next J
    Holder = sum2
  GoTo up
End If
ox: For J = 1 To Nterms
  A(J) = A(J) + DA(J): Next J
ychi = A(Nterms)
Draws
LeastSquares
  sum3 = sum
  If sum3 < sum2 Then
    sum1 = sum2: sum2 = sum3
  GoTo ox
End If
  If sum2 = sum3 Then
    Delta = 0
  Else Delta = 1 / (1 + (sum1 - sum2) / (sum3 - sum2)) + .5
End If

```

P3MOD.BAS - 9

```

  For J = 1 To Nterms
    A(J) = A(J) - Delta * DA(J)
    Sigma(J) = DD(J) * Sqr(Free * Abs(Alpha(J, J)))
  Next J
ychi = A(Nterms)
Draws
LeastSquares
  If sum2 < sum Then
    For J = 1 To Nterms

```

```

    A(J) = A(J) + (Delta - 1) * DA(J)
  Next J
  sum = sum2
  End If
ychi = A(Nterms)
Draw
End Sub
Sub hider ()
Form1.Hide
'GraphForm.Hide
'FitForm.Hide
End Sub
Sub LeastSquares ()
sum = 0
Nfree = Pts
If Peak > 0 Then Nfree = Pts / (4 * Peak)
For h = 1 To Pts
sum = sum + (Y(h) - YF(h)) ^ 2
Next h
sum = sum / Nfree
'Debug.Print sum
sums = Str$(sum)
FitForm.ResidualLabel.Caption = "Residuals = " + sums
End Sub
Sub MatrixInvert ()
For I = 1 To Nterms
  For J = 1 To Nterms
    Bray(I, J) = Alpha(I, J)
    Bray(I, J + Nterms) = 0
  Next J
  Bray(I, I + Nterms) = 1
Next I
For Solv = 1 To Nterms
  it = 1 / Bray(Solv, Solv)
  For Col = Solv To Nterms * 2
    Bray(Solv, Col) = Bray(Solv, Col) * it
  Next Col
  For Row = 1 To Nterms
    If Row = Solv Then GoTo sr
    TI = Bray(Row, Solv)
    For Col = Solv To Nterms * 2
      Bray(Row, Col) = Bray(Row, Col) - TI * Bray(Solv, Col)
    Next Col
sr: Next Row
Next Solv
  For I = 1 To Nterms
    For J = 1 To Nterms
      Alpha(I, J) = Bray(I, J + Nterms)
    Next J
  Next I
End Sub

```

P3MOD.BAS - 10

Sub MatrixInvert2 ()

For G = 1 To Nterms

amax = 0

righty: For I = G To Nterms

For J = G To Nterms

If Abs(amax) > Abs(Alpha(I, J)) Then GoTo ja

amax = Alpha(I, J)

IK(G) = I

JK(G) = J

ja: Next J: Next I

If amax = 0 Then

Det = 0

Exit Sub

End If

I = IK(G)

If I = G Then GoTo lefty

If I < G Then GoTo righty

For J = 1 To Nterms

save = Alpha(G, J)

Alpha(G, J) = Alpha(I, J)

Alpha(I, J) = save

Next J

lefty: J = JK(G)

If J = G Then GoTo down

If J < G Then GoTo righty

For I = 1 To Nterms

save = Alpha(I, G)

Alpha(I, G) = Alpha(I, J)

Alpha(I, J) = -1 \* save

Next I

down: For I = 1 To Nterms

For J = 1 To Nterms

If I = G Then GoTo jb

If J = G Then GoTo jb

Alpha(I, J) = Alpha(I, J) + Alpha(I, G) \* Alpha(G, J)

jb: Next J: Next I

For J = 1 To Nterms

If J = G Then GoTo jc

Alpha(G, J) = Alpha(G, J) / amax

jc: Next J

Alpha(G, G) = 1 / amax

Det = Det \* amax

Next G

For L = 1 To Nterms

G = Nterms - L + 1

J = IK(G)

If J > G Then

For I = 1 To Nterms

save = Alpha(I, G)

Alpha(I, G) = -Alpha(I, J)

```

    Alpha(I, J) = save
  Next I
End If
I = JK(G)
If J > G Then
  For J = 1 To Nterms
    save = Alpha(G, J)
    Alpha(G, J) = -Alpha(I, J)
    Alpha(I, J) = save
  Next J
End If
Next L

```

P3MOD.BAS - 11

```

  End Sub
  Sub OffsetDown ()
  For h = 1 To 100000
  Next h
  Do While BringDown = 1
  Offset = Offset - .001 * ymax
  For h = StartPointReal To EndPointReal
  yc(h) = (Y(h) + Offset) / FilterFac
  Next h
  replot
  DoEvents
  Loop
  End Sub
  Sub OffsetUp ()
  For h = 1 To 100000
  Next h
  Do Until BringUp = 0
  Offset = Offset + .001 * ymax
  For h = StartPointReal To EndPointReal
  yc(h) = (Y(h) + Offset) / FilterFac
  Next h
  replot
  DoEvents
  Loop
  End Sub
  Sub Plot ()
  GraphForm.Cls
  GraphForm.ScaleMode = 0
  GraphForm.Left = 0
  GraphForm.Top = 0
  GraphForm.Height = 9000
  GraphForm.Width = 12000
  xmax = 0: xmin = 40000: ymax = 0
  For h = 1 To Pts
  If X(h) > xmax Then xmax = X(h)
  If X(h) < xmin Then xmin = X(h)
  If Y(h) > ymax Then ymax = Y(h)

```

```

Next h
xmaxx = xmax + (xmax - xmin) * .05
xminn = xmin - (xmax - xmin) * .05
ymaxx = ymax + ymax * .05
yminn = 0 - ymax * .05
GraphForm.Scale (xminn, ymaxx)-(xmaxx, yminn)
GraphForm.Line (xmin, ymax)-(xmin, 0), RGB(200, 0, 0)
GraphForm.Line -(xmax, 0), RGB(200, 0, 0)
diffx = (xmax - xmin) / 4
diffy = ymax / 100
GraphForm.Line (xmin + diffx, -diffy)-(xmin + diffx, diffy), RGB(200, 0, 0)
GraphForm.Line (xmin + 2 * diffx, -diffy)-(xmin + 2 * diffx, diffy), RGB(200, 0, 0)
GraphForm.Line (xmin + 3 * diffx, -diffy)-(xmin + 3 * diffx, diffy), RGB(200, 0, 0)
For h = 2 To Pts
GraphForm.Line (X(h - 1), Y(h - 1))-(X(h), Y(h)), RGB(200, 0, 0)
Next h
GraphForm.MousePointer = 3
End Sub

```

### P3MOD.BAS - 12

```

Sub replot ()
GraphForm.Cls
GraphForm.ScaleMode = 0
GraphForm.Left = 0
GraphForm.Top = 0
GraphForm.Height = 9000
GraphForm.Width = 12000
xmax = 0: xmin = 40000: ymax = 0
For h = StartPoint To EndPoint
If X(h) > xmax Then xmax = X(h)
If X(h) < xmin Then xmin = X(h)
If yc(h) > ymax Then ymax = yc(h)
Next h
xmaxx = xmax + (xmax - xmin) * .05
xminn = xmin - (xmax - xmin) * .05
ymaxx = ymax + ymax * .05
yminn = 0 - ymax * .05
GraphForm.Scale (xminn, ymaxx)-(xmaxx, yminn)
GraphForm.Line (xmin, ymax)-(xmin, 0), RGB(0, 200, 0)
GraphForm.Line -(xmax, 0), RGB(200, 0, 0)
diffx = (xmax - xmin) / 4
diffy = ymax / 100
GraphForm.Line (xmin + diffx, -diffy)-(xmin + diffx, diffy), RGB(200, 0, 0)
GraphForm.Line (xmin + 2 * diffx, -diffy)-(xmin + 2 * diffx, diffy), RGB(200, 0, 0)
GraphForm.Line (xmin + 3 * diffx, -diffy)-(xmin + 3 * diffx, diffy), RGB(200, 0, 0)
For h = StartPoint + 1 To EndPoint
GraphForm.Line (X(h - 1), yc(h - 1))-(X(h), yc(h)), RGB(200, 0, 0)
Next h
End Sub
Sub ScalesDown ()
For h = 1 To 100000

```

```

Next h
Do While ScalDown = 1
ychi = ychi - .01 * ychi
Draw
DoEvents
Loop
End Sub
Sub ScalesUp ()
For h = 1 To 100000
Next h
Do While ScalUp = 1
ychi = ychi + .01 * ychi
Draw
DoEvents
Loop
End Sub
Sub SinglePeak ()
V = 0: MS = 26
WF = X(Pts)
W0 = X(1)
Del = (WF - W0) / Pts
W = W0 - Del
For h = 1 To Pts
W = W + Del
YRI = 0

P3MOD.BAS - 13

YII = 0
CHIRL = 0
CHIIM = 0
CHI2(h) = 0
WJ = A(1) - W
If V = 1 Then GoSub VGTPFL1
C11 = WJ
C12 = (A(2) / (4 * C11 * C11 + A(3) * A(3)))
XR = 2 * C11 * C12
XI = A(3) * C12
CHIRL = CHIRL + XR
CHIIM = CHIIM + XI
CHI2(h) = (CHIRL + A(Nterms - 1)) ^ 2 + CHIIM * CHIIM
Next h
For h = 1 To Pts
YF(h) = CHI2(h)
Next h
GoTo EN
VGTPFL1:
SQTPI = 1.772453851
ALPD = .00000043014 * A(1) * Sqr(A(4) / MS)
XV = WJ / ALPD
YV = A(3) / (2 * ALPD)
GoSub CPF1

```

```

AC = SQTPI / (2 * ALPD)
XR = A(2) * WI * AC
XI = A(2) * WR * AC
Return
CPF1:
T(1) = .314240376
T(2) = .947788341
T(3) = 1.59768264
T(4) = 2.27950708
T(5) = 3.02063703
T(6) = 3.8897249
C(1) = 1.01172805
C(2) = -.75187147
C(3) = .012557727
C(4) = .0100220082
C(5) = -.000242068135
C(6) = .000000500848061
S(1) = 1.393237
S(2) = .231152406
S(3) = -.155351466
S(4) = .00621836624
S(5) = .0000919082906
S(6) = -.000000627525958
WR = 0
WI = 0
Y1 = YV + 1.5
Y2 = Y1 ^ 2
If YV > .85 Then GoTo TWOs
If Abs(XV) < 18.1 * YV + 1.65 Then GoTo TWOs
If Abs(XV) < 12 Then WR = Exp(-XV * XV)
Y3 = YV + 3
For I = 1 To 6
  R1 = XV - T(I)
  R2 = R1 ^ 2
  D = 1 / (R2 + Y2)
  D1 = Y1 * D
  D2 = R1 * D
  WR = WR + TV * (C(I) * (R1 * D2 - 1.5 * D1) + S(I) * Y3 * D2) / (R2 + 2.25)
  R1 = XV - T(I)

```

P3MOD.BAS - 14

```

  R2 = R1 ^ 2
  D = 1 / (R2 + Y2)
  D3 = Y1 * D
  D4 = R1 * D
  WR = WR + YV * (C(I) * (R1 * D4 - 1.5 * D3) - S(I) * Y3 * D4) / (R2 + 2.25)
  WI = WI + C(I) * (D2 + D4) + S(I) * (D1 - D3)

```

Next I

Return

TWOs:

```

  For I = 1 To 6

```

```
R1 = XV - T(I)
D = 1 / (R1 ^ 2 + Y2)
D1 = Y1 * D
D2 = R1 * D
R1 = XV + T(I)
D = 1 / (R1 ^ 2 + Y2)
D3 = Y1 * D
D4 = R1 * D
WR = WR + C(I) * (D1 + D3) - S(I) * (D2 - D4)
WI = WI + C(I) * (D2 + D4) + S(I) * (D1 - D3)
Next I
Return
EN:
End Sub
```